Aus dem Bereich der Physiologie
Theoretische Medizin und Biowissenschaften
der Medizinischen Fakultät
der Universität des Saarlandes, Homburg/Saar

# AMPA receptor trafficking and regulation by prominent auxiliary subunits in cultured hippocampal neurons

**Dissertation**

**zur Erlangung des Grades eines Doktors der Naturwissenschaften**

**der Medizinischen Fakultät**

der UNIVERSITÄT DES SAARLANDES

2019

vorgelegt von: Ali Harb

geb. am: 10 August 1986 in Serhin El Faouka, Libanon

| | |
|---|---|
| Tag der Promotion: | 29.08.2019 |
| Dekan: | Prof. Dr. M. D. Menger |
| Berichterstatter: | Prof. Dr. R. Mohrmann |
| | Prof. Dr. M. Boehm |

**Doctoral supervisor:** Prof. Dr. Ralf Mohrmann

*I want to dedicate this work to my beloved parents and brothers, especially my brother Mohammed who I hope is proud watching me from heaven!*

# Table of contents

# List of Figures

# List of Tables

# Abbreviations

| | |
|---|---|
| % | percentage |
| Ab | antibody |
| ABP | AMPAR binding protein |
| AMPAR | α-amino-3-hydroxy-5-methyl-4-isoxazole propionate receptors |
| AOTF | Acousto Optical Tunable Filter |
| APV | 2-amino-5-phosphonopentanoic acid |
| Arf6 | ADP-ribosylation factor 6 |
| ATD | amino-terminal domain |
| AU | Airy Unit |
| β2AR | β2 adrenergic receptor |
| BiP | immunoglobulin-binding protein |
| °C | degrees Celsius |
| $Ca^{2+}$ | calcium |
| CI | $Ca^{2+}$ impermeable |
| CKAMP | Cystine-Knot AMPAR modulating protein |
| CKAMP44a | Cystine-Knot AMPAR modulating protein44a |
| CNIH | cornichon |
| CP | $Ca^{2+}$ permeable |
| CTD | C-terminal domain |
| DG | dentate gyrus |
| DIV | days in vitro |
| DMEM | Dulbecco's Modified Eagle Medium |
| DPBS | Dulbecco’s Phosphate Buffered Saline |
| DPSS | Diode Pumped Solid State |
| EE | early endosome |

| | |
|---|---|
| EM | electron microscopy |
| EMCCD | Electron Multiplying Charge Coupled Device |
| ER | endoplasmic reticulum |
| EPSC | excitatory postsynaptic current |
| EX | extracellular domain |
| EZ | endocytic zone |
| fC | femtoCoulomb |
| FCS | fetal calf serum |
| FUdR | 5 - Fluoro - 2’ deoxyuridine |
| g | gram |
| GABAR | ɣ-amino butyric acid receptors |
| GFAP | glial fibrillary acidic protein |
| GFP | green fluorescence protein |
| GluN | NMDA glutamate receptor |
| GluR | glutamate receptor |
| GPCR | G protein-coupled receptors |
| GRIA | glutamate receptor ionotropic AMPA |
| GRIK | glutamate receptor ionotropic kainate |
| GRIN | glutamate receptor ionotropic NMDA |
| GRIP | glutamate receptor-interacting protein |
| GRM | glutamate receptor metabotropic |
| GSG1L | Germ Cell-Specific Gene 1-Like |
| h | hour |
| HBSS | Hanks' Balanced Salt solution |
| HEPES | 4-(2-hydroxyethyl)-1-piperazineethanesulfonic acid |
| Hz | hertz |
| iGluR | ionotropic AMPA receptor |

| | |
|---|---|
| $K^+$ | potassium |
| kDa | kilo Dalton |
| KO | knockout |
| LBD | ligand-binding domain |
| LDCV | large dense core vesicles |
| LE | late endosome |
| LTD | long term depression |
| LTP | long term potentiation |
| M | molar |
| MAGUK | membrane-associated guanylate kinase |
| MAP | microtubule-associated protein |
| MΩ | MegaOhm |
| mEPSC | miniatureEPSC |
| mGluR | metabotropic glutamate receptors |
| min | minutes |
| ml | milliliter |
| µl | microliter |
| µm | micrometer |
| µM | micromolar |
| mm | millimeter |
| mM | millimolar |
| mRNA | messenger RNA |
| ms | millisecond |
| mV | millivolt |
| MVB | multivesicular bodies |
| NA | numerical aperture |
| NARP | Neuronal activity-regulated pentraxin |

| | |
|---|---|
| NBA | Neurobasal A medium |
| nm | nanometer |
| NMDA | N-methyl-D-aspartate |
| NP1 | neuronal pentraxin1 |
| nPIST | neuronal isoform of protein-interacting specifically with TC10 |
| NR | NMDA receptor |
| NSF | N-ethylmaleimide-sensitive fusion |
| NTD | N-terminal domain |
| pA | picoAmpere |
| Pen | penicillin |
| PFA | paraformaldehyde |
| PICK | Protein Interacting with C Kinase 1 |
| PKC | protein kinase C |
| PMT | photomultiplier |
| PSD | postsynaptic density |
| PSD93 | postsynaptic density protein93 |
| PSD95 | postsynaptic density protein95 |
| RE | recycling endosome |
| RFP | red fluorescent protein |
| RNA | ribonucleic acid |
| ROI | regions of interest |
| rpm | round per minute |
| s | second |
| SAP97 | synapse-associated protein 97 |
| SAP102 | synapse-associated protein102 |
| SD | standard deviation |
| SEM | standard error mean |

| | |
|---|---|
| SEP | superecliptic phluorin |
| SNAP25 | Synaptosomal-associated protein 25 |
| SNARE | soluble N-ethylmaleimide-sensitive-factor attachment protein receptor |
| Strep | streptomycin |
| STP | short term plasticity |
| SV | synaptic vesicle |
| SynDig1 | Synapse Differentiation Induced Gene I |
| TARP | transmembrane AMPA receptor regulatory protein |
| TARPγ2 | transmembrane AMPA receptor regulatory proteinγ2 |
| TARPɣ8 | transmembrane AMPA receptor regulatory proteinɣ8 |
| TIRF | total internal reflection fluorescence |
| TfR | transferrin receptor |
| TMD | transmembrane domain |
| TTX | tetrodotoxin |
| U | unit |
| VGCC | voltage gated calcium channel |

# Summary

*α-Amino-3-hydroxy-5-methyl-4-isoxazole propionate* type receptors (AMPARs) are ligand-gated cation channels that reside at glutamatergic synapses throughout the vertebrate central nervous system and play a prominent role in excitatory synaptic transmission. Regulated plasma membrane delivery and reuptake of AMPARs are critical for synaptic receptor accumulation, synaptic homeostasis, and neurotoxicity. While AMPARs are thought to continuously cycle between plasma membrane and intracellular compartments via exocytosis and endocytosis (Ehlers*, 2000; Yudowski et al., 2007), many organizational and regulatory aspects of AMPAR turnover are still unclear to this date. Here, we have analyzed AMPAR dynamics in dendritic and somatic areas of cultured hippocampal neurons in live cell imaging, taking advantage of genetically encoded tags for the visualization of receptors.

To study the membrane delivery of AMPAR from transport organelles, GRIA1 subunits were N-terminally fused with the pH-dependent GFP derivative superecliptic pHluorin, which is quenched in the acidic lumen of transport organelles but regains its full fluorescence in a neutral environment during exocytosis. In a basic characterization of our model system, we show that AMPARs are predominantly (>80% of all events) inserted from recycling endosomes into adjacent plasma membrane areas. Interestingly, AMPAR delivery was associated with fluorescence transients that exhibit considerable variation, ranging from fast flickers to long-lasting events, in accord with previous work (Jullie et al., 2014; Yudowski et al., 2007). These varying signal types likely represent mechanistically different fusion events, with the fluorescence decay frequently reporting reacidification of recycling endosomes after transient membrane merger rather than an actual receptor dispersion on the plasma membrane. To analyze receptor uptake, we employed genetically-encoded self-labelling tags that allow for pulse-chase assays. Using an N-terminal HaloTag-GRIA1 fusion protein, we established an acute staining procedure to label the surface pool of AMPAR in neurons. For this purpose, HaloTag-GRIA1-expressing neurons were incubated with membrane-impermeable fluorescently-labelled ligands for short intervals, resulting in covalent attachment of the fluorophores to the HaloTag domain due to its enzymatic activity. By using fluorescently-labeled synaptic markers, we could specifically follow the progressive uptake of labelled HaloTag-GRIA1 at synaptic as well as extrasynaptic sites.

It has become evident during recent years that native AMPARs are generally associated with auxiliary subunits, which modulate channel function and facilitate forward trafficking from the ER towards the plasma membrane. Two prominent auxiliary subunits, TARPγ8 and

CKAMP44a, have been shown to govern AMPAR function in hippocampal neurons (Khodosevich et al., 2014; Rouach et al., 2005). While auxiliary subunits putatively contribute to the synaptic anchorage of AMPARs via C-terminal interactions with scaffolding proteins, little is known about the influence of these auxiliary subunits on the local dendritic turnover of AMPARs. Here, we have investigated how changes in the abundance of TARPγ8 or CKAMP44a affect the trafficking of AMPAR under basal conditions. For this purpose, we overexpressed each type of auxiliary subunit and investigated AMPAR behavior in live cell imaging experiments. Strikingly, we found that overexpression of TARPγ8 or CKAMP44a did not significantly change surface expression of AMPAR but exerted profound effects on receptor cycling: First, the fusion rate of AMPAR-containing transport organelles with the plasma membrane appeared dramatically reduced when assayed by pHluorin-GRIA1 after overexpression of TARPγ8 or CKAMP44a. This change was accompanied by a reduced pool of AMPAR in recycling endosomes, pointing to an overall reduced recycling of AMPARs. Second, the endocytic reuptake of receptors was significantly reduced in cells overexpressing either auxiliary subunit, as indicated by a decelerated constitutive incorporation of labelled HaloTag-GRIA1-containing receptors under basal conditions. This effect was specific for the extrasynaptic receptor pool, excluding the possibility that enhanced synaptic anchorage of receptors led to an apparent stabilization of the surface receptor pool. A similarly reduced receptor uptake in the presence of the auxiliary subunits was also observed, when endocytosis of AMPARs was directly stimulated by application of insulin, suggesting that the effect on endocytosis is not restricted to constitutive turnover. These novel data indicate that association with auxiliary subunits protects AMPARs from rapid recycling processes, in effect stabilizing the extrasynaptic receptor pool. Noteworthy, TARPγ8 and CKAMP44a exhibit a similar capacity to increase surface lifetime of AMPARs, suggesting that they employ a similar mechanistic avenue to inhibit endocytosis despite belonging to different protein families.

In summary, we provide here new insight into the local dendritic turnover of AMPAR in hippocampal neurons, demonstrating that association of receptors with auxiliary subunits affects their propensity to be rapidly incorporated and recycled. It will be highly interesting to explore how auxiliary subunits mechanistically delay endocytosis in future experiments.

# Zusammenfassung

Glutamat gesteuerte AMPA Rezeptoren (AMPAR, *α-amino-3-hydroxy-5-methyl-4-isoxazole propionate* auf englisch genannt) bilden Kationenkanäle, die sich in glutamatergen Synapsen im zentralen Nervensystem von Wirbeltieren befinden. AMPA Rezeptoren sind hauptsächlich für die schnelle Komponente des postsynaptischen Stroms verantwortlich. Die regulierte Bereitstellung des AMPA Rezeptors auf der Zelloberfläche und die entsprechende Wiederaufnahme in die Zelle sind wichtige Prozessen für die synaptische Akkumulation von Rezeptoren, die synaptische Homöostase und Neurotoxizität. Der regulierte Transport an die Plasmamembran und die Wiederaufnahme des AMPA Rezeptors sind für die synaptische Akkumulation von Rezeptoren, die synaptische Homöostase, und Neurotoxizität entscheidend. Auch wenn grundsätzlich beschrieben ist, dass AMPA Rezeptoren in einem ständigen Zyklus zwischen Plasmamembran und intrazellulärem Bereich durch Exo- und Endozytose wechseln (Ehlers*, 2000; Yudowski et al., 2007), sind viele Fragen über die Dynamik und Regulierung dieses Prozesses ungelöst. Die vorliegende Arbeit beschäftigt sich im wesentlichen mit der Dynamik von AMPA Rezeptoren im dendritischen und somatischen Bereichs von hippokampalen Neuronen der Maus in Kultur. Dazu wurden mit bildgebenden Verfahren (*live cell imaging*) und unter Verwendung genetischer Marker (englisch: *Tag*) die AMPA Rezeptoren visualisiert und ihre Membranrecycling als Zeitverlauf gemessen und analysiert.

Um den Transport der AMPA Rezeptoren (*Glutamate Ionotropic Receptor AMPA subtype1* (*GRIA1)*) in Transportorganellen zu untersuchen, haben wir GRIA1 (Untereinheit des AMAPA Rezeptors) mit pH-abhängigem *Green Fluorescent Protein* (*GFP*), auch *Superecliptic Phluorin* (*SEP*) genannt, N-Terminal fusioniert. *SEP* Fluoreszenz ist im saueren Medium der Transportorganellen unterdrückt, emittiert jedoch zunehmend Licht, wenn der pH Wert des Mediums ansteigt, was während der Exozytose der Fall ist. Es zeigte sich, dass die Mehrheit der AMPA Rezeptoren (>80 %) von *Recycling Endosomes* in nahliegende Abschnitte der Plasmamembran durch Exozytose eingefügt werden. Interessanterweise konnten wir beobachten, dass die Exozytoseereignisse, bestimmt als Fluoreszenzzunahme, sehr variabel sowohl im zeitlichen Verlauf als auch der Intensität der Fluoreszenz waren, was auf verschiedene Fusionstypen hinweist. Auffällig war ein häufig auftretender Fluoreszenzabfall unmittelbar nach Exozytose, den wir als Reazidifizierung nach Endozytose des zuvor exozytierten Vesikels (*recycling Endosome*) interpretieren. Um diese Hypothese zu prüfen, haben wir selbstmarkierende *Tags* für *Pulse-Chase* Experimente kloniert. Mit Hilfe des N-

Terminalien *HaloTag-GRIA1* Fusionsproteins, haben wir eine akute Färbungsprozedur etabliert um den Bestand an Oberflächen- AMPA Rezeptoren in Neuronen zu markieren. *HaloTag-GRIA1* exprimierende Neurone wurden kurzzeitig mit fluoreszierenden Membranimpermeblen Liganden inkubiert. Durch die entstehende kovalente Bindung zwischen *Tag* und Ligand entsteht eine spezifische Färbung. Gleichzeitig wurde ein Fluoreszenz markierter Synapsen-Marker benutzt. So konnte das Schicksal von markiertem *HaloTag-GRIA1* sowohl in den Synapsen als auch im extrasynaptischen Bereich verfolgt werden.

Es hat sich über die letzten Jahre gezeigt, dass native AMPA Rezeptoren generell mit auxiliar (Helfer) Untereinheiten assoziieren, die die Kanal Funktion modulieren und den vorwärts Transport des Proteins vom endoplasmatisches Retikulum zur Plasmamembran fördern. Es wurde gezeigt, dass zwei bekannte auxiliare Untereinheiten, *TARPγ8* und *CKAMP44a*, die Funktion der AMPA Rezeptoren in hippokampalen Neurone modulieren (Khodosevich et al., 2014; Rouach et al., 2005). Anscheinend helfen diese Untereinheiten bei der Verankerung der AMPA Rezeptoren in den Synapsen. Wenig ist hingegen über den Einfluss der Helferuntereinheiten auf das lokale *Recycling* der Rezeptoren bekannt. Deshalb haben wir den Effekt der beiden Helferuntereinheiten auf den Transport der AMPA Rezeptoren bei basale neuronaler Aktivität untersucht. Wir haben die Helferuntereinheiten zu diesem Zweck überexprimiert und das Verhalten der AMPA Rezeptoren mit *Live Imaging* beobachtet. Überraschenderweise war die Oberflächenexpression der AMPA Rezeptoren mit der Überexpression der *TARPγ8* oder *CKAMP44a* nicht verändert, wohingegen das Rezeptor *Recycling* stark beeinflusst war. Erstens war die Fusionsrate von AMPA Rezeptor enthaltenden Transportorganellen mit der Plasmamembran stark verringert. Diese Veränderung war mit einer reduzierten Anzahl von *Recycling Endosomen* verbunden, was ein reduziertes Recycling der AMPA Rezeptoren nahelegt. Zweitens konnten wir beobachten, dass die Endozytose der AMPA Rezeptoren bei Überexpression der Helfer Untereinheiten ebenfalls stark reduziert war, was durch die verlangsamte Internalisierung der *HaloTag-GRIA1* unter basale Bedingungen gezeigt werden konnte. Die Effekte der Helferuntereinheiten waren auf die extrasynaptischen Bereiche beschränkt, was synapsenspezifische Effekte, wie eine stärkere Verankerung der AMPA-Rezeptoren, als Ursache des reduzierten *Recyclings* ausschließt. Die Helferuntereinheiten entfalteten ihre Effekte nicht nur bei basaler neuronaler Aktivität. Bei Stimulation mit Insulin trat die gleiche inhibitorische Wirkung auf das *Recycling* von AMPA Rezeptoren auf, was dafür spricht, dass Helferuntereinheiten eine Rolle in aktivitätsabhängiger als auch in konstitutiven Endozytose spielen. Unsere Ergebnisse sprechen dafür, dass die Assoziierung von auxiliar Untereinheiten die AMPA Rezeptoren vor einer schnellen

Endozytose schützen, um auf diese Weise das extrasynaptische Rezeptorenangebot zu stabilisieren. Obwohl *TARPγ8* und *CKAMP44a* zu zwei verschiedene Proteinfamilien gehören, zeigen sie eine vergleichbare Fähigkeit die Lebensdauer der AMPA Rezeptoren auf der neuronalen Oberfläche zu vergrößern.

Zusammenfassend lässt sich sagen, dass wir einen Einblick in das lokale *Recycling* von AMPA Rezeptoren in den Dendriten der hippokampalen Neurone gewonnen haben. Wir konnten zeigen, dass mit Hilfe der auxiliar Untereinheiten das *Recycling* von AMPA Rezeptoren verlangsamt wird. In der Zukunft wird es sehr interessant sein, die Mechanismen, die hinter der verzögerten Endozytose von AMPA Rezeptor liegen zu entschlüsseln.

# 1. Introduction

## 1.1 General background

The last two centuries have brought an enormous revolution in the study of brain function, greatly expanding our knowledge of molecular neurophysiology. The brain is probably the most complex matter in the universe. Cajal showed that a brain is composed of distinct neurons, a realization that initiated the birth of modern neuroscience (Cajal, 1899, 1904). It has been estimated that the human brain contains around 105 billion neurons that interact with each other in an organized way (Andersen et al., 1992). Nerve cells communicate with each other and organize in functional circuits that enable motor behaviors, such as walking, but also more complex actions like cognition, learning, and memory. The basic concept of localized brain function originated nearly two centuries ago by the German neuroanatomist Franz Joseph Gall (1758-1828). Neurons coordinate and communicate through highly specialized connections known as synapses (Foster and Sherrington, 1887). A chemical synapse is a complex structure that conveys information between neurons by transient conversion of electrical activity into chemical signals. A chemical synapse consists of a presynaptic and a postsynaptic specialization, where the latter contains receptors that receive the output message of the former as a released chemical substance called neurotransmitter (glutamate, GABA, dopamine etc.) (Otto Loewi, 1921; and John Eccles, 1951). Furthermore, it has been realized that correlated neuronal activity in neuronal network may affect the strength of synaptic connections and thus define functional circuits, as experimentally supported by the phenomenon of synaptic plasticity (Bliss and Lomo, 1973) and theoretically predicted by the Canadian neuroscientist Donald Hebb in 1940. One of the determinants of synaptic identity, in addition to neuronal strength, is the composition of receptors that reside on the postsynaptic site. Glutamate receptors represent the majority throughout the mammalian brain and are responsible for the main excitatory neurotransmission (Monaghan et al., 1989). Glutamate receptors are part of a protein complex that belongs to the postsynaptic density (*PSD*) protein family. Trafficking of glutamate receptors to the postsynaptic membrane involves members of the PSD protein family. I am studying in my thesis the turnover of glutamate receptors [Glutamate receptor 3ionotropic AMPA type subunit (GRIA) 1-containing receptors] to the postsynaptic membrane and the involvement of underlying PSD auxiliary proteins.

## 1.2 Glutamate receptors

Glutamate receptors are predominantly found in the central nervous system of vertebrates, but are also located at neuromuscular junctions in invertebrates. They are present in neuronal and non-neuronal cells and mediate the most excitatory neurotransmission. Glutamate receptors have been divided into two principle families, ionotropic glutamate receptors "iGluR" and metabotropic glutamate receptors "mGluR". Ionotropic glutamate receptors are ligand-gated ion channels permeable to cations, and metabotropic glutamate receptors are G-protein coupled receptors that get activated upon glutamate binding (Collingridge and Lester, 1989; Curtis et al., 1960; Sugiyama et al., 1987).

Metabotropic glutamate receptors are membrane proteins with seven transmembrane spanning domains which activate a downstream signaling through the G-protein subunits upon glutamate binding. They have eight isoforms that are divided into three classes according to their amino acid sequence, signal transduction, and channel pharmacology (Nakanishi, 1994). Class I receptors are adenylyl cyclase activator whereas class II and class III are inhibitors of adenylyl cyclase machinery (Cartmell and Schoepp, 2000) (**Table 1**). They have a broad range of electrophysiological effects, and are mainly involved in the inhibition of voltage gated calcium and potassium channels although activation of non-selective cationic channels may also occur (Anwyl, 1999). Mammalian ionotropic glutamate receptors are encoded by 18 genes, and are divided according to their pharmacology and physiology into three subtypes: α-amino-3-hydroxy-5-methyl-4-isoxazole propionate (AMPA) receptors, N-methyl-D-aspartate (NMDA) receptors, and kainate (KA) receptors. Each subtype constitutes several subunits where AMPARs include GRIA1-4, NMDARs include GRIN1, GRIN2A-D, and GRIN3A-B, and KARs include GRIK1-5 (**Table 1**). Initially glutamate receptors were known as NMDARs and non-NMDARs according to their kinetic and pharmacological properties. Although all three subtypes bind glutamate neurotransmitter, their permeability to calcium ($Ca^{2+}$) is different. However, sodium ($Na^{+}$) and potassium ($K^{+}$) permeability is quite similar among subtypes (**Figure 1)** (Dingledine et al., 1999). Different subunits of the same subtype can assemble and form

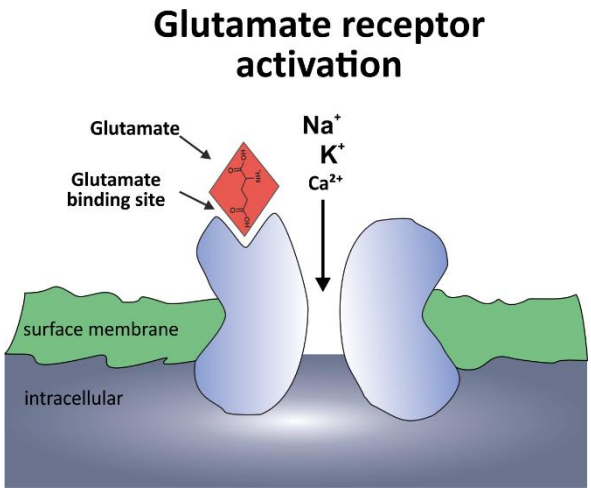


**Figure 1. Glutamate receptor activated by glutamate neurotransmitter**

various conformations. Functional NMDARs assemble as GRIN1 dimer with either GRIN2 or GRIN3 dimers (Monyer et al., 1992). NMDARs are calcium permeable channels that are primarily blocked by magnesium ($Mg^{2+}$) ions. In addition, activation of NMDARs requires the binding of glycine and glutamate molecules. GRIN1 and GRIN3 contain the glycine binding sites, and GRIN2 contains a glutamate binding site (Furukawa et al., 2005; Johnson and Ascher, 1987; Yao et al., 2008). Knowing that more than two subtypes can assemble to form a channel, ionic conductance is dependent on the different subunit make up (Traynelis et al., 2010). It is well known that NMDAR channels are the main initiators of neuronal plasticity, which is an increased synaptic activity producing short and long-term potentiation (STP and LTP, respectively). Synaptic potentiation may last for hours where AMPAR recruitment to the site of activation is critical for such plastic changes. LTP is divided into three phases known as LTP1 (early-LTP phase), LTP2 (late-LTP phase), and LTP3 phase that involves transcription. All synaptic potentiation require NMDARs; however, each phase is dependent on different subunit assembly (Benke et al., 1998; Bliss and Collingridge, 1993; Collingridge et al., 1983; Reymann and Frey, 2007; Volianskis et al., 2013).

| ***Ionotropic receptor*** | | | ***Metabotropic receptor*** | | |
|---|---|---|---|---|---|
| **AMPA** | **NMDA** | **Kainate** | **Class I** | **Class II** | **Class III** |
| GRIA1 | GRIN1 | GRIK5 | GRM1 | GRM2 | GRM4 |
| GRIA2 | GRIN2A | GRIK6 | GRM5 | GRM3 | GRM6 |
| GRIA3 | GRIN2B | GRIK7 | | | GRM7 |
| GRIA4 | GRIN2C | GRIK1 | | | GRM8 |
| | GRIN2D | GRIK2 | | | |
| | GRIN3A | | | | |

**Table 1.** Classification of glutamate receptors

Unlike NMDARs, KARs and AMPARs share structural similarities that renders them sensitive to both kainate and AMPA; however, their functional role is distinct. KARs activate downstream second messengers, and mediate currents as AMPARs do. Plenty of evidences show that KARs are ubiquitous and present on the pre- and postsynaptic sites of neurons (Rodriguez-Moreno et al., 1997). KARs assemble as homomers or heteromers from GRIK1, GRIK2, and GRIK3 subunit, and GRIK1, GRIK2, and GRIK3 can form heteromers with GRIK4 or GRIK5 subunits. Similar to AMPARs, KARs are non-selective cationic channels with moderate permeability to calcium ions, but they have a slower kinetic decay and rise time than AMPARs (Lerma, 2006; Perrais et al., 2010). However, kainate receptors, like NMDARs and AMPARs, may also play a role in synaptic plasticity (Rebola et al., 2007). Kinetic

properties and subunit assembly of AMPARs will be detailed in the next paragraph. Generally, glutamate receptors play different roles according to their sites of expression in the brain, spinal cord, retina, and even in the peripheral nervous system (Curtis and Watkins, 1960; Davidson and Carlton, 1998). A consequence of dysfunction of any of these receptors, leads to various neurodegenerative diseases like epilepsy, Alzheimer's and Parkinson's diseases, or psychiatric disorders like schizophrenia or depression, may arise (Johnson et al., 2009; Mattson et al., 1992; Russo et al., 2013). Glutamate receptors met the interest of many researchers in the field of neuroscience due to their importance in memory and learning. The property of information storage has been strongly attributed to synaptic plasticity and potentiation, even though it is not fully understood (Bliss and Lomo, 1973; Harvey and Svoboda, 2007; Shaib et al., 2018). Trafficking of glutamate receptors to and from synaptic membranes and changing synaptic activity plays a crucial role in the process of potentiation in addition to their important roles at normal homeostatic activity. Glutamate receptor synaptic targeting and trafficking is a tightly controlled process which underlying mechanisms still need to be clarified.

## 1.3 AMPA receptors

AMPA receptors (AMPARs), also known as *"Quisqualate"* receptors, mediate predominantly fast excitatory neurotransmission. As mentioned previously, AMPARs include four different subunits GRIA1, 2, 3, and 4 with GRIA1 and 2 being most abundant. AMPAR, as well as KAR and NMDAR, have a quaternary structure that consists of four large subunits forming ligand gated ion channels. Tetrameric complexes of AMPARs are made of dimers of dimers with either identical or different subunits and form homomers or heteromers, respectively (Safferling et al., 2001; Sobolevsky et al., 2009). This complex assembly of different subunits adds structural as well as functional diversity to the signaling machinery of the synapse. The type of subunit assembly determines the distinct biophysical properties as well as the conductivity of the channel (Gan et al., 2015), which will be detailed next. Moreover, subunit composition and recruitment of AMPARs is changed according to the synaptic activity (Wang et al., 2012). Out of the three iGluR subtypes, AMPARs are known for their highly dynamic trafficking to and from synapses (Benke et al., 1998).

The different AMPA receptor subunits have similar size of around 900 amino acids and share 68-73% sequence similarity (Hollmann and Heinemann, 1994). An AMPAR subunit consists of four distinct domains having a structure similar to other ligand-gated ion channels

like ɣ-amino butyric acid receptors (GABAR), however; a GABAR has four real transmembrane domains unlike AMPARs (Olsen and Sieghart, 2008). Each AMPAR subunit contains an extracellular N-terminal domain (NTD), also known as an amino-terminal domain (ATD), an extracellular ligand-binding domain (LBD), a membrane spanning transmembrane domain (TMD), and a C-terminal domain (CTD) in the cytoplasmic region. The major variation among the four subunits lies in the cytoplasmic region of AMPARs. The extracellular domain, on the other hand, represents the biggest part of the receptor (**Figure 2**). Within the extracellular part, the N-terminal region has been recently shown to play an important role in AMPAR subunit assembly and receptor anchorage at synapses (Jin et al., 2009; Watson et al., 2017). Large parts of the extracellular region also contribute to the ligand-binding domain (LBD) of the receptor, which is essential for binding of glutamate and the induction of the conformational changes leading to channel opening. The polypeptide chain of all GRIA subunits contains four membrane-embedded sections (M1, M2, M3, and M4), with M2 not forming a regular transmembrane domain (TMD) but establishing a re-entrant loop that does not pass through the membrane. The LBD is assembled out of a segment of the N-terminal subunit loop (S1) and a segment of the extracellular loop connecting M3 and M4 (S2) (**Figure 3**) (Armstrong and Gouaux, 2000; Wo and Oswald, 1995). The membrane-spanning regions M1, M3, and M4 of all subunits within a tetramer arrange into a channel structure in the lipid bilayer, which is lined by the M2 loop at its inner core. The C-terminal domain has a variable sequence and length

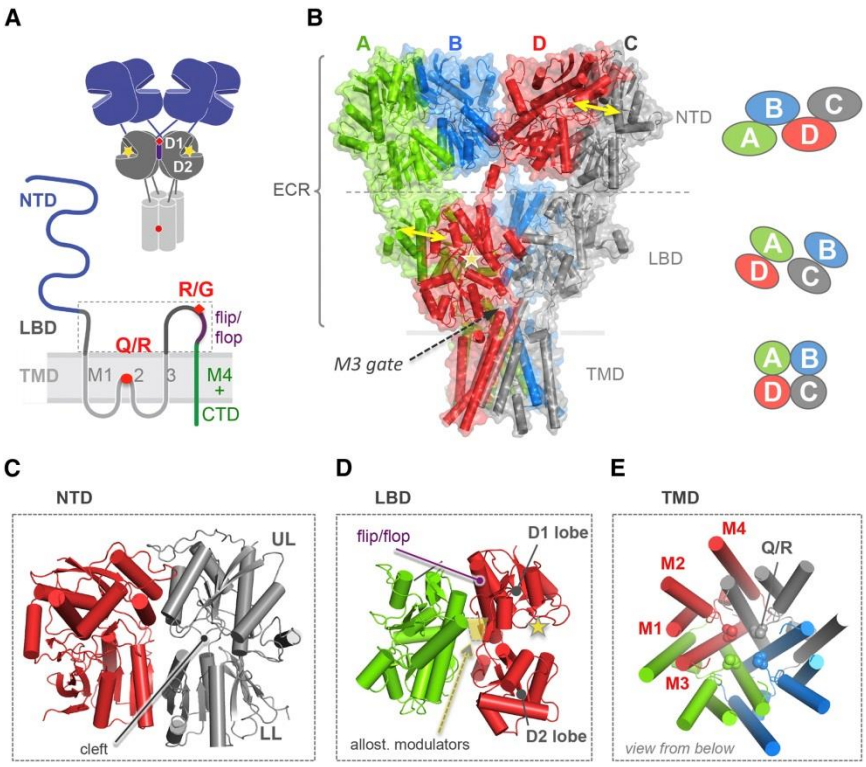


**Figure 2. Three-dimensional structure of AMPAR tetramer and its different domains**
(**A**) Schematic drawing of AMPAR tetramer with its D1 and D2 ligand-binding domain (upper), and a membrane AMPAR structure in a with its different domains (lower). (**B**) Organization of domains in an AMPAR tetramer in a three dimensional structure (NTD: N-terminal domain, LBD: ligand binding domain, TMD: transmembrane domain). (**C-E**) Association of AMPAR dimers in the NTD (UL: upper lobe, LL: lower lobe), in the LBD, and in the TMD. (Greger et al., 2017)

among the four subunits, which has been shown to play significant roles in AMPAR trafficking, stabilization at synapses, and channel gating. This domain has various binding sites for intracellular proteins some of which are scaffold proteins that phosphorylate/dephosphorylate amino acid residues upon different signal transduction pathways. Extensive studies have shown that Protein Kinase A (PKA) and calcium/calmodulin (CaM)-dependent protein kinase II (CaMKII) phosphorylate the C-terminal domain at Ser845 and Ser831 amino acid residues, respectively, and enhance synaptic plasticity. Phosphorylation of Ser845 by PKA has shown to increase the open probability of homomeric GRIA1 channels, and to be involved in AMPAR surface trafficking (Banke et al., 2000; Esteban et al., 2003; Hosokawa et al., 2015; Lee et al., 2003; Roche et al., 1996). Phosphorylation of Ser831 by CaMKII also increases channel conductance of homomeric GRIA1 receptors by enhancing the open probability (Derkach et al., 1999).

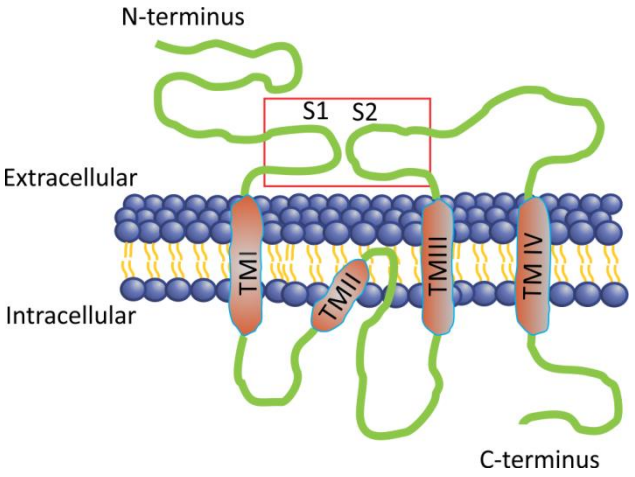


**Figure 3. Association of S1 and S2 domains in an AMPAR subunit in the plasma membrane**
Extracellular S1 and S2 associate to form the ligand-binding domain of the receptor.

Furthermore, it has been shown that transmembrane proteins form complexes with AMPARs and play crucial roles in their trafficking, membrane targeting and stabilization although it is not fully clear how this regulation occurs (Boehm et al., 2006; Granger et al., 2013). The role of transmembrane proteins will be expanded later. Native hippocampal AMPARs primarily (~ 80%) consist of GRIA1/GRIA2 heteromers, with the residual population being made up by GRIA2/GRIA3 heteromers. Hippocampal pyramidal neurons express GRIA4 only predominantly in early developmental stages (Zhu et al., 2000). In addition, all surface receptors on the post-synapse contain a GRIA2 subunit (Lu et al., 2009). AMPARs are cationic channels mainly permeable to sodium ($Na^+$) and potassium ($K^+$) ions (Boulter et al., 1990), and to a lesser extend to calcium ($Ca^{2+}$) ion (**Figure 4**). The presence of GRIA2 subunits in a receptor complex

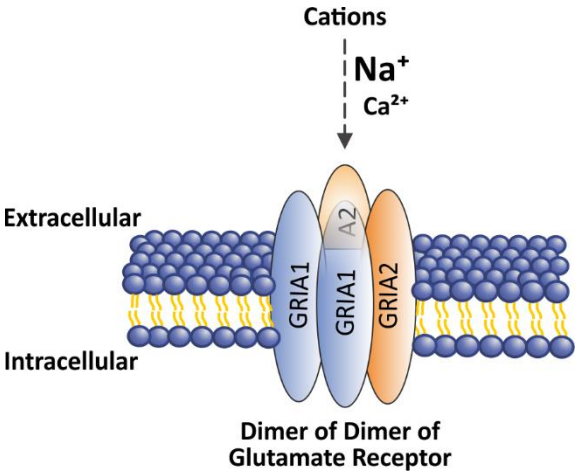


**Figure 4. Ion permeability of AMPAR channel**
Heterotetramers of AMPARs containing GRIA2 subunit have low permeability to calcium ions.

critically determines the calcium permeability of a channel. GRIA2 are calcium impermeables, and they gain this specificity during RNA editing. RNA editing is especially prominent in the M2 transmembrane domain of GRIA2, where the RNA modification causes a glutamine → arginine substitution (Q/R editing) (Sommer et al., 1991). It has been shown that mice lacking Q/R editing suffered from epileptic seizures and died early after birth (Brusa et al., 1995). AMPAR channels containing the GRIA2 subunit, which is the case for the majority of hippocampal pyramidal neurons, are $Ca^{2+}$ impermeable (CI-AMPAR), and AMPARs lacking GRIA2 are $Ca^{2+}$ permeable (CP-AMPAR). Calcium permeable AMPAR channels constitute a minority, yet play an important role in the activity of synapses in neurons (Toth and McBain, 1998).

## 1.4 AMPA receptor assembly and exit from ER

Transcription of the messenger RNAs (mRNAs) for AMPAR subunits is largely limited to neurons and some glial cells. Interestingly, mRNA editing plays an important role in subsequent receptor complex formation and targeting (Greger et al., 2002). It has been also shown that mRNA is abundant in dendrites and at synaptic sites to ensure “on site” protein synthesis (Grooms et al., 2006). AMPA receptor trafficking starts after protein synthesis with the maturation of the subunits and receptor assembly in the endoplasmic reticulum (ER). Identical subunits emerging from polyribosomes first form homodimers due to high affinity of their NTDs (Herguedas et al., 2016). A subsequent assembly of different dimers (dimer of dimers) leads to the formation of tetrameric complexes, involving interactions of all subunit domains (Sobolevsky et al., 2009). A proper assembly and conformational topology of the subunits trigger a signal for AMPARs to leave the ER for their subcellular destination. Dimers that fail to associate with their corresponding partners in heterotetramers accumulate in the ER and cannot be exported (Coleman et al., 2006). It has also been shown that glycosylation of the first part of an AMPAR N-terminus is important for ER export to the Golgi apparatus and for their further transport (Greger et al., 2002).

The export of AMPAR from the ER has been well studied, and several critical factors have been identified. Two important ER chaperons, immunoglobulin-binding protein (BiP) and calnexin, have been shown to play a role in AMPAR folding and ER retention (Rubio and Wenthold, 1999). Auxiliary proteins, some of which will be discussed in detail later, have also been shown to contribute to ER sorting, export, and even AMPAR folding and assembly.

Auxiliary proteins include transmembrane AMPA receptor regulatory proteins (TARPs) like TARPγ2, γ3, γ4, and γ8, and cornichons. TARPs, cornichons, synapse-associated protein 97 (SAP97), in addition to other receptor interacting proteins bind AMPARs either directly or indirectly and regulate their modification and exit from the ER compartment (Brockie et al., 2013; Leonard et al., 1998; Vandenberghe et al., 2005). It has also been shown that TARPγ2 binds at the C-terminal of nPIST (neuronal isoform of protein interacting specifically with TC10), a protein enriched in the Golgi apparatus, and facilitates AMPAR exit from the Golgi network. It is still unclear how these different proteins regulate AMPAR transport from the ER, but impairing these interacting proteins dramatically increased ER retention and diminished surface expression. Taking for example TARPγ8, its impairment causes an increased retention of AMPARs in the ER and Golgi network of hippocampal neurons (Rouach et al., 2005).

## 1.5 AMPAR trafficking

The recruitment of AMPARs to postsynaptic sites is dynamically regulated and requires a network of intricate protein interactions (Anggono and Huganir, 2012; Greger et al., 2017; Kessels and Malinow, 2009; Luscher et al., 1999). AMPARs are enriched in the postsynaptic structure, but their synaptic residence depends on a continuous recruitment of "new" receptors to compensate for the ongoing loss of receptors due to a high turn over rate (Heine et al., 2008). Interestingly, postsynaptic aggregation and/or liberation of receptors are believed to be subject to activity-dependent regulation during synaptic plasticity (Bredt and Nicoll, 2003). Local exocytosis and endocytosis near spines as well as lateral diffusion represent the key mechanisms determining AMPAR trafficking at synapses. According to current ideas, these processes are under precise regulation by AMPAR interacting proteins and auxiliary subunits: One of the first identified binding partners of AMPAR were scaffolding proteins containing PDZ (PSD-95/Discs-large/ZO-1) domains. PDZ domains constitute

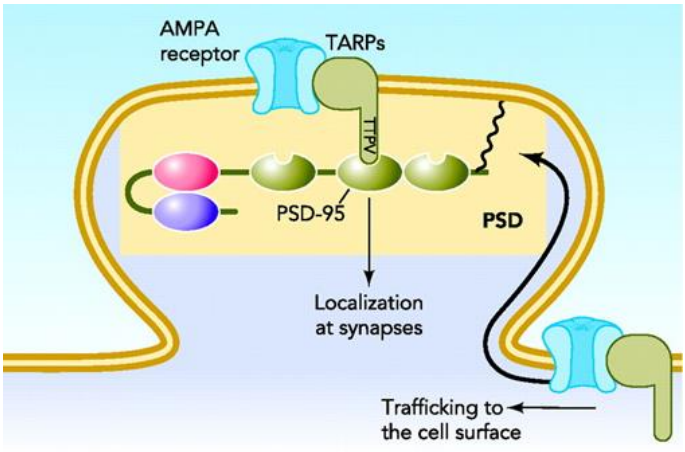


**Figure 5. AMPAR stabilization by PSD95 protein**
Schematic figure showing AMPAR/TARP complex stabilized by PSD95 protein in the synaptic membrane after trafficking of the complex to the synapse. (Tomita, 2010)

common interaction domains of 80 to 90 amino acid residues, which recognize short (up to 7 aa) C-terminal PDZ-binding motifs and may be categorized in several classes due to specificity (Tonikian et al., 2008). As PDZ domains are frequently found in multiple copies within structural proteins, they are able to form large protein complexes (Doyle et al., 1996). Membrane-associated guanylate kinases (MAGUK) represent a prominent PDZ protein family, which includes several members that are found at postsynaptic sites and interact with glutamate receptors. In particular, PSD95 (post-synaptic density protein 95), PSD93 (post-synaptic density protein93), SAP102 (synapse-associated protein102), and SAP97 (synapse-associated protein97) have been proposed to interact with the C-termini of glutamate receptor subunits (El-Husseini et al., 2000; Leonard et al., 1998; Muller et al., 1996; Parker et al., 2004). The MAGUK PSD-95 is among the most abundant proteins in the postsynaptic density (Chen et al., 2005) and possesses three PDZ domains apart from a non-functional guanylate-kinase domain (Tavares et al., 2001). Electron microscopic tomography showed a clear reduction in clustering of PSD proteins when PSD93, PSD95, and SAP102 were knocked down, in line with a role of these MAGUKs in organizing glutamate receptors in the PSD (Chen et al., 2015). Interestingly, none of the MAGUKs in the PSD -except SAP97- were found to directly interact with AMPA subunits. SAP97, however, interacts with the PDZ-binding at the C-terminus of GRIA1 subunit and is thought to chaperon it from the endoplasmic reticulum for actin based trafficking (Wu et al., 2002). PSD95, PSD93, and SAP102 bind AMPARs indirectly through auxiliary subunits like members of the transmembrane AMPA receptor regulatory protein (TARP) family. TARP proteins also have a PDZ binding motif and can bind to PSD95 as an intermediate between AMPARs and PSD95 (Chen et al., 2000) (**Figure 5**).

Other PDZ-containing proteins include glutamate receptor-interacting protein (GRIP)/AMPAR binding protein (ABP), and Protein Interacting with C Kinase1 (PICK1) that bind to GRIA2 and GRIA3 subunits at their C-terminal domain and regulate their expression at the synapse (Dong et al., 1997; Xia et al., 1999). Two homologous GRIP isoforms exist, GRIP1 and GRIP2 that are differentially expressed in the different developmental stages of the rat brain. GRIP1 is expressed in earlier stages of the embryonic development whereas GRIP2 is expressed in later stages (Dong et al., 1999). The later identified ABP has been identified as a shorter splice variant of GRIP2. Moreover, GRIP1, GRIP2, and ABP have been found to form homo and heterodimers (Srivastava et al., 1998). Unlike the MAGUK family, GRIP/ABP have seven PDZ domains, and bind GRIA2 and GRIA3 through the fourth and fifth PDZ motif although GRIA subunits do not have PDZ binding domains. GRIP/ABP complex targets and stabilizes AMPARs at a synapse and is involved in synaptic formation upon increased

expression of GRIA2 subunit (Dong et al., 1999). GRIP/ABP play a role in synaptic up scaling as well, where the complex counteracts synaptic deprivation by increasing synaptic AMPARs and enhances synaptic activity (Gainey et al., 2015). On the other hand, PDZ-containing PICK1 protein has only one PDZ motif and also binds GRIA2 and GRIA3 at their C-terminal domains (Xia et al., 1999). However, unlike GRIP/ABP, PICK1 direct interaction to GRIA2 leads to long term depression (LTD) (Kim et al., 2001). PICK1 competes with GRIP/ABP to internalize AMPARs from the synapse. Calcium increase and activated Protein kinase C (PKC) promote the dissociation of GRIP1 and N-ethylmaleimide-sensitive factor (NSF) from GRIA2, and on the other hand increased binding of PICK1 and β-SNAP (vesicle fusion protein) lead to the internalization of membrane AMPARs (Hanley and Henley, 2005; Hanley et al., 2002). Other types of proteins have been identified that bind AMPARs and regulate their clustering at synapses. Neuronal activity-regulated pentraxin (NARP) and neuronal pentraxin1 (NP1) are known to interact with all AMPAR subunits and involved in AMPAR recruitment and synapse formation. However, NARP and NP1 do not contain PDZ domains; and NARP was the first identified protein that binds the AMPARs at their N-terminal domains (O'Brien et al., 1999). Non-PDZ domain containing proteins also include the prominent AMPAR auxiliary proteins that are being heavily studied and investigated due to their crucial roles in AMPAR trafficking and regulation.

## 1.6 Exocytosis and membrane insertion of AMPARs

AMPA receptors subunits are synthesized by ribosomes at the endoplasmic reticulum (ER), wherein they assemble into functional tetramers before being transported to the Golgi network for further modification (Hanus and Ehlers, 2008). In dendrites, local synthesis of AMPAR subunits has been reported to occur at zones of increased ER complexity near dendritic branch points, which also frequently house Golgi-like outposts (Horton and Ehlers, 2003), thus allowing the local transition of the assembled receptors into the secretory pathway and delivery to the plasma membrane in the direct vicinity (Cui-Wang et al., 2012). Noteworthy, recent work also suggested that glutamate receptors may alternatively transit from the *ER-Golgi intermediate compartments* (*ERGIC*) to recycling endosomes (RE), thus bypassing the canonic pathway via Golgi-compartments (Bowen et al., 2017). In this scenario, ERGIC and RE would together form a satellite secretory compartment in most parts of the dendrites, while stack-like GM-130-positive Golgi outposts are mostly restricted to dendritic

shafts (Hanus and Ehlers, 2008; Horton et al., 2005; Pierce et al., 2001). Following the canonic pathway, glutamate receptors enter the Golgi apparatus in the soma, undergo sorting in the *trans*-Golgi-network, and head for the plasma membrane in transport organelles. There is evidence that exocytosis of the transport vesicles delivers AMPARs to extrasynaptic regions on the plasma membrane (Adesnik et al., 2005; Araki et al., 2010; Lin et al., 2009), to dendritic shafts near spines (Makino and Malinow, 2009; Yudowski et al., 2007), or directly in spines close to postsynaptic structures (Gerges et al., 2006; Kennedy et al., 2010) possibly at syntaxin-4-positive exocytotic zones. AMPARs at extrasynaptic sites laterally diffuse on the surface of the cell, which allows for their dynamic capture at synaptic sites, resulting in a recruitment of AMPARs to the postsynaptic density (Ashby et al., 2006; Makino and Malinow, 2009; Rosendale et al., 2017). Recent receptor tracking experiments suggest that synaptic receptor accumulation is at least in part due to activity-dependent diffusional trapping of receptors (Ehlers et al., 2007).

AMPARs are subject to a constant turnover cycle, wherein some receptors are degraded and others are transported to dendritic recycling endosomes for reuse (Ehlers*, 2000). Interestingly, it has been shown that receptors in this resting intracellular pool can be rapidly shuttled to the plasma membrane in an activity-dependent manner, which is essential for different forms of synaptic plasticity including long-term potentiation (Park et al., 2004). The frequency of exocytotic receptor delivery depends on the subunit composition of the AMPAR cargo, with GRIA1-containing receptors being inserted in activity-dependent fashion (Araki et al., 2010; Makino and Malinow, 2009; Passafaro et al., 2001). Specific interactions of the different AMPAR subunits via their C-terminal tails may account for the different behavior in receptor turnover. In particular, it has been shown that NSF binding to GRIA2 is important for efficient insertion of new AMAPRs into the plasma membrane (Araki et al., 2010). Moreover, phosphorylation of serine 816 (S816) and S818 residues on GRIA1 C-terminal tail by PKC enhance the binding of 4.1N protein that mediates activity dependent GRIA1 membrane insertion. In addition, impaired 4.1N protein decreases long term potentiation as a result of reduced AMPAR surface expression (Lin et al., 2009). Live Cell imaging using fluorescently labeled GRIA subunits revealed the existence of two kinetic categories for AMPAR insertion events (Jullie et al., 2014; Yudowski et al., 2007). On the one hand, ‘transient’ or ‘short burst’ fluorescence signals were observed, wherein fluorescently-labeled receptors remain for ~ 1 s or less within a small membrane area before rapidly dispersing on the surface. In the second group, fluorescently labelled receptors appeared to rest for roughly 5-10 s at the insertion site, resulting in a ‘persistent’ or ‘long display’ event. Interestingly, it has been shown that

fluorescently-marked transferrin receptors (TfR) exhibit a similar behavior to tagged AMPARs, indicating that the different event types may reflect different fusion modes of recycling endosomes (Jullie et al., 2014). Still, the specific type of cargo clearly influences the fusion kinetics, as different cognate 7-TM receptors exhibited 'long display' events with different frequency (Jullie et al., 2014; Yu et al., 2010) analyzed fusion pore dynamics during 'persistent display' events by application of a (low pH) quencher solution testing access to the pHluorin-tagged cargo in the vesicular lumen. Interestingly, this delivered evidence that 'long display' events primarily represent kiss-and-run fusion of the recycling endosome, in which the fluorescence decay reports re-acidification of the resealed organelles rather than cargo dispersion on the plasma membrane. In agreement with this conclusion, another study recently demonstrated that bafilomycin-treatment, which prevents the re-acidification of vesicles, indeed altered the decay kinetics of 'persistent' events (Roman-Vendrell et al., 2014).

## 1.7 Endocytosis of AMPARs

Endocytosis is the first step of recycling where AMPARs are internalized and sorted afterwards into different organelles (Glebov et al., 2015). Intracellular sorting of AMPARs is quite dependent on the way the receptors are endocytosed in neurons (Hausser and Schlett, 2017; Parkinson and Hanley, 2018). The classical mode of receptor endocytosis is clathrin-dependent requiring the action of the clathrin adaptor protein 2 (AP2) and the GTPase dynamin. AMPARs destined to be endocytosed associate with AP2, and clathrin coated pits with the help of dynamin mediate the membrane invagination and pinching off of vesicular organelles containing the receptors (Carroll et al., 1999; Cosker and Segal, 2014; Mukherjee et al., 1997). Clathrin-dependent endocytosis of AMPARs is activity dependent and is up regulated during long-term depression (LTD) (Ashby et al., 2004; Man et al., 2000). It has been shown that insulin treatment of CA1 hippocampal neurons induced clathrin dependent GRIA2 internalization. Insulin exists in the CNS, and neurons exhibit insulin receptors that regulate neuronal activity by inducing LTD upon increased AMPAR insertion (Man et al., 2000). When internalized, AMPAR organelles are uncoated via Rab5 protein and driven towards the early endosome (EE) (Brown et al., 2005). In addition, Rab5 bound organelles bind EE antigen 1 (EEA1) that associates phosphatidylinositol-3-phosphate (PI3P) and facilitate the fusion of endocytic vesicle into EE (Gaullier et al., 2000; Murray et al., 2016). Early endosomes continue either towards becoming recycling endosomes (RE) (van der Sluijs

and Hoogenraad, 2011) via Rab11 or towards late endosome (LE) via Rab7 and end up in lysosomal compartments (Hu et al., 2015; Parkinson and Hanley, 2018). Receptors destined to be recycled back to the synaptic surface are packaged in recycling endosomes (RE) that fuse again with the membrane upon signaling and LTP (Park et al., 2004; Parkinson and Hanley, 2018). Upon LTD, AMPAR intracellular retention increases and is directed towards degradation through the lysosomal pathway (Fernandez-Monreal et al., 2012). On the other hand, AMPAR constitutive trafficking and homeostatic downscaling are thought to be mediated by clathrin-independent endocytosis (Glebov et al., 2015). Experiments have shown that alteration of F-actin protein disrupts endocytosis under basal activity, and suggested that F-actin and Rac1 proteins are required for clathrin-independent endocytosis (Glebov et al., 2015). Unlike clathrin-dependent endocytosis, clathrin-independent requires Rab4, Rab7, and Rab11 for the sorting, late, and recycling endosomes, respectively (Gu et al., 2016b; Hausser and Schlett, 2017). Not only Rab11, but also Rab4 can target AMPARs, precisely GRIA2, towards the surface membrane (Gu et al., 2016b). It is not clear whether AMPARs are endocytosed in spines, or migrate through lateral diffusion to extrasynaptic sites and then get endocytosed although most evidences are in favor of AMPAR internalization at the extrasynaptic site (Ashby et al., 2004; Luscher et al., 1999; Petrini et al., 2009). Since AMPARs are stabilized by interaction with PSD scaffolding proteins of the MAGUK family

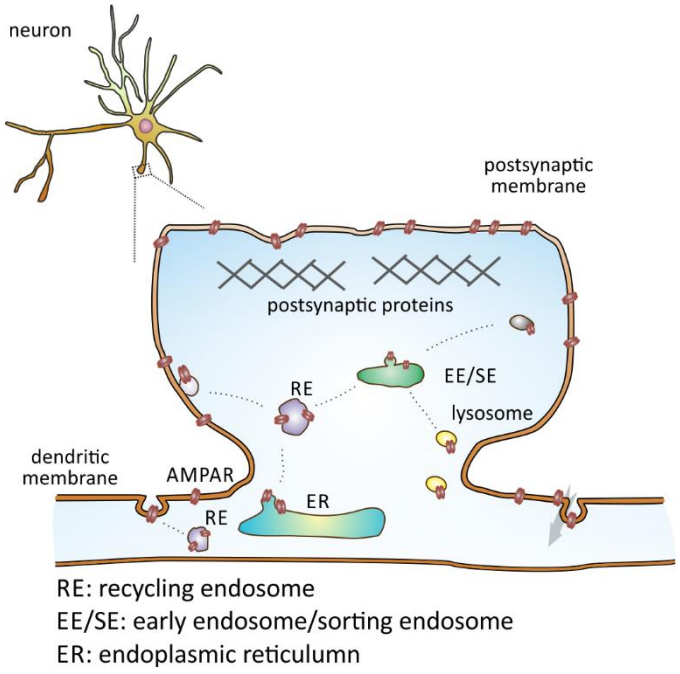


**Figure 6. Endocytosis and exocytosis of AMPARs at the postsynaptic membrane**
AMPARs are synthesized in the endoplasmic reticulum (ER) and transported to the surface membrane through recycling endosomes (REs). AMPARs are internalized in early endosomes (EEs) through endocytosis to be recycled back in REs or become degraded in lysosomes.

like PSD95 at synaptic sites (Chen et al., 2015; Daw et al., 2000), it is likely that endocytosis occurs in extrasynaptic regions as it was stated before (Ashby et al., 2004). AMPARs in extrasynaptic site, unlike synaptic sites, are highly mobile and diffusive (Ashby et al., 2004; Borgdorff and Choquet, 2002). Yet, another active region, termed the endocytic zone (EZ), has been defined to contain mobile AMPARs and is responsible for endocytosis as well (Petrini et al., 2009). EZs are positioned near the postsynaptic density region of neurons. It has been suggested that receptors diffuse from the PSD domain once released from PSD proteins, like auxiliary subunits and PSD95, and move to the EZ for endocytosis. AMPARs endocytosed from EZs are thought to be recycled back to the synaptic region when needed (**Figure 6**) (Blanpied et al., 2002; Petrini et al., 2009).

## 1.8 AMPAR auxiliary subunits

The subunit composition critically determines the functional properties of AMPARs. However, the "opening and closing"-kinetics of AMPAR channels is additionally modulated by a variety of associated cytosolic/ transmembrane proteins. Binding of these factors to AMPARs in many cases also regulate their initial export from the ER and transport to the plasma membrane (Schwenk et al., 2012). AMPAR binding proteins may either transiently interact or tightly bind to an AMPAR. Core interacting proteins that stay bound to AMPARs have been called AMPAR auxiliary subunits. The most prominent auxiliary subunits identified to play crucial roles in AMPAR regulation in mammalian brains include TARP (Transmembrane AMPA receptor regulatory proteins) family (Tomita et al., 2003), CKAMP (Cystine-Knot AMPAR modulating proteins) family (von Engelhardt et al., 2010), CNIH (cornichon) family (Schwenk et al., 2009), a recently identified protein called GSG1L (Germ Cell-Specific Gene 1-Like) (Shanks et al., 2012), and SynDIG1 (Synapse Differentiation Induced Gene I) (Diaz, 2010) (**Figure 7**). In addition, SOL-1 and NETO were also identified as auxiliary subunits that are expressed in C. elegans binding the GLR1 glutamate receptor or responsible for regulating kainate type- glutamate receptors, respectively (**Figure 7**) (Zhang et al., 2009; Zheng et al., 2006).

Although it is generally accepted that auxiliary proteins positively regulate AMPAR trafficking and enhance channel kinetics like TARP, CKAMP, and CNIH proteins at synapses, recently found GSG1L is shown to negatively regulate these processes. Auxiliary subunits generally represent transmembrane proteins that exhibit a differential expression pattern within

the vertebrate brain. Moreover, AMPARs being part of a proteome, which is a large protein complex of around thirty proteins, that comprises auxiliary subunits as well as soluble proteins, accounts for the diversity of these macromolecules on synapses (Schwenk et al., 2012). The structure of AMPAR complex consists of a core that includes TARPs, CNIHs, and GSG1L subunits that define the function of the AMPAR, and a periphery that includes CKAMP transmembrane proteins and soluble proteins of the MAGUK family for example (Schwenk et al., 2012; Schwenk et al., 2009; Shanks et al., 2012; Tomita et al., 2003). Although it has been previously thought that TARP subunits dominate the binding of AMPARs, recent identification of CNIH1 and CNIH2 showed that these auxiliary subunits are more abundantly distrubuted and bind more AMPARs in the rat brain (Schwenk et al., 2009). CNIHs are closely related to a conserved family of a *Drosophila* transmembrane protein designated by *Cni*, which is responsible for the recruitment of Gurken, an EGF-like protein, into COPII vesicles. Without Cni, export of Gurken from the endoplasmic reticulum (ER) is defected (Bokel et al., 2006). CNIHs, as will be detailed later for the TARPs as well, increase surface expression of AMPARs and transport receptors from the ER similar to Cni protein (Brockie et al., 2013). On the other hand, SynDIG1 has also been shown to interact with AMPARs as well as NMDARs, but its effect on AMPAR showed controversy among studies. Some studies state that the absence of SynDIG reduces AMPAR content in developing synapses (Diaz, 2010; Kalashnikova et al., 2010) whereas others prove no effect on AMPARs in the synapses when tested in slices (Lovero et al., 2013). The variety of roles that these auxiliary subunits play in

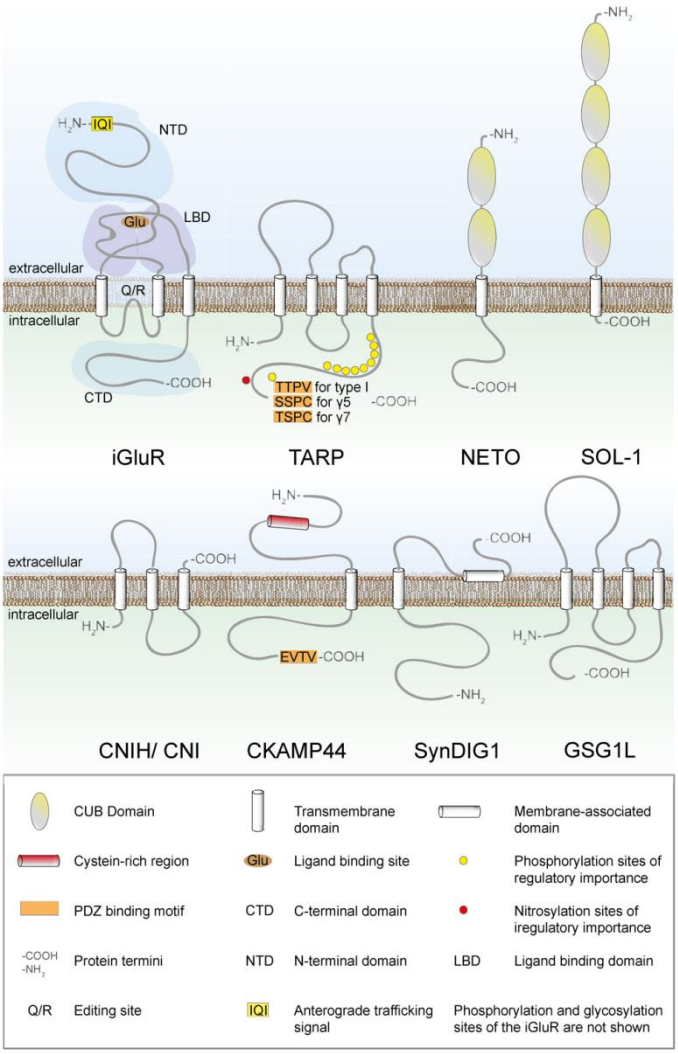


**Figure 7. Schematic structures of most prominent AMPAR auxiliary subunits**
GRIA (iGluR) and AMPAR transmembrane auxiliary proteins presented on the surface membrane of neurons. (Haering et al., 2014)

terms of AMPAR regulation determines the basic features of these receptors and adds a bit complexity to the synaptic system of neurons. Our focus was mainly on TARP and CKAMP proteins, in addition to GSG1L in which we are going into details next.

### 1.8.1 TARP auxiliary proteins

*Transmembrane AMPA receptor regulatory proteins* (TARPs) were the first family of AMPAR auxiliary subunits that was found in the mammalian brain. The most prominent member of the TARP family, "stargazin" or TARPγ2, was identified in the mutant strain of *stargazer* mice (Chen et al., 2000) which suffer from absence epilepsy and cerebellar ataxia (Noebels et al., 1990). Neurophysiological studies showed that the phenotype of *stargazer* mice results from a reduced surface expression of AMPAR in cerebellar granule cells (Hashimoto et al., 1999), highlighting the essential role of stargazin in intracellular transport of receptors. TARPγ2 belongs to a larger protein family that includes TARPγ3, γ4, γ5, γ7, and γ8 (also known as *Cacng2*, *3*, *4*, *5*, *7*, and *8*) which have a homology to the voltage gated calcium channel (VGCC) "γ1" subunit (Klugbauer et al., 2000) of the skeletal muscle calcium channel subunit and the integral membrane claudin proteins. γ1 is closely related to "γ6" where both lack the PDZ binding motif (Chu et al., 2001). Claudin proteins are cell adhesion molecules of epithelial cells forming tight junctions (Morita et al., 1999). Neuronal TARPs may also be part of membrane calcium channels, thus possibly serving a dual function. TARPs, as their name says, are proteins exhibiting tetraspan transmembrane domains, with two extracellular domains (loops) known as EX1 and EX2, and a cytoplasmic N- and C-terminal domain. It has been shown that the first extracellular domain (EX1) controls channel properties and thus regulating desensitization and gating of AMPARs (Tomita et al., 2005b). The second loop EX2 contains a PDZ interacting motif at its intracellular C-terminal domain that interacts directly with PSD95 and increases the number of synaptic AMPARs (Schnell et al., 2002). TARPs are divided according to their structure and function into two main types, type I and type II (**Figure 8)**. Type I includes TARPγ2, γ3, γ4 and γ8 subunits, whereas type II includes TARPγ5, and γ7 subunits. Type I TARPs show a higher degree of slowdown of deactivation and desensitization than type II TARPs, whereby it should be mentioned that type II TARPs exhibit unique properties. In this context, TARPγ5 was shown to only interact and increase peak whole cell current of AMPARs containing GRIA2 subunit unlike type I TARPs, which do not show this distinction. AMPAR glutamate affinity is also reduced in the presence of TARPγ5 (Kato et al., 2008). TARPγ7 also does not show this distinction among GRIA subunits yet it shows a rapid

and sustained desensitization of AMPARs, and it augments glutamate affinity to the receptors. Upon coexpression of GRIA and TARPγ7, glutamate evoked currents rapidly desensitize and show a unique feature of prolonged large steady state current (Kato et al., 2007). Generally, glutamate and kainate affinity and gating of AMPARs is regulated by the EX1 domain of TARPs that is more pronounced in type I than in type II subunits (Milstein et al., 2007). Another prominent difference between type I and type II TARP subunits, is the PDZ binding domain in the C-terminal domain that is in the form of T-T-P-V and S/T-S-P-C amino acid sequence in type I and II, respectively. The PDZ binding motif of type I matched the PDZ domain of PSD95 and related proteins whereas the PDZ binding motif of type II binds weakly to PDZ domains. Moreover, type I TARPs mediate AMPAR trafficking whereas type II do not (Tomita et al., 2005a). Furthermore, type I is divided according to sequence and function into two subfamilies: type Ia and Ib. Type Ia includes TARPγ2 and γ3, and type Ib includes TARPγ4 and γ8. Functional analysis shows that TARPγ4 and γ8 slowdown deactivation and desensitization of AMPARs to a higher degree than TARPγ2 and γ3 (Milstein et al., 2007).

TARP proteins are heterogeneously expressed throughout the brain, although some may be co-expressed in the same neuronal subtypes. Analysis of mRNA content by in situ hybridization of developing and adult mouse brain revealed that TARPγ2 and γ7 are highly expressed in the cerebellar cortex and precisely in the Purkinje and granule cells of the adult brain. In addition, TARPγ3 and γ8 are mainly expressed in the telencephalon, with TARPγ8 being predominantly expressed in the hippocampus. TARPγ4 is significantly expressed in the olfactory bulb, striatum, thalamus and hypothalamus, and TARPγ5 is profoundly present in the olfactory bulb, hippocampal CA2 region, thalamus, inferior colliculus and Bergmann glia cells of the adult brain. In the embryonic brain, expression of TARPγ2, γ5, γ7, and γ8 is spatially

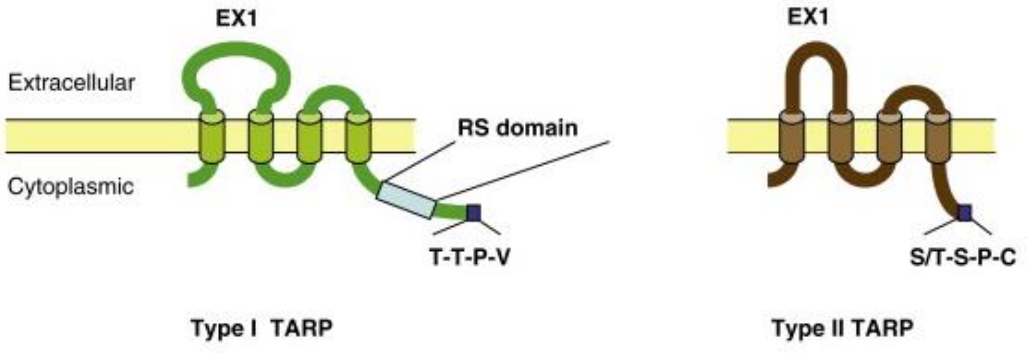


**Figure 8. Structure of type I and type II TARP auxiliary proteins**
(**A**) Extracellular domain (EX1) of type I is bigger than type II of TARP subunit. Type I has a more frequent PDZ binding domain (T-T-P-V) than in type II (S/T-S-P-C) in its C-terminal domain. Type I exclusively has an arginine/serine rich sequence (RS domain) that plays a role in synaptic plasticity. (Kato et al., 2010)

well preserved whereas TARPγ3 and γ4 are respectively up and down regulated (Fukaya et al., 2005).

### 1.8.1.1 TARPγ8 protein

TARPγ8 is preferentially expressed in hippocampal neurons (Tomita et al., 2003). It has high sequence homology to other TARPs, especially to the prototypic group I TARP *stargazin*, but possesses an elongated C-terminal tail (Burgess et al., 2001). Among all TARPs, the C-terminus of TARPγ8 possesses three unique stretches of amino acids that are not present in other TARP subunit (Chu et al., 2001; Milstein and Nicoll, 2009). Multiple studies have shown that TARPγ8 directly modulates the function of GRIA1, 2, and 3-containing receptor channels. It has even been shown to differentially modulate the gating of channels containing homomers or heteromers, or even the flip or flop splice variants of GRIA subtypes. Enhanced kainate response and steady state currents have been recorded in GRIA1/GRIA2 heteromers than in GRIA1 or GRIA2 homomers (Cho et al., 2007; Kott et al., 2007; Tomita et al., 2003). In heterologous cells, coexpression of AMPAR channels with TARPγ8 especially decelerated desensitization and deactivation, thus increasing overall charge transfer during receptor activation (Cho et al., 2007). TARPγ8, similar to other TARPs, binds the AMPAR channel at its extracellular N-terminal domain (NTD) and regulates its gating (**Figure 9**). The role of the AMPAR distal N-terminus is not well known; however, the N-terminus with part of the ligand binding domain (LBD), connected via a N-glycosylated linker of ~17 amino residues, forms a binding site for TARPs mediating the gating of the channels. In case of TARPγ8, mutation of this linker results in a slowdown of recovery from desensitization due to the NTD acquiring a different position and reducing the interaction with the TARPγ8 (Cais et al., 2014).

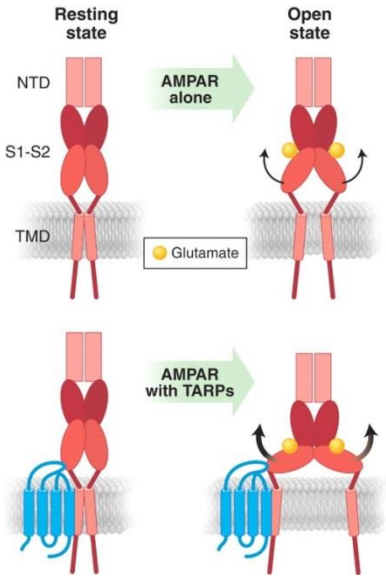


**Figure 9. Possible function of TARP on AMPAR channel**
AMPAR shown in its resting state and open state when bound to glutamate. S1-S2 domain closes like a clam-shell when bound to glutamate to open the channel pore (**upper figure**). Clam-shell closes more when TARP (blue) is bound to the AMPAR to efficiently open the channel (**lower figure**) (Nicoll et al., 2006).

In analogy to other members of the TARP family like stargazin/TARPγ2 (Vandenberghe et al., 2005), TARPγ8 is believed to be involved in ER export and forward trafficking of GRIAs (GRIA2/3 or GRIA1). Indeed, elimination of TARPγ8 in a KO mouse model not only resulted in a decreased overall cellular pool of AMPARs but also led to an increased population of receptors with immature glycosylation in intracellular compartments (Rouach et al., 2005). Intriguingly, the stoichiometry of AMPAR and TARPγ8 is variable where AMPARs are functional with four, two, or even no TARPγ8. The number of associating TARPγ8 depends on the region and expression level in the brain. It has been shown that native AMPARs may associate with four TARPγ8, a saturated state of assembly, in the pyramidal neurons of the CA1 region whereas less than four associate with the receptors in the granule cells of the dentate gyrus. The variability in stoichiometry is related to the mechanistic role played in the different regions (Shi et al., 2009). A later study showed that the number of assembled TARPγ8 to the AMPAR is controlled by CNIH2 suggesting a modulating effect of the AMPAR channel gating and pharmacology (Gill et al., 2011). Precisely, GRIA1 containing AMPARs can bind TARPγ8 and CNIH2 simultaneously, and non-GRIA1 containing AMPARs are prevented from CNIH2 binding by TARPγ8 explaining why not all AMPARs have the same number of associated TARPγ8 subunits (Herring et al., 2013). In addition, it was reported that glycosylation of TARPγ8 itself is critical for the transport of GRIA1-containing receptors to the plasma membrane, as a reduced surface/total receptor expression and a changed glycosylation status of GRIA1-receptors was observed in neurons expressing non-glycosylated TARPγ8 (Zheng et al., 2015a). Interestingly, TARPγ8 loss reduces the synaptic receptor population much less than extrasynaptic receptors, which are almost abolished in KO neurons (Rouach et al., 2005). The persistence of synaptic AMPAR localization likely reflects a compensatory action of other auxiliary subunits that can still efficiently recruit AMPARs to synaptic sites, even if overall receptor abundance is dramatically low. While TARPγ8 is clearly not essential for synaptic localization of AMPARs, its C-terminal PDZ binding motif still is involved in normal postsynaptic aggregation of receptors, as C-terminal truncation of TARPγ8 in a corresponding knock-in mouse model (TARPγ8Δ4) significantly decreased AMPA EPSC

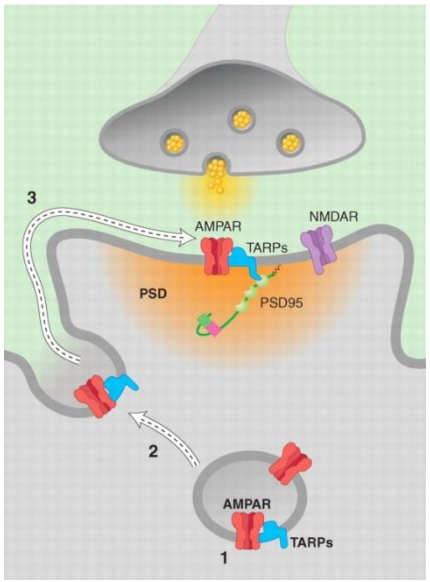


**Figure 10. AMPAR trafficking is regulated by TARP auxiliary subunit**
TARP subunit conveys AMPARs early in trafficking (**1**), insertion in the postsynaptic membrane (**2**), and stabilization at the synapse via PSD95 protein (**3**). (Nicoll et al., 2006)

amplitude (Sumioka et al., 2011). The synaptic receptor aggregation has been attributed to the disruption of C-terminal interactions of TARPγ8 with PDZ domains of PSD95 (**Figure 10**) (Sumioka et al., 2011), similar to the role of PDZ interactions of other group I TARPs in synaptic anchorage (Schnell et al., 2002). Elimination of TARPγ8 abolishes expression of long term potentiation (LTP) (Rouach et al., 2005). Given the strong reduction in the extrasynaptic receptor population, this functional deficit might be a simple consequence of hampered receptor recruitment. However, elimination of the PDZ binding motif in TARPγ8Δ4 did not interfere with the expression of LTP, even though TARP-mediated synaptic receptor aggregation is compromised (Sumioka et al., 2011). Upon LTP initiation and calcium increase, CaMKII phosphorylates TARPγ8 at its S277 and S281 residues to increase the binding between PSD95 and TARPγ8, a process necessary to enhance AMPAR trapping on the postsynaptic membrane (Park et al., 2016). Recent work identifies new routes of AMPAR trafficking from the dendritic ER to the surface. Unlike somatic ER, AMPARs originating from dendritic ER do not pass through the Golgi apparatus, which makes the transport of receptors faster to the dendritic surface. Half of the surface GRIA1 and GRIA2 exist in a mannose glycosylated state indicting that these subunits did not pass through the glycosylation process in a the Golgi apparatus (Bowen et al., 2017). On the other hand, it has been shown that TARPγ8 has a complex glycosylation when present on the surface membrane (Zheng et al., 2015a) suggesting that AMPARs and TARPγ8 have different maturation routes before arriving to the dendritic surface. Therefore, other auxiliary subunits, like CNIHs and SynDIG4, have been proposed to assist the transport of AMPARs originating from the dendritic ER (Buonarati et al., 2019; Matt et al., 2018; Schwenk et al., 2009). These findings show that a lot of work has to be done to understand the role of TARPγ8 in AMPAR trafficking and local recycling in the dendrites.

### 1.8.2 CKAMP44 protein

In hippocampal neurons, especially in granule cells of the dentate gyrus, AMPARs are associated with a second type of auxiliary subunit called *cystine-knot AMPAR modulating protein 44 kDa* (CKAMP44) (von Engelhardt et al., 2010). CKAMP44 (alternative nomenclature: Shisa9) belongs to a subgroup of the Shisa adaptor protein family (Pei and Grishin, 2012), which also comprises the brain-specific isoforms CKAMP39, 52, and 59 (Farrow et al., 2015). All CKAMPs represent type I transmembrane proteins with only one

transmembrane domain, an extracellular N-, and an intracellular C-terminal domain (**Figure 11**) (Farrow et al., 2015). As its name-giving feature, CKAMPs possess a conserved cysteine rich motif (eight cysteines), with six cysteine residues that likely form disulfide bridges similar to the cysteine knot found in *ω-conotoxin* (Farrow et al., 2015; von Engelhardt et al., 2010). CKAMP44 contains 424 amino acids and exists in two splice variants, CKAMP44a and CKAMP44b, which differ by 48 base pairs (von Engelhardt et al., 2010). CKAMP44 has a pronounced C-terminal domain of 253 amino acids and contains a type II PDZ, which putatively binds to PSD95. CKAMP44 binds to AMPARs without apparent subunit-specificity, involving a short juxtamembrane part of its cytosolic domain (Khodosevich et al., 2014).

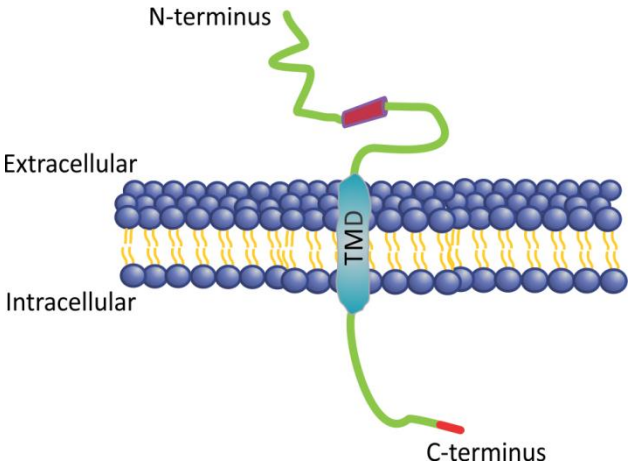


**Figure 11. Schematic structure of CKAMP auxiliary subunit**
CKAMP auxiliary subunit has an extracellular N-terminal domain with a cysteine-rich sequence (dark red), an intracellular C-terminal domain, and one transmembrane domain (TMD).

On the functional level, CKAMP44 promotes surface expression of AMPARs, slows down deactivation of AMPAR channels, and increases apparent glutamate affinity, very similar to the effects of TARPγ8. Unlike the effects of TARPγ8; however, in the presence of CKAMP44, receptor desensitization is more pronounced showing a decreased desensitization time constant and increased recovery time constant. Mutation of the cysteine residues in CKAMP44 renders the protein fully non-functional, despite a persistent binding of the mutant to GRIA1-containing AMPAR. Interestingly, almost the full C-terminal tail (except the juxtamembrane region) of CKAMP44 could be truncated without any functional consequences in hippocampal neurons, derogating its mechanistic requirement (Khodosevich et al., 2014). However, a recent study showed that the C-terminal domain binds PKC, and phosphorylation of C-terminus is modulated by PICK protein indicating a possible role of the C-terminal domain in synaptic plasticity (Kunde et al., 2017). Moreover, screening the eight PDZ binding domains of the C-terminus showed that PSD95 is a binding partner which assembly enhances the anchoring of AMPARs on the surface membrane (Karataeva et al., 2014). The CKAMP44-mediated modulation of AMPAR channel properties also seem to significantly affect short term plasticity (STP), highlighting how CKAMP44 function determines synaptic physiology (Khodosevich et al., 2014; von Engelhardt et al., 2010). In contrast to TARPs, loss of

CKAMP44 however did not affect synaptic plasticity. Interestingly, it has been recently shown that TARPγ8 and CKAMP44 can be present in the same receptor complex in hippocampal neurons to differentially fine tune AMPAR channel and synaptic activity in addition to their role in forward trafficking of AMPARs to the surface membrane (Khodosevich et al., 2014). In addition to CKAMP44, related CKAMP39 (shisa8), CKAMP52 (shisa6), and CKAMP59 (shisa7) also modulate AMPAR function. However, unlike CKAMP44 that is expressed in the majority of the brain regions as well as in embryonic stages (von Engelhardt et al., 2010), the novel CKAMPs' expression is region and age specific specific. CKAMP39 was exclusively found in the olfactory bulb and cerebellum. CKAMP52 is expressed in the hippocampus, cerebellum, and septum, and CKAMP59 is expressed in the cortex and olfactory bulb as well as in the hippocampus. On the embryonic level, only CKAMP59 is strongly expressed in contrast to CKAMP39 or CKAMP52, which are completely absent and weakly expressed, respectively (Farrow et al., 2015). On the structural level, CKAMPs differ in the length of their extracellular signal peptide being 22, 23, 30, and 36 amino acids for CKAMP59, 44, 52, and 39, respectively. All CKAMPs interact with GRIA1 and GRIA2, but they differentially modulate the channel gating and according to the subunit composition of the AMPAR. When CKAMP39 and 52 were coexpressed with either GRIA1 or GRIA2 in heterologous systems, they increased deactivation and reduced desensitization of GRIA2-mediated currents but did not affect GRIA1-mediated currents. When testing the recovery from desensitization, CKAMP39 had similar effects as CKAMP44 suggesting that CKAMP39 also mediates STD (Farrow et al., 2015; von Engelhardt et al., 2010). Although CKAMP59 did neither change deactivation nor desensitization of GRIA1 or GRIA2-mediated currents, a recent study showed that CKAMP59 knockout slows AMPAR decay kinetics without affecting amplitude or frequency (Farrow et al., 2015; Schmitz et al., 2017). Furthermore, overexpression of CKAMP44 in oocytes showed no change in GRIA1 surface expression (von Engelhardt et al., 2010) in contrast to CKAMP39 and CKAMP59 where GRIA1 and GRIA2 surface expression was reduced and in CKAMP52 was increased in HEK293/T17 cells (Farrow et al., 2015). These different findings suggest that CKAMPs differentially modulate forward trafficking and AMPAR stabilization on the dendritic surface.

### 1.8.3 GSG1L protein

GSG1L (Germ Cell-Specific Gene 1-Like) protein is an auxiliary subunit that has been recently identified and shown to form a stable complex with AMPARs (Shanks et al., 2012). According to its topology, GSG1L is also related to the *claudin* protein family, and has a high similarity to TARP proteins. As for TARP proteins, GSG1L also has a tetraspan transmembrane domain with two extracellular loops, and an intracellular N- and C-terminal domain. GSG1L is expressed in the hippocampus, striatum, and the cortex. However, it is unique in its functional properties among the four core auxiliary subunits of AMPARs although it has a structural similarity to TARPs (**Figure 12)** (Shanks et al., 2012). In contrary to other auxiliary subunits, GSG1L negatively regulates AMPAR trafficking and synaptic transmission in glutamatergic synapses of hippocampal neurons. GSG1L is known to reduce the single channel conductance and calcium permeability of calcium permeable AMPARs (CP-AMPARs) as it has been shown in the cerebellar and hippocampal neurons. Absence of GSG1L showed an increase in inward rectification and mEPSCs in cerebellar neurons and increased mEPSC amplitude in hippocampal neurons, respectively (McGee et al., 2015). In line with that, a recent study showed via cryo-electron microscopy (EM) that GSG1L stabilizes the closed conformation structure of the AMPAR channel (Twomey et al., 2017). Thus, GSG1L suppresses synaptic currents and fastens deactivation and desensitization in CA1 hippocampal neurons. Its effect on the AMPAR is mediated by the first extracellular loop and the C-terminus (Gu et al., 2016a). Coexpression of Cre with GRIA1 and GSG1L showed a reduction in forward trafficking of AMPARs to the synapses in hippocampal neurons, and overexpression of GSG1L also resulted in reduced surface expression of AMPARs in neurons (Gu et al., 2016a). Interestingly, GSG1L knockout reduced AMPAR endocytosis and increased its forward trafficking which consequently enhanced LTP. Furthermore, it was shown that the extrasynaptic pool of AMPARs was greatly increased in GSG1L knockout hippocampal neurons which is in agreement with the concept that LTP requires an extrasynaptic AMPAR reserve pool (Gu et

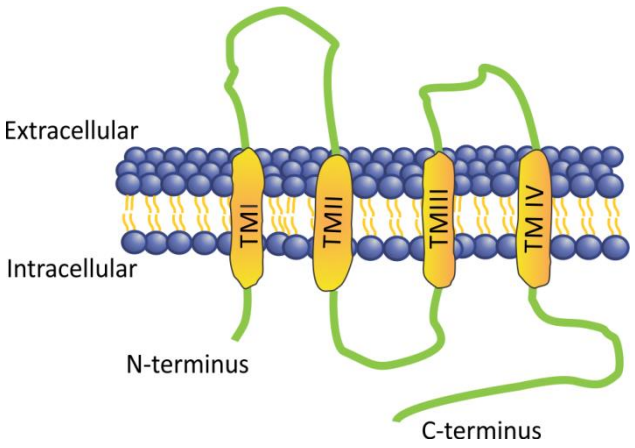


**Figure 12. Schematic structure of GSG1L auxiliary subunit**
GSG1L auxiliary subunit has an intracellular N- and C-terminal domain, and four transmembrane domains (TMDs).

al., 2016a). The fact that GSG1L inhibits the function of other auxiliary subunits like CNIH2 and mediates a negative role on AMPAR trafficking and channel gating, indicates that GSG1L indeed ensures a balance in neuronal activity (Gu et al., 2016a). It is worth mentioning that in contrast to CA1 hippocampal neurons, absence of GSG1L in hippocampal dentate granule neurons did neither affect LTP nor deactivation or desensitization of the AMPAR channel, indicating a region specific role of GSG1L (Mao et al., 2017).

# Aims of study

1. AMPAR trafficking to and from the surface membrane of neurons is a dynamic process, but its precise mechanism is still not clear. Our first aim was to characterize the trafficking system of AMPARs. Therefore, GRIA1 subunits were N-terminally fused with the pH-dependent GFP derivative superecliptic pHluorin (*SEP*) to track AMPARs during their surface insertion via exocytosis in hippocampal neurons. By using SEP-GRIA1 construct, we were also able to detect intracellular trafficking organelles storing AMPARs and quantify their content. We also aimed to identify the type of AMPAR trafficking organelles; therefore, we cotransfected hippocampal neurons with endosomal markers like the transferrin receptor (*TfR*)- fused to *tagRFPt* to stain recycling endosomes.

2. Our second aim was to study the activity dependent regulation of AMPAR surface delivery in the soma of hippocampal neurons. By chronically depressing the activity of mouse hippocampal neurons using TTX or using *Snap25*$^{-/-}$ neurons having a disabled exocytotic machinery, we studied the exocytosis rate of SEP-GRIA1 in an activity dependent manner.

3. AMPARs are known to associate with several proteins that regulate their trafficking and channel properties. We aimed to study the impact of two prominent auxiliary proteins, precisely TARPγ8 and CKAMP44a, on AMPAR trafficking mainly under basal activity. Using SEP-GRIA1, we examined the effect of both auxiliary subunits on AMPAR surface expression and local recycling. For the local recycling, we studied the exocytosis rate and intracellular stores of SEP-GRIA1 in dendrites upon auxiliary subunit overexpression. To further elucidate the effect of auxiliary subunits on AMPAR trafficking, we studied the basal AMPAR endocytic rate in extrasynaptic and synaptic sites that were differentiated using the synaptic marker PSD95-tagRFPt. Moreover, using the self-labelling HaloTag-GRIA1, we aimed to stain exclusively the surface membrane of dendrites with a cell impermeable ligand tagged to a fluorescent dye to observe a gradual uptake of fluorescence indicating GRIA1 endocytosis.

# 2. Materials and Methods

## 2.1 Solutions

### 2.1.1 Hippocampal neuron - glial sandwich co-culture (Gary Banker Culture)

Poly-D-Lysine (Poly-D-Lysine Hydrobromide, Sigma P6407)

- MW: 70000-150000 Da
- Concentration: 0.227 mg/ml dissolved in Borate buffer

Borate buffer

- $H_3BO_3$ (Sigma B-0252): 0.05 M
- $B_4O_7.10H_2O$ (Merck A688908): 0.024 M
- Components are dissolved in double distilled water ($ddH_2O$), and pH is adjusted to 8.5 with NaOH. Solution is then stored at 4 °C after filtration.

Collagen, Rat Tail (Corning, 90 % purity, Product No. 35426)

- Concentration: 1 mg/ml,
- Diluted in $ddH_2O$
- Stored at 2 to 8 °C

Enzyme Solution

- 250 ml DMEM (gibco, 31966-021), 50 mg L-Cysteine (Sigma, C7352), 2.5 ml $CaCl_2$ (100 mM), 2.5 ml Ethylenediaminetetraacetic acid (EDTA, pH=8.5) (50 mM) (Sigma, E1644)
- Stored at -20 °C

Inactivation Solution

- 225 ml DMEM, 25 ml FBS (gibco, 10270-106), 625 mg Bovine Serum Albumin (BSA) (Sigma, A7906), 625 mg Trypsin Inhibitor (Sigma, T9253)
- Stored at -20 °C

Papain (Worthington, CAT #: LS003126)

- Concentration: 20 U/ml in enzyme solution
- Stored at 4 °C

Neurobasal A (NBA) medium with supplements

- 250 ml NBA (gibco, 10888-022), 5 ml B27 (gibco, 17504-044), 2.5 ml Glutamax (gibco, 35050-038), 0.5 ml penicillin and streptomycin (Pen/Strep) (ThermoFisher, 15140122)

Dulbecco's modified Eagle medium (DMEM) with supplements

- 225 ml DMEM, 25 ml FBS (10 %), 0.5 ml Pen/Strep, 250 µl MITO (Corning, 355006)

Hank's Balanced Salt Solution (HBSS) (gibco, 24020-091)

- With calcium and magnesium

Dulbecco's Phosphate Buffered Saline (DPBS) (gibco, 14190-094)

- With calcium and magnesium

Trypsin-EDTA enzyme (10x)

- Trypsin enzyme (ThermoFisher, 15400054) is diluted 10 times with DPBS to obtain a concentration of 0.05 %

Astrocyte inhibitor

- 5 - Fluoro - 2’ deoxyuridine (Sigma, F0503): is a thymidylate synthase inhibitor: 3.2 mM
- Uridine (Sigma, U3003): 79.8526 mM

**All media were stored at 4 °C.**

## 2.1.2 Other materials

- Culture Coverslips (VWR, 25 mm)
- Paraffin Wax (Fischer Scientific UK, P/0600/90): sterilized by autoclaving
- Six-well plates (Fischer scientific, 10799541)
- T-25 culture flasks
- Cell strainer (100 µm, Easy strainer, greiner bio-one)

## 2.1.3 Calcium phosphate transfection of hippocampal neurons

- Plasmid DNA in $H_2O$
- $CaCl_2$ (2.5 M)
- Sigma $H_2O$
- Fresh DMEM
- 2xHeBS (HEPES Buffered Saline) (Sigma, H7523)

For 50 ml (2xHeBS)

- NaCl: 0.8 g
- KCl: 0.0355 g
- $Na_2HPO_4.2H_2O$: 0.013 g
- D-Glucose: 0.135 g (Sigma, G6152)
- HEPES: 0.5 g

Three HeBS solutions with pH 7.06, 7.1, and 7.14 are prepared by adjusting the pH with NaOH solution. Neurons are then transfected with the three different HeBS solutions, and the one with the highest transfection efficiency is stored (-20 °C) for further transfections.

### 2.1.4 Extracellular solution

- NaCl: 145 mM
- KCl: 2.4 mM
- $MgCl_2$: 1 mM
- $CaCl_2$: 2 mM
- HEPES: 10 mM
- D-Glucose: 10 mM

pH≈7.4

### 2.1.5 Ammonium chloride solution (modified extracellular solution with ammonium chloride)

- NaCl: 95 mM
- $NH_4Cl$: 50 mM
- KCl: 2.4 mM
- $MgCl_2$: 1 mM
- $CaCl_2$: 2 mM
- HEPES: 10 mM
- D-Glucose: 10 mM

pH≈7.4

### 2.1.6 Low pH solution (5.5) (modified extracellular solution with low pH=5.5)

- NaCl: 95 mM
- KCl: 2.4 mM
- $MgCl_2$: 1 mM
- $CaCl_2$: 2 mM
- HEPES: 10 mM
- D-Glucose: 10 mM

pH≈5.5

### 2.1.7 Insulin solution (modified extracellular solution with insulin)

- NaCl: 145 mM
- Insulin: 50 µM (Sigma, 11376 497 001, human recombinant)
- KCl: 2.4 mM
- $MgCl_2$: 1 mM
- $CaCl_2$: 2 mM
- HEPES: 10 mM
- D-Glucose: 10 mM

pH≈7.4

### 2.1.8 Patch clamp intracellular solution

- potassium-gluconate 137.5 mM
- NaCl 11 mM
- MgATP 2 mM
- $Na_2GTP$ 0.2 mM
- EGTA 1.1 mM
- HEPES 11 mM
- D-glucose 11 mM

pH was adjusted with KOH to 7.3

### 2.1.9 Patch clamp extracellular solution

- NaCl: 145 mM
- KCl: 2.4 mM
- $MgCl_2$: 1 mM
- $CaCl_2$: 2 mM
- HEPES: 10 mM
- D-Glucose: 10 mM
- D-APV 50 µM (Tocris, 0106)
- TTX 1 µM (Abcam, ab120055)

pH≈7.4

### 2.1.10 Immunocytochemistry

- PBS (1x)

  For 1L:

  - NaCl: 8 g
  - KCl: 0.2 g
  - $Na_2HPO_4.2H_2O$: 1.78 g
  - $KH_4PO_4$: 0.24 g

  pH≈7.4

- PFA (4 %)

  For 50ml:

  - PFA: 2 g (MERCK, 1040051000)
  - PBS(1x): 50 ml

  pH≈7.4; pH measured with a litmus paper

- Blocking Buffer

  For 200ml:

  - BSA: 6 g
  - TritonX100: 0.3 g (MERCK, 1 08603 1000)
  - PBS(1X): 200 ml

- Quenching Buffer

  For 40 ml:

  - $NH_4Cl$: 0.1 g
  - PBS(1X): 40 ml

## 2.2 Preparation of culture coverslips

### 2.2.1 Acid wash

Coverslips were first put in 37 % HCl acid solution for 2 to 3 h, and then washed three times with $ddH_2O$ each time for 1 h. A second acid wash with 65 % $HNO_3$ was done in the same manner as with HCl solution. Acid washing of coverslips increases the cleanliness and etches the surface allowing for a better neuron attachment. In case 3 h is not enough for acid treatment, coverslips can be left in HCl or $HNO_3$ overnight. After the last washing step with $ddH_2O$, the coverslips were washed with 70 % and 100 % ethanol for 2 to 3 h. Coverslips can

also be left in dd$H_2O$, 70 %, or 100 % ethanol overnight. Eventually, the coverslips are put in a glass petri-dish and dried at 153 °C for 2 h. Coverslips are eventually exposed to UV light before use, for sterilization.

If the coverslips were used for neuron-glial sandwich culture (Gary Banker culture), three paraffin dots (wax dots) were added on the edge of a coverslip in a triangle. Wax dots serve as spacers between neurons and astrocyte feeding layer (**Figure 15**).

### 2.2.2 Poly-D-Lysine coating of acid washed glass coverslips

In order to enhance neuron cell adhesion to solid substrates, culture coverslips are coated with Poly-D-Lysine. Poly-D-Lysine is a positively charged amino acid polymer that binds negatively charged ions on cell membranes.

Poly-D-Lysine was dissolved in Borate buffer and aliquots were stored at -20 °C. Coverslips, in six-well plate, were coated with 100 µl of Poly-D-Lysine overnight. The six-well plates were then covered with parafilm to prevent dryness of coverslips. On the next day, remaining Poly-D-Lysine was removed and coverslips were washed with dd$H_2O$ three times each time for about 1 h. The coverslips were dried and sterilized prior to use.

## 2.3 Astro-glial culture preparation

For optimal imaging of neurons, we optimized the neuron-glial sandwich culture, which is also known as the Gary Banker culture. Astrocytes were prepared at least 8 to 9 days before the neuron culture. To prepare an astrocyte primary culture, three newborn (P0/P1) C57/Black6 mice (**Figure 13**) were decapitated and the skull was then cut carefully with a small surgical micro scissor. The brain was then taken out with the help of a small spoon and put in cold HBSS medium. The two hemispheres of the brain were pulled apart with two forceps and the hippocampal regions were carefully dissected out (**Figure 14**). All hippocampi were collected and put in a cell strainer (pore size of 100 µm) set on a sterile 50 ml falcon tube to mechanically dissociate the tissue with a sterile plastic stick. Cells were filtered with fresh and cold DMEM medium into a falcon tube until no tissue was visible. Cell suspension was then centrifuged at 1800 rpm for 5 min. The supernatant was removed and 1 ml of warm DMEM medium (with supplements) was added to re-suspend the astrocytes. Finally, 5 ml of warmed DMEM medium was added to the


**Figure 13. Image of a new born mouse (P0)**

cell suspension and mixed slowly then transferred to a collagen coated T-25 culture flask. The cells were cultured in a 12 % $CO_2$ incubator at 37 °C for one day. Then they were fed with fresh DMEM medium and left for about a week to grow for confluence. After one week, astrocytes were harvested and seeded in six-well plates. To harvest astrocytes, they were shortly washed with 5 ml warmed DPBS and detached from their adhesive layer through addition of 0.005 % tryspin-EDTA for 5min in 12 % $CO_2$ incubator at 37 °C. About 3 ml of warmed DMEM medium (with supplements) were then added to deactivate trypsin and to re-suspend them with 5 ml pipette. The cell suspension was put in a 15 ml falcon tube and centrifuged for 5 min at 1300 rpm at 20 °C. The supernatant was removed and the cell pellet was re-suspended in 1 ml DMEM medium (with supplements). With the help of a Neubauer hemocytometer chamber astrocytes were counted and an estimate of ≈ 3 x $10^5$ cells were calculated for each culture coverslip of a diameter 25 mm of a six-well plate. The astrocytic feeding layer was incubated in DMEM medium (with supplements) for two to three days to grow 40 % to 60 % confluence before addition of hippocampal neurons.

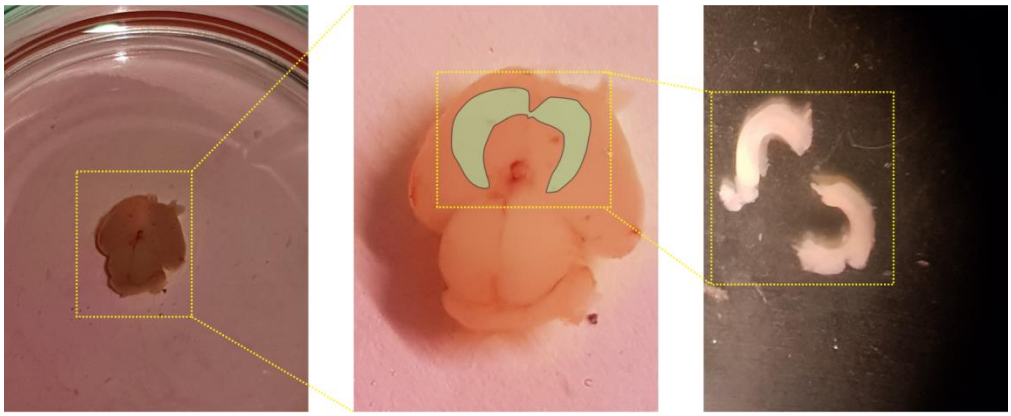

**Figure 14. Brain and hippocampi of a P0 Mouse**
Dissection of a mouse brain to obtain the hippocampus (right image) for primary culture.

## 2.4 Hippocampal neuron primary culture preparation

To prepare neuron primary culture, newborn (P0/P1) C57/Black6 mice were decapitated and the skull was then cut carefully with a small surgical micro scissors. The brain was then taken out with the help of a small spoon and put in cold HBSS medium. The two hemispheres of the brain were pulled apart with two forceps and the hippocampal regions were carefully taken out. In the meantime, the enzyme solution containing 20 units (20 U) papain was put in an 11 % $CO_2$ incubator for pH adjustment, and culture plates containing treated coverslips were

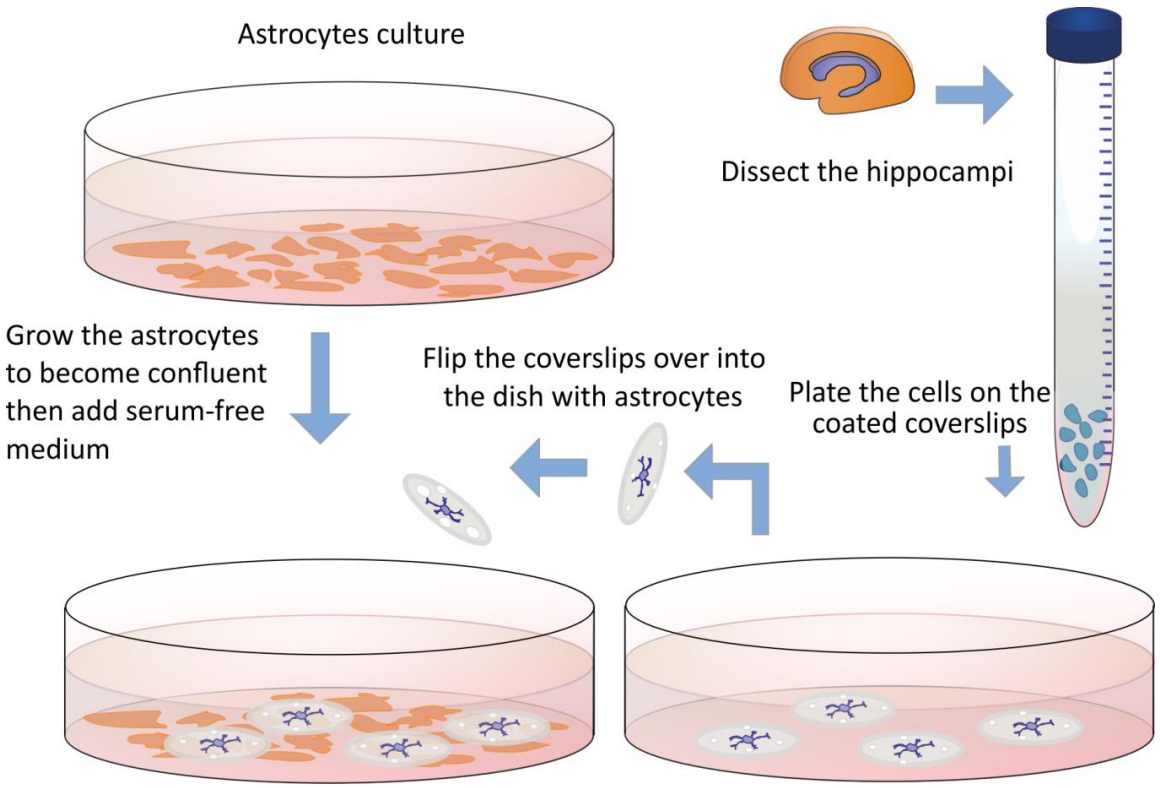


**Figure 15. Gary Banker culture of hippocampal neurons and astrocytes**
A Gary Banker culture is a sandwich culture of astrocytes on a bottom of a well and neurons on coverslips facing the astrocytes upside down. Neurons and astrocytes are separated by wax dots that serve as spacers.

sterilized with UV light. DMEM medium (with supplements), NBA medium, and inactivation solution were also warmed up (37 °C) to use in later steps. The cleaned hippocampi were put in 400 µl papain-enzyme solution for ≈ 20 min in a 37 °C water bath under shaking condition. Following digestion, the enzyme solution was removed and the tissue was incubated in 400 µl inactivation solution and returned back into the shaking water bath for 5 min. The inactivation medium was then removed and 600 µl of warm DMEM medium (with supplements) was added to the hippocampi. The tissue was carefully dissociated by multiple pipetting. The cell suspension was left for 2-3 min for allow non-dissociated cellular tissue to precipitate. The 600 µl cell suspension was then put in a 1.5 ml eppendorf tube with 400 µl DMEM medium and mixed carefully. We then counted the cells using a Neubauer hemocytometer chamber and an estimate of about 3 x $10^4$ cells per 25 mm coverslip was calculated. We incubated the plated hippocampal neurons for 30 min in 5 % $CO_2$ incubator then added carefully 2 ml warmed (37 °C) NBA medium to each well.

In a case of a continental culture (≈ 6.8 x $10^4$ cells/coverslip), every 3 days a medium change was done until use the ($9^{th}$ to $13^{th}$ day). In case of a low density culture (≈ 3.2 x $10^4$ cells/coverslip), FUdR astrocyte inhibitor was added on the third day after preparation, to block overgrowth of astrocytes. FUdR is a thymidylate synthase inhibitor that blocks DNA

synthesis. At the second day NBA medium was exchanged with a fresh one. In addition, medium change (~1 ml) was done every three days to maintain the integrity of neurons. Blocking astrocytes' growth was done to allow better imaging of overlaying hippocampal neurons.

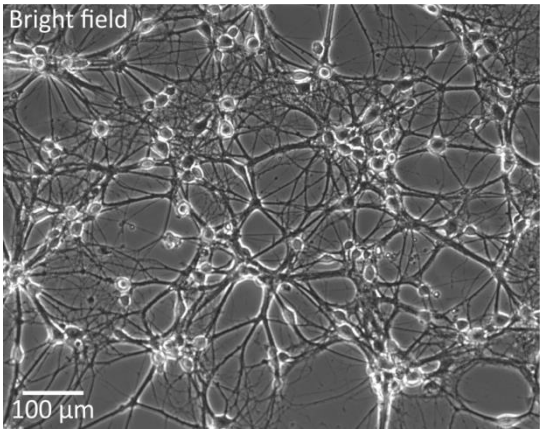


**Figure 16. Typical hippocampal primary neuron culture**
Image of hippocampal neurons (DIV 9-10) grown in a Gary Banker culture

For the neuron-glial sandwich culture (**Figure 15, Figure 16**), the medium of cultured astrocytes was exchanged with NBA medium for pre-conditioning at the day of neuron preparation. On the second day, the coverslips containing neurons were transferred upside down to the astrocyte feeding layers (**Figure 15**). At the third day, the culture was treated with FUdR astrocyte inhibitor followed by a medium exchange every three days as mentioned previously.

## 2.5 Calcium phosphate transfection of hippocampal neurons

To transfect hippocampal neurons with a cloned DNA, the cells were washed one time with pre-warmed fresh DMEM medium then incubated in 2 ml fresh DMEM medium (transfection medium) for 45-60 min at 37 °C in 5 % $CO_2$. Conditioned NBA medium of the neurons is preserved to be added again at the end of transfection procedure. In the meanwhile, the DNA-calcium phosphate precipitate was prepared. For the precipitate, 34 µl Sigma $H_2O$, 4 µl $CaCl_2$ (2.5 M), 2 µl DNA (1 µg), and 40 µl of HeBS are required per 25 mm coverslip. First, Sigma $H_2O$, $CaCl_2$, and the DNA were gently mixed together, and then it was added dropwise to the HeBS and mixed through bubbling with a pipette. The mixture was put in dark for 30-40 min at room temperature to allow the DNA/calcium phosphate precipitate to build. After ~30 min, the solution should look somewhat cloudy compared to the HeBS stock solution and ready to be added dropwise over the neurons. Eighty microliters of the precipitate solution were added in each well during which the six-well plate was moved gently to ensure homogeneous distribution of the precipitate on the neurons. Neurons were put back in the incubator with 5 % $CO_2$ for 30-35 min to allow transfection to take place whereby fine precipitate was seen after ~20 min all over the coverslip. Then the transfection medium was removed and coverslips were washed with fresh warm DMEM medium two times for 10-15 min. Finally, DMEM medium

was exchanged with the conditioned NBA medium and incubated one to two days to allow the expression of the desired gene.

## 2.6 Immunocytochemistry of hippocampal neurons

Hippocampal neurons were fixed with 4 % freshly prepared paraformaldehyde (PFA) solution for 20 min on a shaker after a short wash with PBS. PFA is prepared by adding 2 g PFA powder to 50 ml PBS (1x), and then put for 1.5 to 2 h in a 65 °C water bath to dissolve. PFA was removed, and the cells were washed three times (5 min each) with PBS. Neurons were then quenched with the quenching buffer for 10 min followed by one wash with PBS (1x). Then blocking buffer was added to the cells for 30-45 min to prevent unspecific binding of antibodies. Neurons were then incubated overnight with primary antibody in a wet chamber at 4 °C. Primary antibody was washed away on the second day with blocking solution (three times, 10 min each), and cells were incubated with the secondary antibody in a wet chamber at room temperature for 2 h in the dark. Finally, cells were washed with PBS and mounted with glycerol on microscope slides for imaging.

## 2.7 Blocking astrocyte growth in hippocampal neuron culture

Since our study was based on imaging primary hippocampal neuron cultures of 9-12 days old, we had to make sure that astrocytes did not contaminate the neuronal cultures with their overgrowth in the coverslips. Hence, astrocytes lying under neurons block imaging of soma and/or dendrites making it sub-optimal. To circumvent this problem, we treated the neuron-glia culture with an astrocyte inhibitor *5 - Fluoro - 2' deoxyuridine* (*FUdR*) to block astrocytic overgrowth at the time keeping neurons healthy. To identify the optimal day to treat the neuron-glial culture with FUdR, we treated cultures on the second (DIV 2) or third (DIV 3) day after preparation and fixed and stained astrocytes and neurons to test the effect of FUdR. We fixed the cultures on the following day, and immunostained against microtubule-associated protein (MAP) and glial fibrillary acidic protein (GFAP) that are neuron and astrocytic markers, respectively. Primary antibodies (Ab) against MAP (abcam, Cat.No. ab32454) and GFAP were diluted 1:1000 in blocking buffer (anti-MAP: mouse monoclonal; and anti-GFAP: rabbit polyclonal). As for secondary antibodies, both were also diluted 1:1000 in blocking buffer (secondary Ab against anti-MAP Ab: Alexa 488 nm goat anti-mouse; secondary Ab

against anti-GFAP Ab: Alexa 546 nm donkey anti-rabbit). After mounting the coverslips in glycerol, they were imaged using confocal microscopy (LSM 780). Interestingly, FUdR treated coverslips, on the second (DIV 2) and third (DIV 3) day, showed a clear decrease in astrocyte number compared to non-treated coverslips (**Figure 17**).

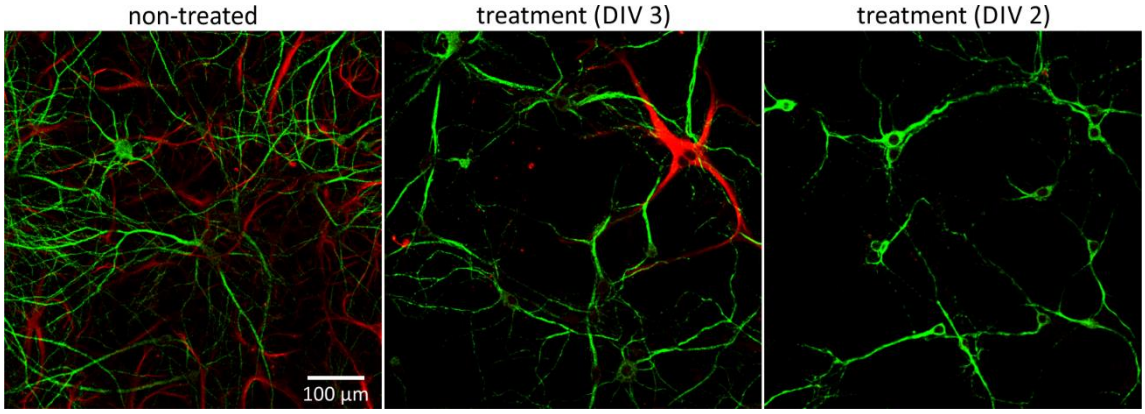


**Figure 17. Astrocyte growth inhibition via FUdR treatment**
Hippocampal neuron culture immunostained against microtubule-associated protein (MAP, green) in neurons and glial fibrillary acidic protein (GFAP, red) in astrocytes. Culture not treated with FUdR shows normal growth of astrocytes (**left**). Cultures treated with FUdR at DIV 3 and DIV 2 show a noticeable reduction in astrocyte growth (**middle and right**). Images were smoothed for better presentation.

## 2.8 Epifluorescence and TIRF imaging

Epifluorescence imaging of transfected neurons was done on two inverted microscopes depending on the purpose of the experiment. Olympus IX70 microscope setup with custom installments for a wide range of experiments was mostly used for epifluorescence imaging. It is equipped with manual and automated perfusion systems that were used during recording. An EMCCD camera (Evolve Photometrics, 512) was used for capturing images during recording. The camera is connected with a Dual-View (565dcxr) from Optical Insights. Two laser systems were used to excite fluorophores. A green 488 nm laser from Spectrophysics, and a red 561 nm laser from Melles Riot (model: 85-YCA-615). Laser paths are modulated through an Acousto Optical Tunable Filter (AOTF) from Visitron Systems (model VS AOTF-2). The setup is equipped with different AHF filters, and we used the green/red filter in our experiments. For our imaging purposes a 100x TIRF objective with NA 1.45 Apochromat was used. Data were acquired using VisiView software version 2.1.2 from Visitron Systems.

The same setup was used to do total internal reflection fluorescence (TIRF) microscopy. TIRF illumination excites fluorophores that lay in the evanescent field generated through the

total reflection of the excitation rays. The evanescent field penetrates 150-180 nm in a sample between glass-sample interface (**Figure 18**) (Funatsu et al., 1995). TIRF microscopy enables the observation of fluorescent organelles near the membrane with low background fluorescence and increased signal to noise ratio.

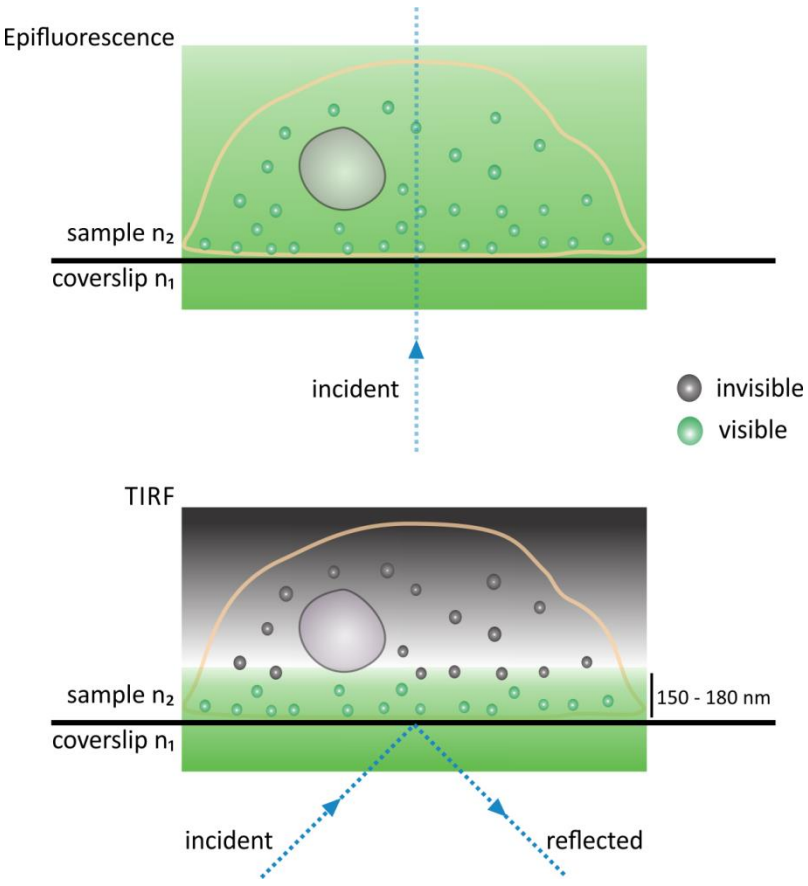


**Figure 18. Epifluorescence and TIRF microscopy**
In epifluorescence mode, whole cell is illuminated that makes all fluorophores fluorescent (**upper diagram**). In total internal reflection fluorescence (TIRF) mode, an incident light wave is totally reflected and an evanescent wave with a penetration range of 150 - 180 nm illuminates fluorophores within this region (**lower diagram**).

Additionally, a Carl Zeiss Axiovert 200 microscope with an Evolve EMCCD camera (Visitron, Germany) and a Zeiss Plan Apochromat 40x oil immersion objective (NA 1.3) was used to measure surface expression of fluorophore tagged AMPARs. A polychromator (Till Photonics) was used to excite fluorophores with 488 nm and 561 nm wavelengths. This setup is also equipped with an automated perfusion system suitable for our experimental purposes.

### 2.8.1 Detection of intracellular quenched SEP-GRIA1 organelles and image processing

To detect internal AMPAR trafficking organelles in neurites of hippocampal neurons, cells were transfected with a pCI expression vector encoding *supercliptic pHluorin* (SEP)-GRIA1 (Kopec et al., 2006). SEP is fused to the N-terminus of GRIA1 subunit positioning the fluorophore in the extracellular space or the lumen of intracellular organelles, respectively. Since SEP is a pH sensitive derivative of GFP (Miesenbock et al., 1998), it is quenched in the acidic milieu of secretory organelles, and becomes fluorescent in neutral medium like the

extracellular medium. To turn internal acidic organelles neutral, neurons were perfused with ammonium chloride ($NH_4Cl$, 45 mM) solution. $NH_3/NH_4^+$ application deprotonates organelles with acidic pH (e.g: vesicles, recycling endosomes, etc.) and changes the lumen to neutral thus unquenching SEP fluorophore and turning it visible (**Figure 19**) (Roos and Boron, 1981). Moreover, $NH_4Cl$ unquenches all SEP-GRIA1 corresponding to the total fluorescence in a neuron. $NH_4Cl$ treatment is reversible and can be washed out with extracellular solution.

***Processing and analysis:*** *We used for all image processing and analysis "Fiji" software (ImageJ 1.52e)***.** To obtain images with internal AMPAR organelles only, we first subtracted background fluorescence of all images. Then we multiplied the fluorescence intensity of the reference image (before $NH_4Cl$ treatment) by two. The multiplied reference image was then subtracted from the image treated with $NH_4Cl$ to obtain a difference image designated by "$NH_4^+$ Δimage". $NH_4^+$ Δimage corresponds to the image containing only the AMPAR internal organelles in a dendrite. (*Exemplary images shown in the results part*)

Formula after background subtraction:

$$\text{Image}_{(\text{AMPAR intrac. organelles})} = NH_4^+ \Delta\text{image} = F_{NH4Cl} - 2 \times F_{\text{baseline image}}$$

Where F corresponds to the fluorescence intensity of the image. $NH_4^+$ Δimage was then thresholded to obtain regions of interest (ROIs) corresponding to the intracellular AMPAR trafficking organelles. In experiments where the fluorescence intensity of internal AMPAR organelles had to be quantified, simple subtraction of the reference image from the image with $NH_4Cl$ treatment was done. Then ROIs obtained from the $NH_4^+$ Δimage, were used to quantify the intensities of individual puncta.

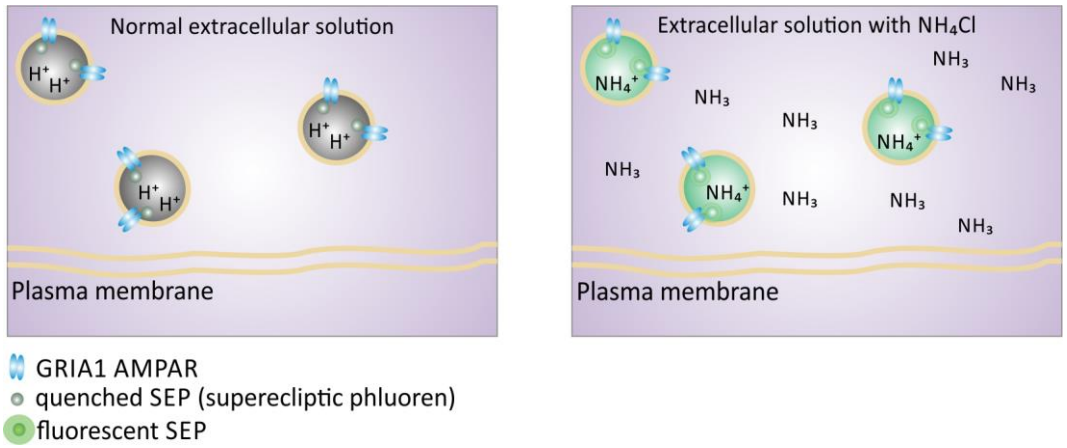


**Figure 19. $NH_4Cl$ unquenches SEP-GRIA1 in trafficking organelles**
Superecliptic phluorin (SEP)-GRIA1 receptors present in vesicles are quenched due to low pH medium (**left**). Addition of $NH_4Cl$ to extracellular medium enables $NH_3$ molecules to penetrate vesicles and bind protons ($H^+$) to become $NH_4^+$ thus making the medium neutral and SEP-GRIA1 fluoresces (**right**).

## 2.8.2 Exocytosis of AMPARs

Exocytosis of SEP-GRIA1 was studied in epifluorescence and in TIRF imaging of hippocampal neurons. SEP-GRIA1 proteins are quenched in intracellular organelles due to acidic pH, and become fluorescent when they fuse with the plasma membrane due to exposure to neutral extracellular medium (**Figure 20**). The sudden increase in fluorescence intensity is captured by an EMCCD camera, and is considered as a fusion event during exocytosis.

***Acquisition:*** Imaging frequency to acquire SEP-GRIA1 exocytotic events was 10 Hz with an exposure time of 100 ms.

***Processing and analysis:*** Exocytosis events in a movie (stack), were first visually detected and marked with ROIs in (ImageJ 1.52e). Then, fluorescence intensity variation of every event was further analyzed in Igor analysis software (Igor Pro 6) with a custom-written routine (macro) to confirm the visually detected events. Only events with an onset time of maximal ~2 s, and an amplitude exceeding four times the standard deviation (4 SD) were included in the analysis.

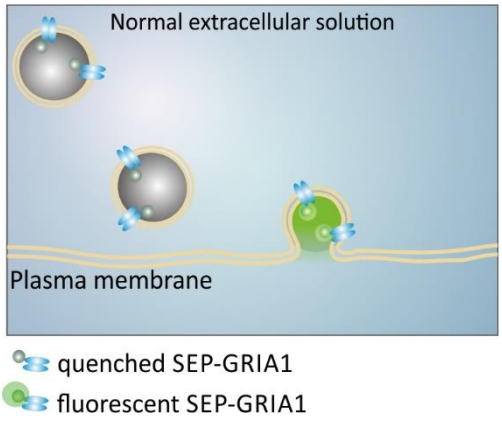


**Figure 20. Exocytosis event of SEP-GRIA1 AMPAR**
A trafficking organelle carrying SEP-GRIA1 becomes fluorescent (green) when fusing with the plasma membrane due to exposure to extracellular neutral medium after being quenched in acidic pH.

## 2.8.3 Discrimination of AMPAR surface fluorescence and image processing

In experiments where surface fluorescence had to be quantified, SEP-GIAR1 transfected neurons were perfused with low pH solution (5.5) during real time recording, and then washed out with extracellular solution that was followed by $NH_4Cl$ treatment (**Figure 21**). Low pH quenches extracellular surface SEP-GRIA1 rendering only internal unquenched SEP-GRIA1 visible (like in the endoplasmic reticulum). Moreover, $NH_4Cl$ solution was applied to obtain the total fluorescence intensities of neurons and calculate the ratio of SEP-GRIA1 surface to total intensities. Application of $NH_4Cl$ or low pH (5.5) solution was for ~3 s followed by washing out with extracellular solution.

***Processing and analysis:*** Due to variability in SEP-GRIA1 fluorescence intensities of neurons, surface fluorescence was normalized to the total fluorescence. First, background fluorescence was subtracted for all images before any processing. To obtain absolute surface fluorescence intensities, we took five frames of the reference images (before low pH (5.5) application) and averaged the fluorescence intensities. The same was done for five frames during low pH (5.5) application. Then, averaged low pH (5.5) image was subtracted from the averaged reference image. The result is an image of absolute SEP-GRIA1 surface fluorescence of a neuron. On the other hand, five frames during $NH_4Cl$ application were averaged to normalize the absolute SEP-GRIA1 surface fluorescence to the total fluorescence (image with $NH_4Cl$).

For low pH treatment: after background subtraction and averaging of frames

$$F_{surface} = F_{baseline\ image} - F_{low\ pH}$$

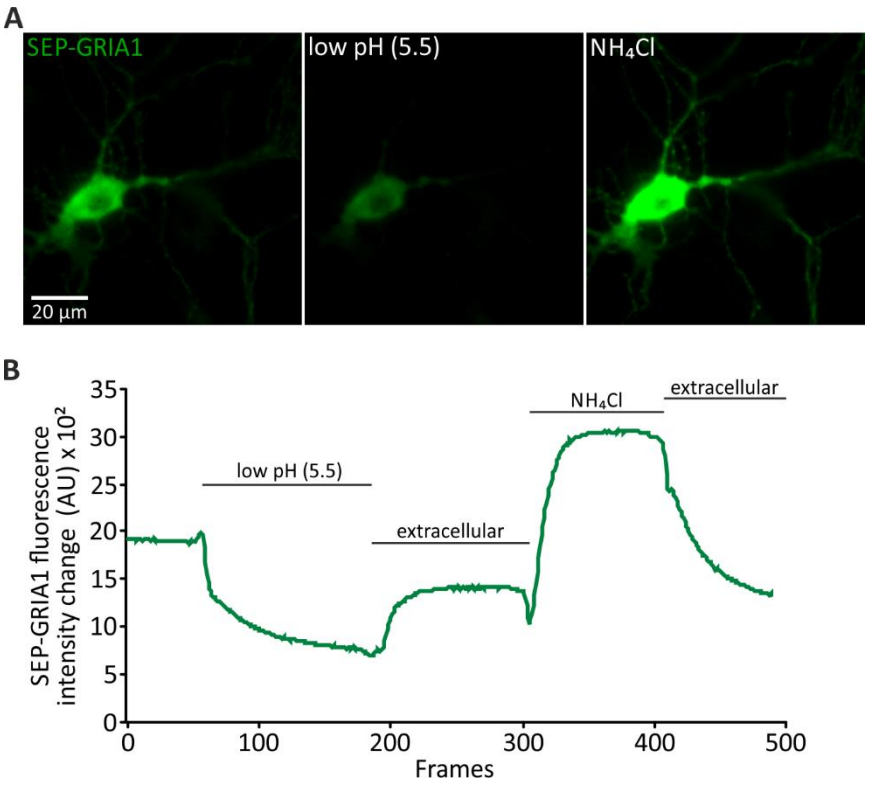


**Figure 21. Fluorescence change of SEP-GRIA1 upon low pH (5.5) and $NH_4Cl$ treatment**
(**A**) Image showing hippocampal neuron transfected with SEP-GRIA1 in extracellular medium (left), in low pH (5.5) that quenches surface fluorescence of SEP protein (middle), and in $NH_4Cl$ that unquenches all SEP molecules in the neuron (right). (**B**) Trace showing fluorescence decrease upon low pH (5.5) application, and fluorescence increase upon $NH_4Cl$ treatment.

## 2.9 Halo-tag staining of AMPARs

To study endocytosis of AMPARs, we designed a construct that stains only surface AMPARs. SEP tag of SEP-GRIA1 construct was exchanged with *HaloTag* sequence (HaloTag-GRIA1) that will be positioned in the extracellular space when the receptor is expressed on the surface membrane. HaloTag is a relatively new designed recombinant protein tag by "*Promega Biosciences"* that favors flexibility and site specific labeling with the suitable synthetic ligands. HaloTag protein is a mutated form and catalytically inactive derivative of a hydrolase enzyme. It has a size of 33 kDa and is expressed as a monomeric protein that can be fused to N- or C-terminal domains of proteins. HaloTag protein catalyzes the formation of a covalent bond with chloroalkane group containing ligand (**Figure 22**). The covalent bond formation is specific, rapid, and irreversible (Urh and Rosenberg, 2012). A HaloTag ligand contains a reactive linker and a fluorescent dye, and it may be cell permeable or impermeable. We used an impermeable Alexa Fluor 488 ligand (Promega, G1001) for surface staining of cultured hippocampal neurons. Transfected neurons were incubated with Alexa Fluor 488 ligand for 35-40 min at 15 °C and in 5 % $CO_2$, to inhibit early endocytosis during incubation. Stacks were then acquired using laser scanning microscopy (confocal imaging).

***Processing and analysis:*** Confocal images showed clear membrane staining of HaloTag-GRIA1 receptors in a neuron. Images were acquired every 4 min over 24 min. At each time point, three slices were acquired. Before quantification of fluorescence intensities, background fluorescence was subtracted. To quantify endocytosis as a function of time, scanlines or circle-like ROIs, were defined to quantify either extrasynaptic or synaptic fluorescence, respectively. For the extrasynaptic site, a scanline of length >3.2 µm was defined along a neurite during each time point and for every slice. The region was straightened to get uniform intensity traces through the membrane. All obtained traces corresponding to the region under the scanline were

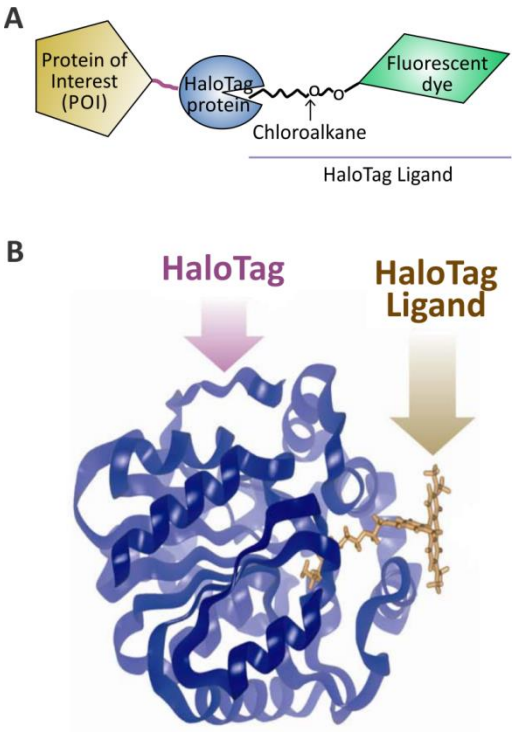


**Figure 22. Concept of HaloTag binding to synthetic ligand**
(A) HaloTag bound to a protein of interest (POI) catalyzes a covalent bond with a synthetic ligand bound to a fluorescent dye. (B) Three dimensional structure of a HaloTag protein bound to HaloTag ligand. (Urh and Rosenberg, 2012)

averaged, and the peak value was taken for the analysis. Eventually, fluorescence intensity of every chosen region was normalized to the first time point, and normalized intensities of all regions for every neuron were averaged to obtain a trace of endocytosis starting from value one. As for the synaptic site, all three slices for every time point were summed, and the image with PSD95-tagRFPt synaptic marker was thresholded to obtain ROIs corresponding to synaptic puncta. ROIs were overlaid on the summed image of HaloTag-GRIA1 for every time point, and fluorescence intensity of each synapse was then quantified. Here also, we normalized the fluorescence intensities to the first time point, and all values of all synapses in a neuron were averaged. (*Exemplary images shown in results part*)

## 2.10 Laser scanning microscopy (LSM)

A confocal Carl Zeiss LSM 780 microscope was used to examine live or fixed immunostained hippocampal neurons. We used Zeiss Efficient Navigation (ZEN) software, which enables a wide variety of controls and configurations of imaging settings to optimize acquisition. The microscope is equipped with autofocus option suitable for relatively long time imaging experiments. In addition, a heating system is used to condition the environment of the container and the head stage where the sample is mounted. Stacks and images were acquired with a C-Apochromat 40x oil objective (NA 1.2). Samples were excited with two lasers, an Argon 488 nm laser and a 561 nm DPSS (Diode Pumped Solid State) laser. Bright field images were also acquired with either wavelength through a T-PMT. In most recordings, a pinhole size of 1 AU (Airy Unit) was applied. Digital images were 12- or 16-bit-encoded. Master gain, gain, laser intensities, laser spectra, pixel size, and dwell time were determined according to the type of experiment and transfection efficiency in neurons.

We also used a confocal Carl Zeiss LSM 710 microscope for imaging immunostained neurons. Settings and features were similar to LSM 780 microscope, and it was also controlled by ZEN software. Measurements were done at room temperature with a 40x oil objective. Digital images were 12- or 16-bit-encoded and for multiple color imaging, sequential scanning was applied to avoid bleed-through or cross-talk between channels.

## 2.11 Electrophysiological measurement (Patch Clamp)

Spontaneous synaptic currents in hippocampal neurons (DIV 10-11) were obtained with whole cell patch clamp recording. Patch clamp was performed on a Carl Zeiss Axiovert 200

microscope with an Evolve EMCCD (Visitron, Germany) camera and a Zeiss Plan Apochromat 40x oil immersion objective (NA 1.3). To detect transfected neurons (SEP-GRIA1 for example), a polychromator (Till Photonics) was used for excitation. Patch pipettes pulled from borosilicate glass capillaries were chosen with size 3.5-6 MΩ for successful sealing. Neurons were voltage clamped at -70 mV. An EPC10 amplifier (HEKA Electronic) controlled by Pulse 8.5 software (HEKA Electronic) was used to record miniature excitatory postsynaptic currents (miniEPSCs or mEPSCs). mEPSCs were measured in the presence of NMDA receptor blocker D-APV (50 µM) and TTX (1 µM) to ensure only AMPAR mEPSC measurement as the drugs prevent voltage gated sodium channel and NMDAR activation, respectively. Analyzed cells had an average access resistance ($R_s$) of 8-20 MΩ and 80 % series resistance compensation. Leak-current had an average value of 20-150 pA. mEPSCs were acquired with a frequency of 50 kHz. Data was analyzed using a commercial software (Mini Analysis, Synaptosoft, Version 6.0.3). To prevent false selection of mEPSC events due to noise fluctuations, a criterion of peak amplitude >15 pA and charge >25 fC were set as thresholds for mEPSC event selection below which is considered a noise.

## 2.12 Statistical analysis

Data are presented as mean ± SEM (standard error mean), unless otherwise mentioned. For data sets with skewed distribution, the median or an average of median was considered for a statistical analysis. Normality test was done by Kolmogorov-Smirnov test. Statistical significance test was performed by *SigmaPlot* software by applying student's two-tailed *t-test* between two groups. To calculate statistical significance among three or more groups, one-way analysis of variance (ANOVA) test was applied. Significance level was assessed according to the following probability values: (*) $p<0.05$; (**) $p<0.01$; (***) $p<0.001$.

# 3. Results

Local AMPAR recycling is a dynamic process wherein receptors are shifted between a surface pool and intracellular compartments via endocytosis and exocytosis. Applying several imaging methods, we tried to address several aspects of neuronal AMPAR trafficking. In particular, we were interested in the properties of the exocytotic events occurring on the membrane of a neuron, and in the origin of the intracellular trafficking organelles of AMPARs. Furthermore, we investigated the role of AMPAR auxiliary subunits on the trafficking of receptors to and from the plasma membrane.

## 3.1 Visualization of AMPAR delivery to the plasma membrane using TIRF microscopy

We used *total internal reflection fluorescence* (TIRF) microscopy to study the dynamic transport of AMPARs in footprint areas of hippocampal neurons cultured on glass coverslips. Neurons in low density culture were transfected with pCI expression vector encoding *superecliptic pHluorin* (SEP)-GRIA1 (Kopec et al., 2006) via calcium phosphate precipitation at DIV 8-11, and imaging experiments were performed 24-48 h later. SEP is fused to the N-terminus of GRIA1 subunit positioning the fluorophore in the extracellular space or the lumen of intracellular organelles, respectively. As a pH sensitive derivative of GFP (Miesenbock et al., 1998), SEP is quenched in the acidic milieu of secretory organelles and becomes brightly fluorescent when exposed to neutral medium during exocytosis. Thus, AMPAR insertion to the plasma membrane is detected by a local, sudden increase in fluorescence intensity. In order to acquire highly resolved images of fusion events, we used an evanescent field with a penetration depth of 150 to 180 nm to illuminate footprint areas of neurons. Images were visually inspected, and fast, point shaped fluorescence signals (**Figure 23B and C**) were considered as fusion events, when the mean fluorescence increased above 4 SD (standard deviation) of the noise within 2 s. Fusion events were bounded by regions of interest (ROIs) with a constant size. We found fusion events in proximal dendrites as well as in the soma of hippocampal neurons with random distribution (**Figure 23A**). On average, 8.2±1.14 events were detected within the recording time of 6 min (**Figure 24A)**.

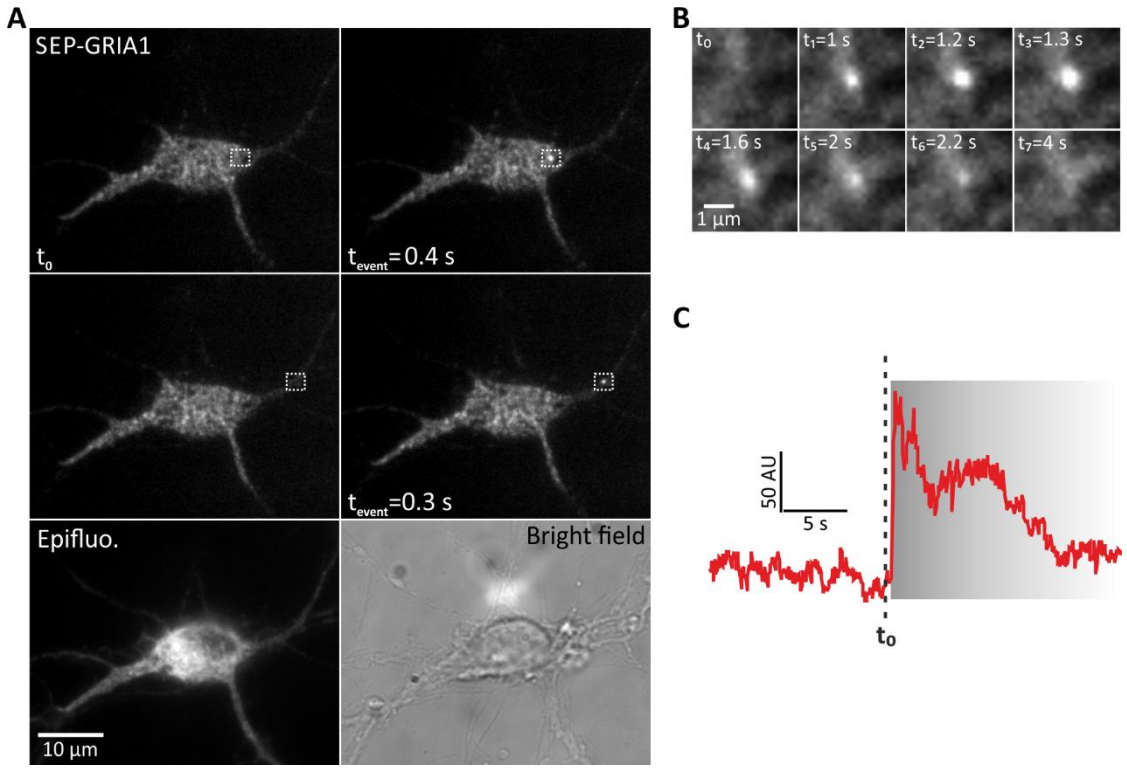


**Figure 23. AMPAR membrane insertion with TIRF microscopy in real time imaging**
(**A**) SEP-GRIA1 transfected hippocampal neuron (DIV 11) in TIRF before (**$t_0$**) and during (**$t_1$**) an exocytosis event in soma (**upper left** and **upper right,** respectively**)** and in dendrite (**middle left** and **middle right,** respectively) (indicated with a white box). Lower panel shows epifluorescence (**left**) and bright field (**right**) image of the measured neuron. (**B**) Time series of exocytotic event in A (**upper panel**). (**C**) Time course of the fluorescence intensity during the exocytosis event shown in B. Imaging frequency is 10 Hz and exposure time is 100 ms.

We analyzed rise-time, amplitude, and decay time constant of fluorescence transients putatively reporting exocytosis events. Amplitude corresponds to the peak fluorescence intensity, and rise-time reports the time from baseline level to peak fluorescence. The decay kinetics was approximated by a monoexponential function, with the time constant (τ) corresponding to the time at which ≈ 63 % of the fluorescence intensity vanished (**Figure 24B)**. We obtained a median amplitude of 45.685 AU, a median rise time of 0.8 s, and a median decay time constant of 11.503 s for putative exocytotic events (**Figure 24C, D, and E**).

The fluorescence decay may be due to a dispersion of exocytosed receptors on the plasma membrane and/or a re-acidification of the persistent secretory organelle after kiss-and-run fusion. The notion of a post-fusional dispersion of glutamate receptors is supported by the observation that fluorescent transients exhibited a lateral "broadening" on the cell surface. A typical example of such a behavior is shown in (**Figure 25A)**. To highlight the expansion of fluorescence, two circular regions of different diameters were defined around the position of an event (**Figure 25B)**. The temporal profiles of fluorescence intensity were plotted in order to

illustrate the signal redistribution. In the narrow region, fluorescence reached its maximum at an earlier time point than in the outer region since fluorophores (SEP-GRIA1) diffused from the center to the periphery (**Figure 25C**). Thus, during SEP-GRIA1 insertion receptors disperse from their point of insertion to neighboring areas. In addition, using TIRF microscopy for detection of SEP-GRIA1 exocytosis is convenient due to its high signal to noise ratio.

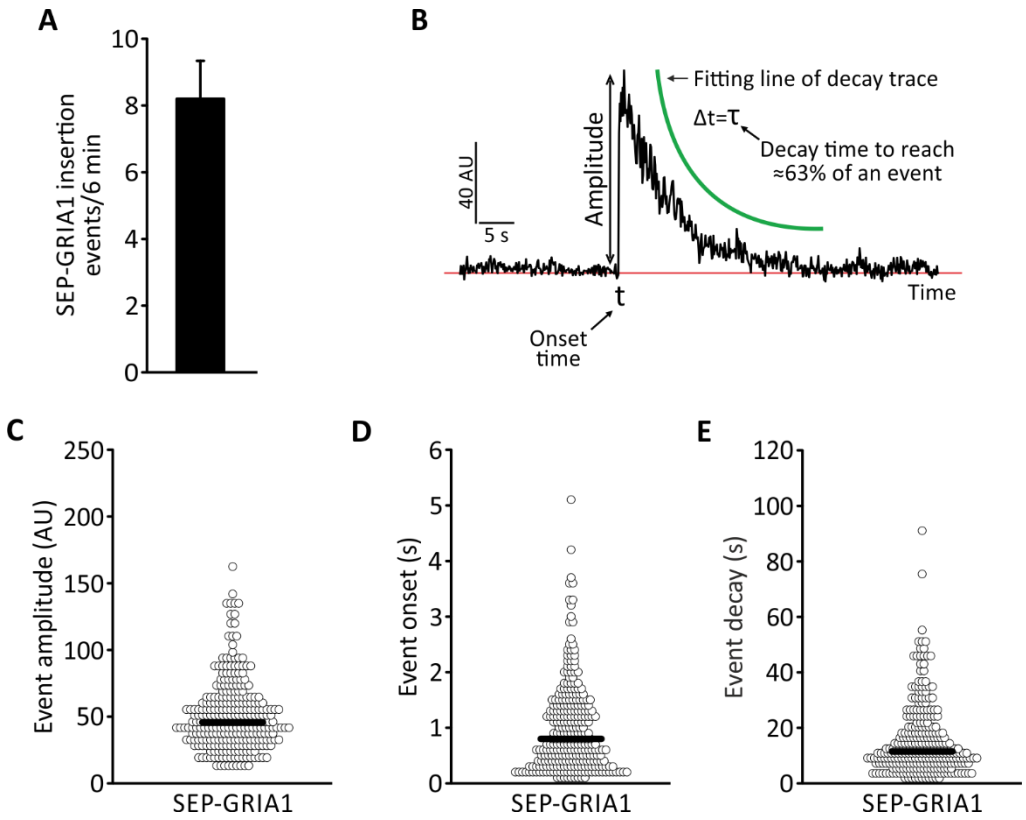


**Figure 24. Frequency and kinetic study of SEP-GRIA1 insertion events in neurons in TIRF microscopy**
(**A**) Average absolute number of SEP-GRIA1 insertion events during 6 min in neurons recorded with TIRF microscopy (number of events/6 min: 8.2±1.14). (**B**) Exemplary trace of a SEP-GRIA1 insertion event indicating its amplitude (AU), onset time (t), and a monoexponential fit of the event decay. Dot density plot illustrating distribution and median of amplitude (**C**), onsets (**D**), and decays (**E**) of SEP-GRIA1 insertion events. Median of amplitude (AU): 45.685, median of onset (s): 0.8, and median of decay (s): 11.503. n=35 cells.

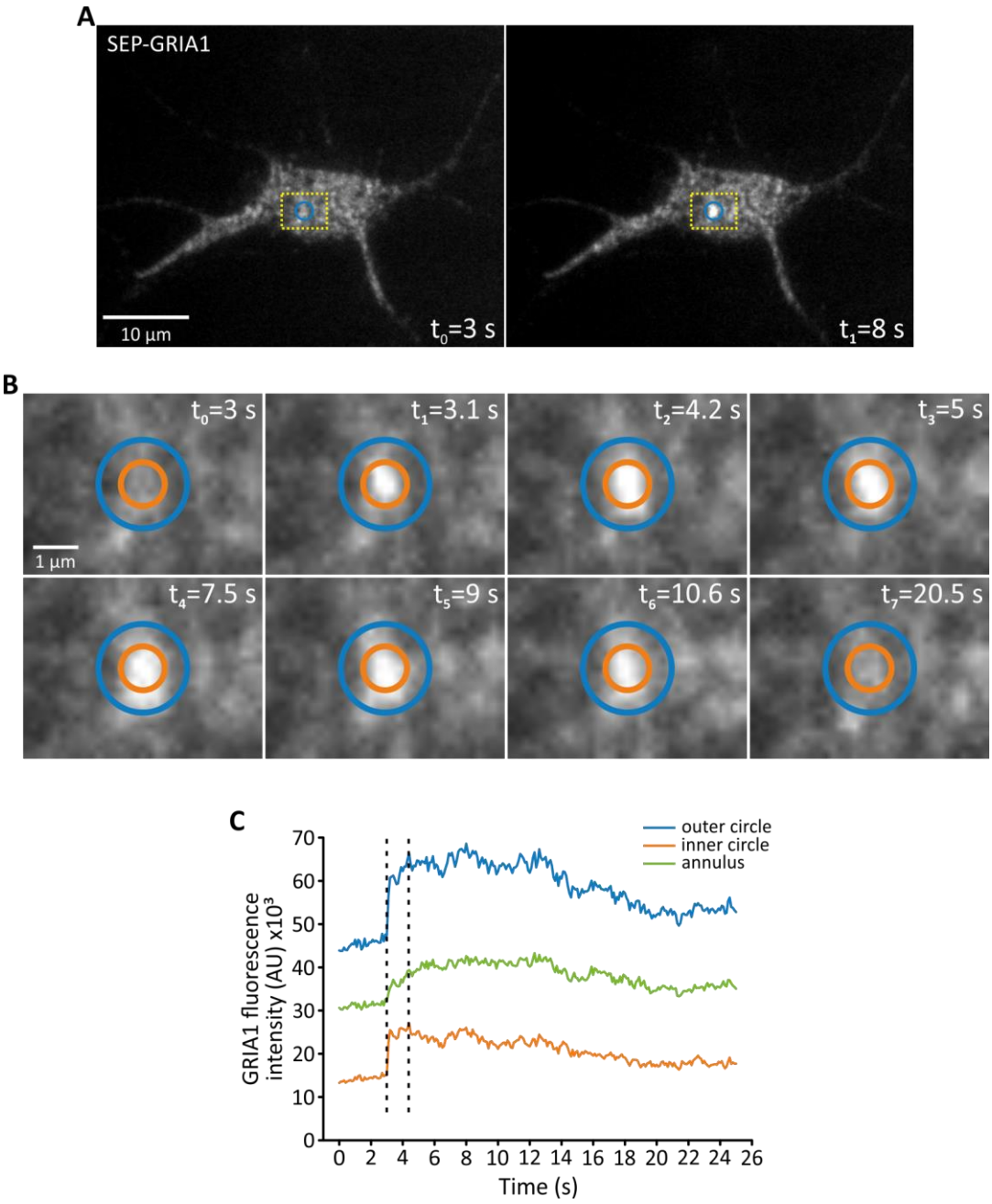


**Figure 25. Spatial dispersion of AMPAR insertion event seen in TIRF microscopy**
(**A**) Exemplary TIRF image of hippocampal neuron (DIV 11) transfected with SEP-GRIA1 before (**left**) and during (**right**) an insertion event (in blue circle). (**B**) Time series images of the insertion event occurring in **A (blue circle**). Event appears first in small orange circle (**t1**) then disperses out towards the big blue circle. (**C**) Graph showing event traces in orange and blue circle. Green trace indicates the annulus. Dotted lines indicate the margin of event onset (orange and blue) and event maximum (orange). Peak of blue trace goes beyond the margin. Size of blue circle=1.92 µm and orange circle=0.96 µm. Imaging frequency is 10 Hz and exposure time is 100 ms.

## 3.2 Activity-dependence of AMPAR delivery to the plasma membrane

Activity-dependent changes in AMPAR trafficking have been proposed to underlie synaptic plasticity (Ehlers et al., 2007; Park et al., 2004). To investigate the role of neuronal activity in delivery of AMPARs in our model system, we pharmacologically inhibited action potential generation by application of tetrodotoxin (TTX) or disrupted synaptic transmission by genetic intervention using neurons derived from *Snap25* knockout (KO) mice (Graham et al., 2002). TTX is a blocker of voltage-gated sodium channels, whose presence at (1 µM) fully suppresses evoked synaptic transmission between neurons, but still allows for spontaneous miniature release. TTX (1 µm) was chronically added to neuronal cultures 3 days before measurement as well as during the measurement. SNAP-25 is an essential part of the SNARE complex driving synaptic neurotransmitter release (Chen et al., 1999), and its ablation also abolishes evoked synaptic transmission in cultured neurons (Delgado-Martinez et al., 2007; Graham et al., 2002; Tafoya et al., 2006). Since *Snap25* heterozygous animals (SNAP25 HZ) were functionally indistinguishable from wild type (Wt) littermates (Graham et al., 2002), neurons from both types of animals were used as controls. As before, control and *Snap25* KO hippocampal neurons (DIV 8-11) were transfected with SEP-GRIA1 via calcium phosphate transfection and used 24-48 h later for TIRF imaging. We compared the frequency of SEP-GRIA1 insertion events in Wt neurons, TTX-treated Wt neurons, and untreated *Snap25* KO cells during 6 min recordings. To account for the variability in the size of neurons, the number of exocytosis events was normalized to the area of the TIRF footprint. This footprint area of a neuron primarily corresponds to the bottom somatic plasma membrane that is involved in the glass/cell interface. Interestingly, the event frequency of SEP-GRIA1 delivery was significantly reduced when neurons were pretreated with 1 µm TTX, and even more so in *Snap25* KO neurons (mean event frequency values ($x10^{-4}$); ctrl without TTX: 6.838±1.605, ctrl with TTX: 2.629±0.93, *Snap25* KO: 1.67±0.396, **Figure 26B**).

The decrease in neuronal activity was also reflected in the fusion kinetics of exocytosis events. As before, we determined amplitude, rise-time, and decay time constant for all detected fusion events in the three experimental groups. Event amplitude was significantly reduced in TTX-treated neurons and in *Snap25* KO cells (median of amplitude (AU): ctrl without TTX: 42.996, ctrl with TTX: 32.386, *Snap25* KO: 28.253, **Figure 26C**), as found by statistical analysis with ANOVA test. In addition, the decay time constant was significantly higher in TTX-treated neurons than in controls, whereas no difference in *Snap25* KO neurons was

observed (median of decay (s): ctrl without TTX: 7.213, ctrl with TTX: 9.806, *Snap25* KO: 10.118, **Figure 26D**). These data show that the loss of synaptic/neuronal activity in *Snap25* KO and TTX-treated neurons clearly influences GRIA1 trafficking. The stronger reduction in exocytosis events in *Snap25* KO cells than in TTX-treated neurons may indicate that SNAP25 also plays a role in the fusion machinery mediating the exocytosis of AMPAR-containing transport organelles.

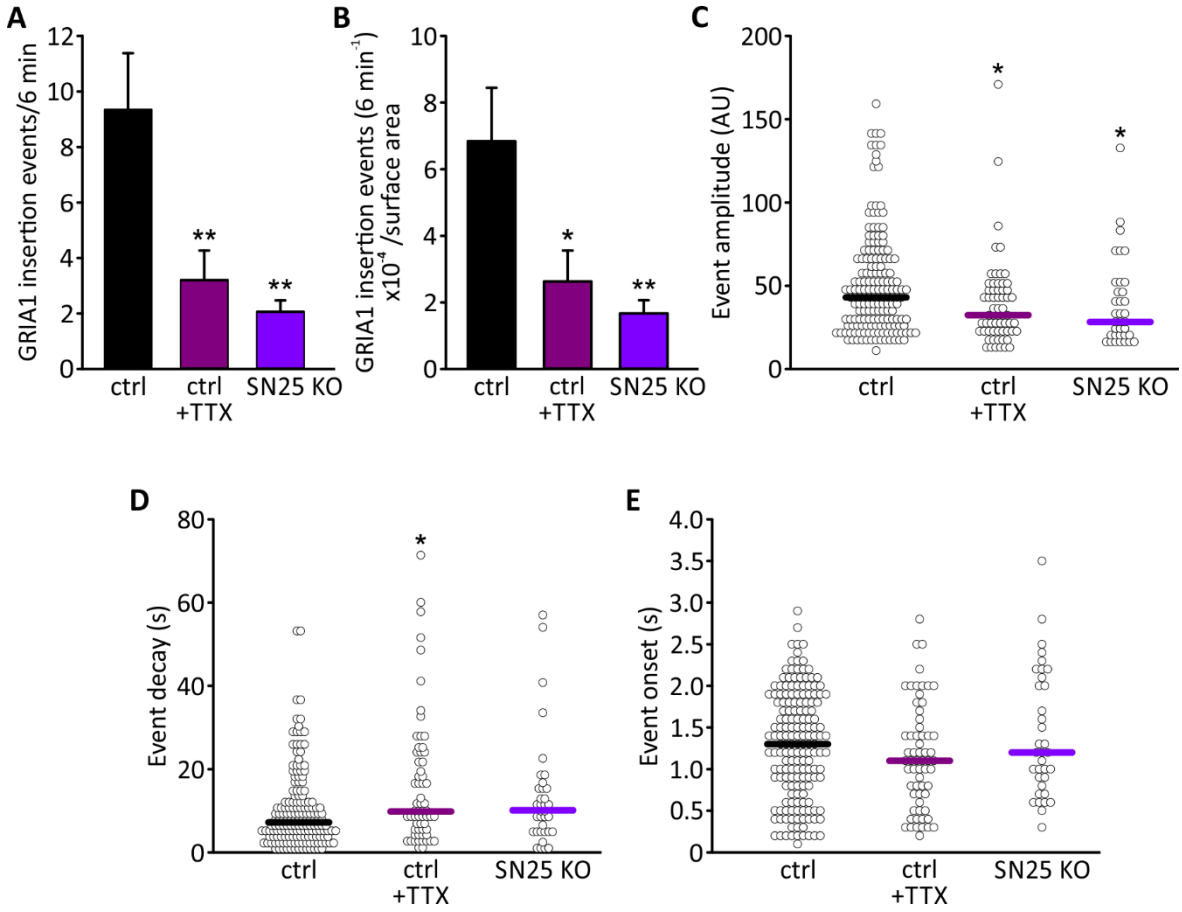


**Figure 26. AMPAR exocytosis detected in TIRF decreases with TTX and in Snap25 knockout neurons** (**A**) Average of absolute number of insertion events of SEP-GRIA1 in 6 min. Ctrl without TTX: 9.333±2.048, ctrl with TTX: 3.2±1.07, *Snap25* KO without TTX: 2.058±0.415. (**B**) Average insertion events of SEP-GRIA1 with and without TTX and in *Snap25* KO neurons were normalized to surface area of TIRF footprint of neuron (x$10^{-4}$). Data are mean ± SEM. Statistical analysis was assessed with one way ANOVA followed by pairwise comparison with the Tukey test. (**p*<0.05, ***p*<0.01). (**C**) Dot density plot illustrating distribution and median of amplitudes(**C**), decays (**D**), and onsets (**E**) of SEP-GRIA1 insertion events. Median of onset (s): ctrl without TTX: 1.3, ctrl with TTX: 1.1, *Snap25* KO without TTX: 1.2. Statistical analysis was assessed with one way ANOVA followed by pairwise comparison with Kruskal-Wallis on ranks test. (**p*<0.05). Ctrl without TTX: n=18 cells, ctrl with TTX: n=20 cells, and *Snap25* KO: n=17 cells.

Previous studies showed that AMPARs are mainly transported in recycling endosomes (REs) (Ehlers*, 2000). To verify that the fusion events detected in our model system indeed

originate from recycling endosomes, we repeated the experiment using a fluorophore-tagged transferrin receptor (TfR) as a marker for REs (Mukherjee et al., 1997). For this purpose, we cotransfected hippocampal neurons (DIV 8-11) with pCI SEP-GRIA1 and pCDNA3 TfR-tagRFPt, and investigated the colocalization of internal SEP-GRIA- and TfR-tagRFPt-containing organelles by TIRF imaging. However, due to the high density of different organelles in soma, we were not able to differentiate specific sub-compartments carrying TfR-tagRFPt (**Figure 27**). Therefore, we continued our investigation in neuritic structures where individual endosomal compartments are more segregated in space. Since neurites are not resting flat on the culture coverslips, imaging of neurites in TIRF mode is not feasable. Therefore, we switched to epifluorescence imaging of hippocampal neurites to overcome these obstacles.

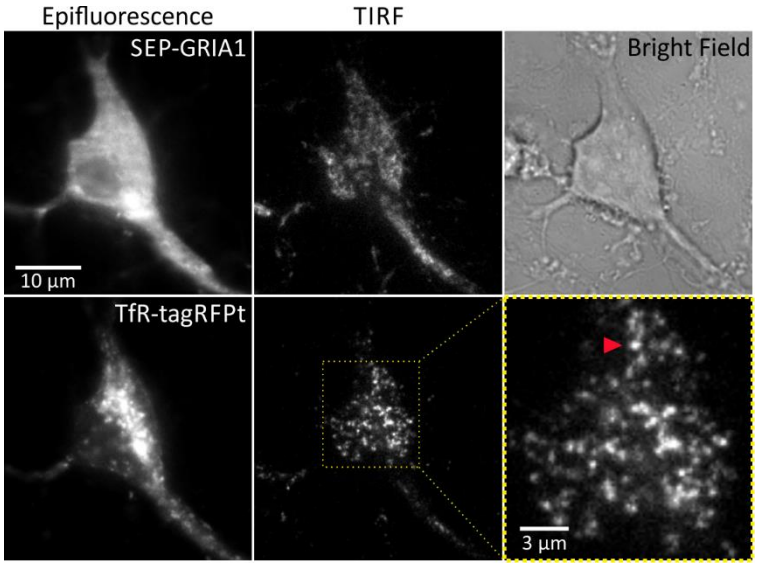


**Figure 27. TfR-tagRFPt trafficking organelles observed in TIRF microscopy in hippocampal neurons**
Epifluorescence image of hippocampal neuron (DIV 8) cotransfected with SEP-GRIA1 (**upper left**) and TfR-tagRFPt (**lower left**). Surface SEP-GRIA1 expression (**upper middle**) and internal TfR-tagRFPt REs (**lower middle**) of neuron seen in TIRF. Enlarged TIRF image of TfR-tagRFPt indicating a RE with a red arrowhead (**lower right**). Bright field image of the neuron (**upper right**). Exposure time=100 ms

## 3.3 AMPAR membrane insertion captured in real-time under epifluorescence imaging in hippocampal neurites

While dendrites of dissociated neurons are not accessible for TIRF microscopy, the small dimensions of dendritic structures still allow to resolve local fluorescence transients during insertion events by epifluorescence microscopy as illustrated in **Figure 28**. To characterize AMPAR delivery in dendrites, we transfected Wt hippocampal neurons (DIV 8-11) with SEP-GRIA1 and recorded 6 min long movies of selected dendritic arbors 24 - 48 h post transfection. We observed instantaneous fluorescence signals whose kinetic properties were largely identical to the signals previously found in TIRF experiments (**Figure 28A, B and C**), in accord with earlier work by Yudowski et al. (2007). As before, we quantified the amplitude, rise-time, and decay time constant. Frequency distribution of event amplitude showed that the majority of events had an intensity of 52.234 AU. As for the event rise-time, most of the events exhibited a time-to-peak 0.3 s. Fusion events differed in their duration from short to long, thus exhibiting variable decay time constants ranging between 0.5 and 23 s (median of decay time: 9.182 s) (**Figure 29A, B and C**).

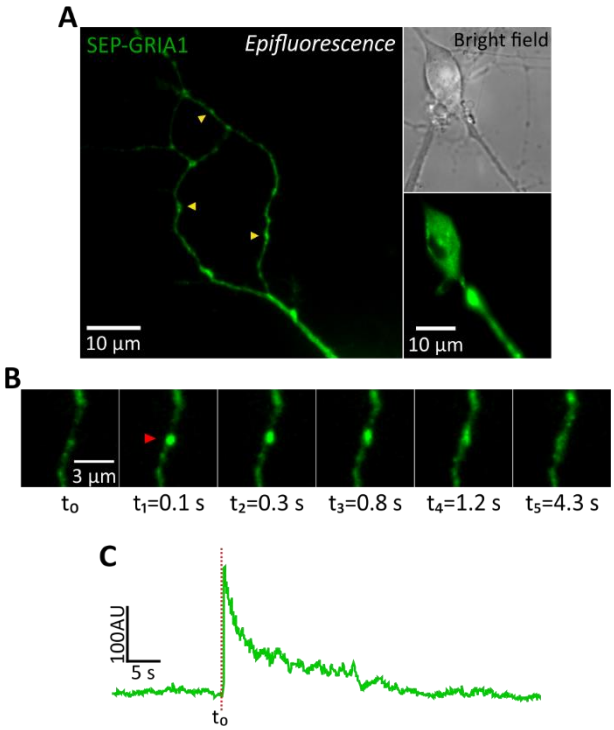


**Figure 28. Membrane insertion of AMPARs detected in real time epifluorescence recording**
(**A**) Exemplary hippocampal neuron (DIV 11) transfected with SEP-GRIA1 showing accumulation of GRIA1 receptors at synaptic sites (yellow arrows) in neurite (**left**). Soma of the same neuron seen in bright field (**upper right**) and epifluorescence (**lower right**). (**B**) Time series of an event. $t_1$ indicates the onset of the event shown by a red arrowhead. (**C**) Exemplary trace of AMPAR insertion event with decay: 12.94 s. Imaging frequency is 10 Hz with 100 ms exposure time.

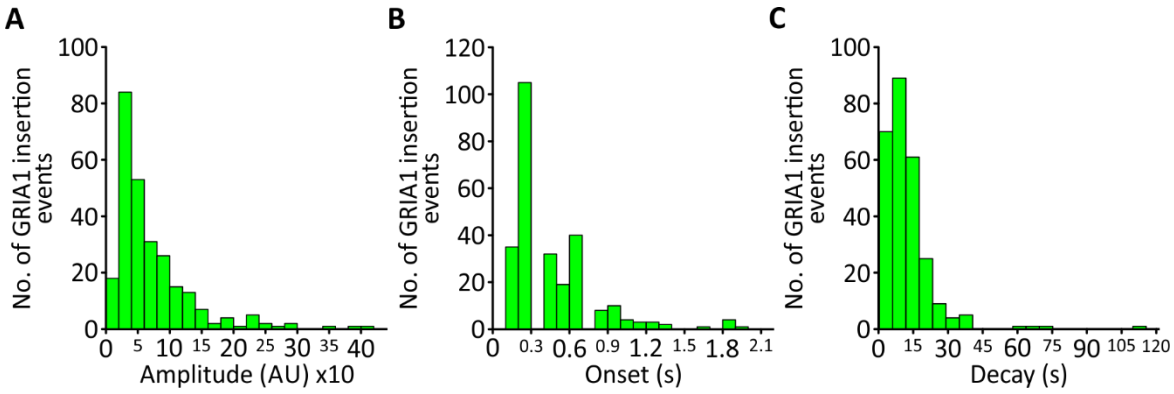


**Figure 29. Fusion kinetics of SEP-GRIA1 insertion in dendritic structures**
Frequency distribution histogram illustrating event amplitude (**A**), event onset (**B**), and event decay (**C**) of SEP-GRIA1 transient fusion events in hippocampal neurites (9-11 DIV). n=24 cells

## 3.4 SEP-GRIA1 overexpression increases spontaneous synaptic transmission (mEPSC)

In the previous experiment, we observed active SEP-GRIA1 receptor insertion in the plasma membrane of dendrites and accumulation at synaptic-like structures. To investigate the effect of synaptic SEP-GRIA1 accumulation on synaptic transmission upon overexpression in hippocampal neurons, we compared miniature excitatory postsynaptic currents (mEPSCs) between transfected and non-transfected neurons. *Postsynaptic density protein95* (PSD95)-tagRFPt was cotransfected with SEP-GRIA1 to confirm that AMPARs concentrated on synaptses (**Figure 30A**). Previously, it had been shown that GRIA1 overexpression increases channel rectification due to formation of homomers (Granger et al., 2013; Shi et al., 1999). We performed whole-cell patch clamp recordings in neurons cultivated for 10-11 days and registered mEPSCs for 2 min after breaking in a neuron (**Figure 30B, C, and D**). Mass cultures were acutely treated with TTX (1 µm) during measurement to inhibit spike-mediated synaptic transmission. Only green cells corresponding to SEP-GRIA1 transfected neurons were patch clamped to be compared afterwards with nontransfected neurons of control cultures. Pipette resistance was 3.5-6 MΩ, and cells analyzed had an access resistance between 8 and 20 MΩ. Only mEPSCs with peak amplitude >15 pA and charge >25 fC were included in the analysis to exclude noise recording. Statistical analysis shows that frequency and amplitude increased significantly in transfected neurons compared to non-transfected neurons (frequency (Hz): non-transfected: 0.915±0.183, SEP-GRIA1: 1.747±0.296; amplitude (pA): non-transfected: 27.847±2.421, SEP-GRIA1: 38.482±3.553; **Figure 30E and F**). In addition, SEP-GRIA1

overexpression increased the charge of mEPSCs (charge (fC): ctrl: 63.218±5.326, SEP-GRIA1: 82.772±6.41, **Figure 30G**). However, decay and rise time were not significantly changed when SEP-GRIA1 was overexpressed (**Figure 30H and I**). Since previous studies showed an effect of GRIA1 overexpression on synaptic transmission, abundance of homomers, and channel properties (Shi et al., 1999), it is very likely that spontaneous mEPSC frequency and amplitude were increased due to increased synaptic clustering.

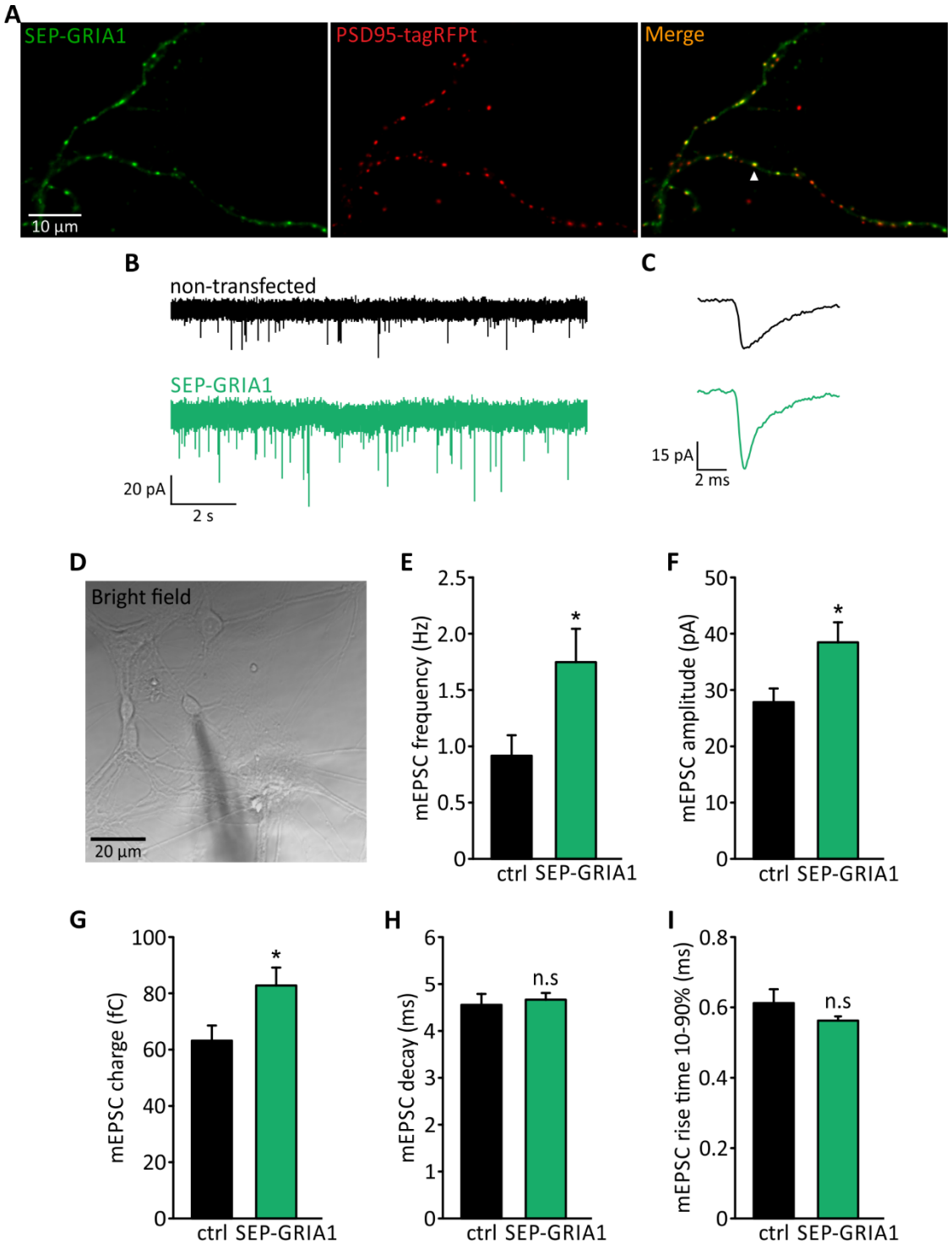

**Figure 30. SEP-GRIA1 overexpression in hippocampal neurons increases mEPSC frequency and amplitude**
(**A**) Exemplary image of coexpressed SEP-GRIA1 and PSD95-tagRFPt in hippocampal neuron. Merged image (**right**) shows colocalization between green SEP-GRIA1 (**left**) and red PSD95-tagRFPt (**middle**) puncta. (**B**) Exemplary traces of spontaneous mEPSCs of non-transfected (black) and SEP-GRIA1 (green) transfected neurons. (**C**) Representative trace of an average mEPSC event in non-transfected (black) and SEP-GRIA1 (green) transfected neurons. (**D**) Bright field image showing a neuron with a patch pipette. (**E**) Overexpression of SEP-GRIA1 in hippocampal neurons (DIV 9-12) causes a significant increase in mEPSC frequency, amplitude (**F**), and charge (**G**). mEPSC decay (**H**) and rise time (**I**) are not significantly changed. Control condition (ctrl) corresponds to non-transfected hippocampal neurons. decay (ms): ctrl: 4.555±0.232, SEP-GRIA1: 4.665±0.142; rise time (ms): ctrl: 0.612±0.039, SEP-GRIA1: 0.562±0.012. Data are mean ± SEM. Ctrl: n=14, SEP-GRIA1: n=13. (*p<0.05).

## 3.5 Dendritic AMPA receptor delivery via recycling endosomes

Following up on our previous experiments in TIRF microscopy, we further investigated whether constitutive AMPAR delivery to the dendritic surface is predominantly due to fusion of receptor-containing recycling endosomes with the plasma membrane. Organelles belonging to the secretory or endosomal pathways are characterized by an acidic pH, and thus the fluorescence of SEP-tagged AMPARs in these structures should be quenched. To visualize the intracellular AMPAR pool in these compartments, we neutralized the luminal milieu by application of ammonium chloride ($NH_4Cl$, 50 mM), which can enter the intracellular compartments as $NH_3$ (**Figure 31Aa, Ab and Ac**). Hippocampal neurons were transfected with SEP-GRIA1 on DIV 8-11 and were used for imaging experiments 24-48h later. Difference pictures were generated to isolate the intracellular fluorescence signal after SEP-dequenching. Fluorescence intensity of the image before $NH_4Cl$ application (baseline fluorescence) was first multiplied by two (2x baseline fluorescence) and then subtracted from the image during $NH_4Cl$ treatment (total fluorescence). The resulting image, which we denoted by "$NH_4^+$ Δimage", was thresholded to generate regions of interest (ROIs) corresponding to the individual puncta of AMPAR organelles (**Figure 31B**) (*Explained in section 2.8.1 in "materials and methods"*).

A strong contribution of endosomal recycling to the maintenance of the AMPAR surface pool was postulated based on previous work (Ehlers*, 2000). To estimate the overlap between the AMPAR-containing dendritic organelles and the endosomal recycling system in our model system, we cotransfected neurons (DIV 8-11) with SEP-GRIA1 and TfR-tagRFPt and visualized internal AMPARs by $NH_4Cl$ application as described above. We performed colocalization analysis between internal SEP-GRIA1-positive organelles of the "$NH_4^+$ Δimage" and TfR-tagRFPt-positive REs (**Figure 32A**, filled arrowheads indicate colocalized puncta). A high colocalization with ~ 79 % between SEP-GRIA1 and TfR-tagRFPt puncta was obtained.

On the other hand, only ~ 25 % TfR-tagRFPt was colocalized with SEP-GRIA1 puncta (Manders' coefficient: GRIA1 to TfR: 0.79±0.05; TfR to GRIA1: 0.25±0.04, **Figure 32B**). Moreover, a Pearson's coefficient of 0.46 indicates only a weak linearity between the signal intensities of SEP-GRIA1 and TfR-tagRFPt-positive puncta (Pearson's coefficient: 0.46±0.04, **Figure 32C**). Based on this data, we conclude that most intracellular SEP-GRIA1-positive

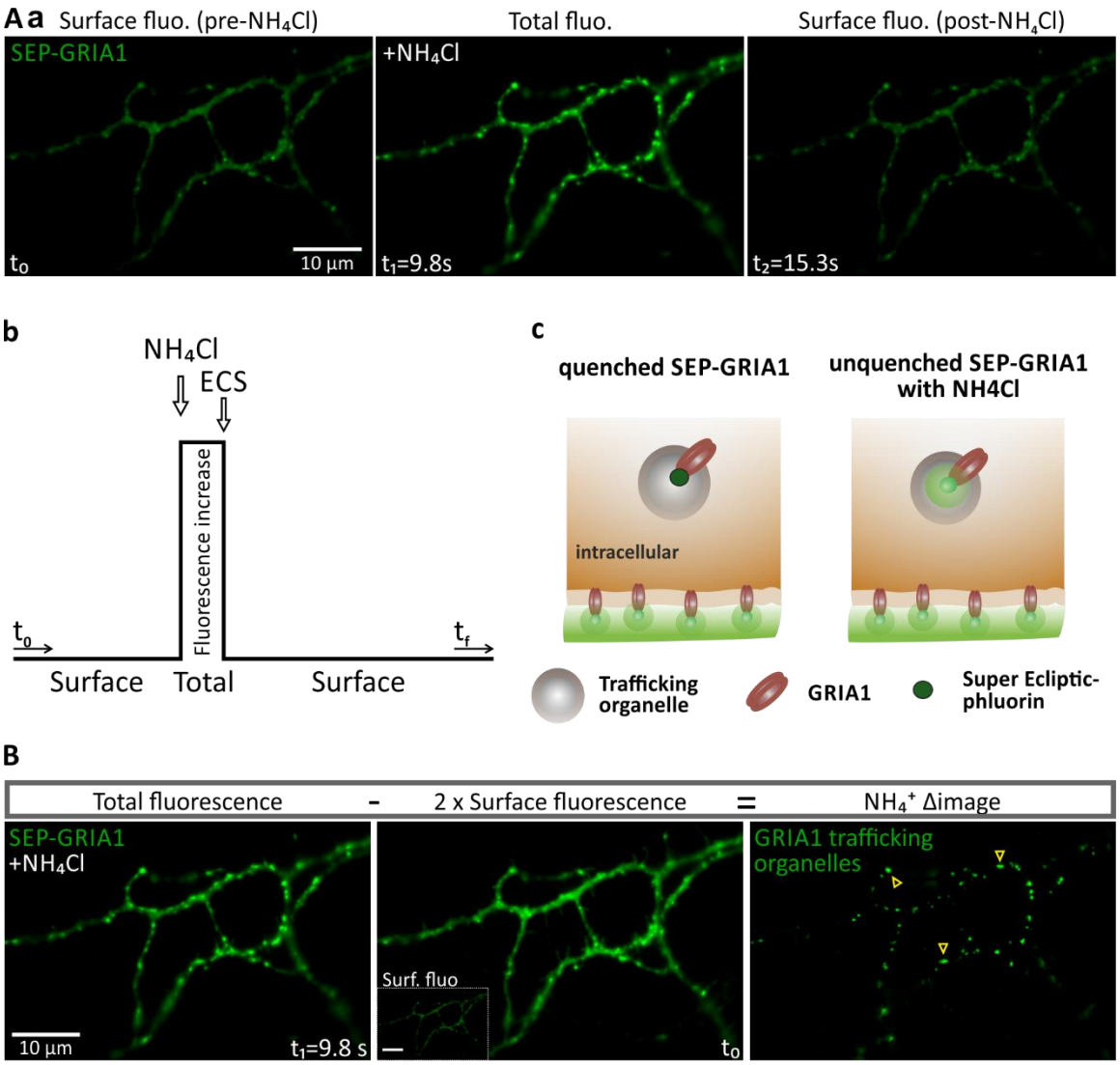


**Figure 31. Internal SEP-GRIA1 unquenching and detection of GRIA1-containing organelle**
(**A**) Epifluorescence images of dendrites of a transfected hippocampal neuron (DIV 13) with SEP-GRIA1 before $NH_4Cl$ (**left**), during $NH_4Cl$ (**middle**), and after $NH_4Cl$ (**right**) treatment. Left and right images correspond to basal surface fluorescence and middle image correspond to the total fluorescence (surface and internal) of the dendritic structure (**a**). (**b**) Schematic drawing showing protocol of ammonium chloride treatment. (**c**) Schematic drawing illustrating a quenched SEP-GRIA1 in a trafficking organelle (**left**) and fluorescent (unquenched) on the surface (**both**) or with $NH_4Cl$ (**right**). SEP tag is bound to the N-terminus of AMPAR. (**B**) Detection of internal GRIA1 trafficking organelles. Image of (2x) surface fluorescence (pre-$NH_4Cl$ treatment) (**middle**) is subtracted from the total fluorescence ($NH_4Cl$ treated image) (**left**). The subtracted image, designated by "$NH_4^+$ Δimage" shows typical GRIA1 internal trafficking organelles (green puncta) indicated by yellow arrowheads (**right**). Basal surface fluorescence of neurites shown in small white dotted box (**middle**, scale bar=10 µm). Imaging frequency is 10 Hz with 100 ms exposure time.

organelles represent recycling endosomes but that GRIA1-marked endosomes only constitute a subset of the population of REs in dendrites.

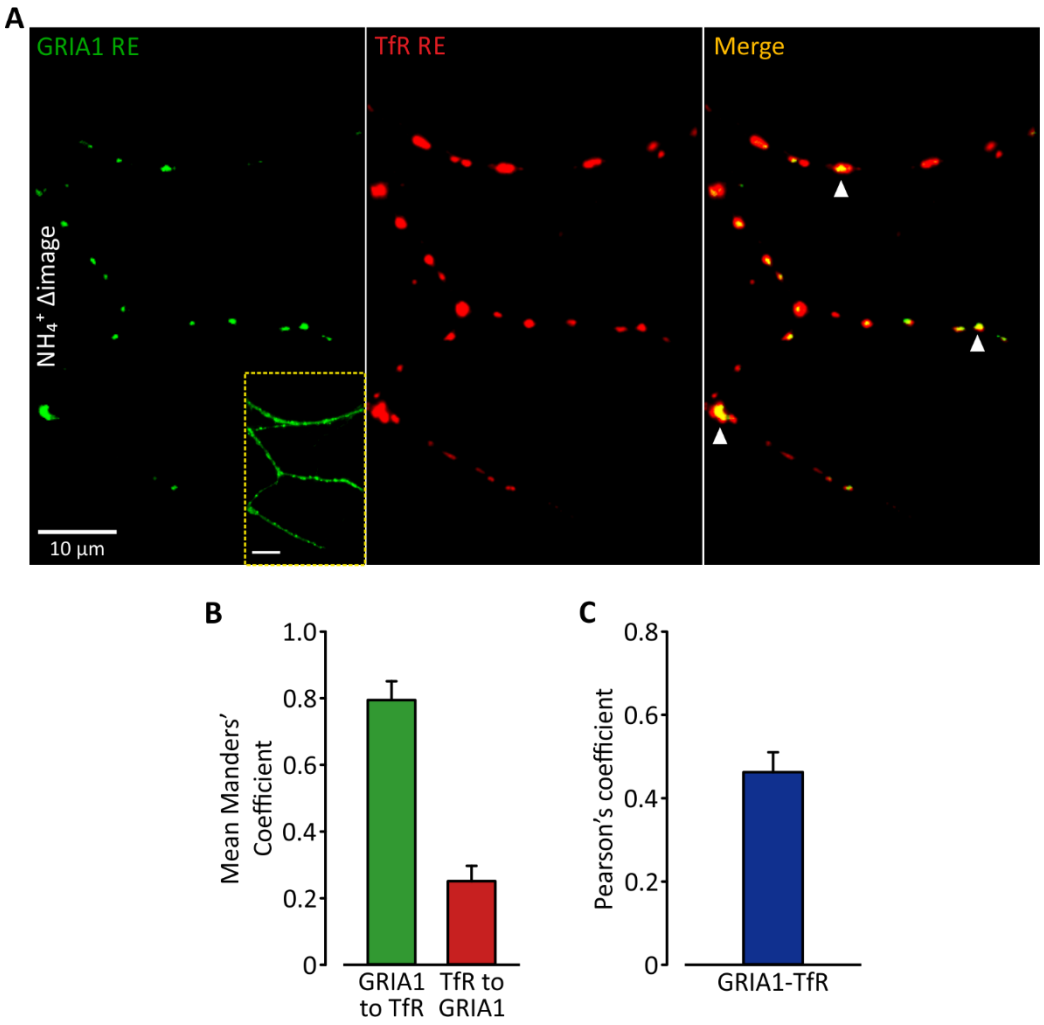


**Figure 32. AMPA-type glutamate receptors are stored in recycling endosomes (REs)**
(**A**) Exemplary image of SEP-GRIA1 (**left**, $NH_4^+$ Δimage) and transferrin receptor (TfR-tagRFPt) (**middle**) recycling endosomes in cotransfected hippocampal neurons (DIV 11) with SEP-GRIA1 (green) and TfR-tagRFPt (red). Image with neurites expressing surface SEP-GRIA1 is shown in yellow box (**left,** scale bar 10 µm). Colocalized SEP-GRIA1 REs with TfR-tagRFPt REs are indicated with white filled arrowheads. Merged image shows the colocalization of SEP-GRIA1 and TfR-tagRFPt puncta. White open arrowheads indicate absence of GRIA1 green puncta in the presence of TfR red puncta (**right**). (**B**) Mean Manders' coefficient of GRIA1 to TfR puncta (green bar), and of TfR to GRIA1 puncta (red bar). (**C**) Quantification of Pearson's coefficient (**right**). Data are mean ± SEM. n=11. ($NH_4^+$ Δimage explained in **Figure 31**)

During dual view imaging, we had to make sure that no bleed-through was occurring between red (561 nm) and green (488 nm) fluorescent signals. We transfected hippocampal neurons either with TfR-tagRFPt or with SEP-GRIA1 and performed imaging experiments on the second day after transfection. When TfR-tagRFPt transfected neurons were excited with 561 nm laser, maximal red fluorescence was seen in the red channel, whereas virtually no

fluorescence was seen in the green channel (normalized fluorescence intensity: 0.00263±0.00231). In reverse, when TfR-tagRFPt transfected neurons were excited with 488 nm laser minimal fluorescence was seen in the green channel (normalized fluorescence intensity: 0.0795±0.0524). Fluorescence intensities were normalized to the intensity captured in red channel with 561 nm excitation in case of TfR-tagRFPt transfected cells (**Figure 33A and**

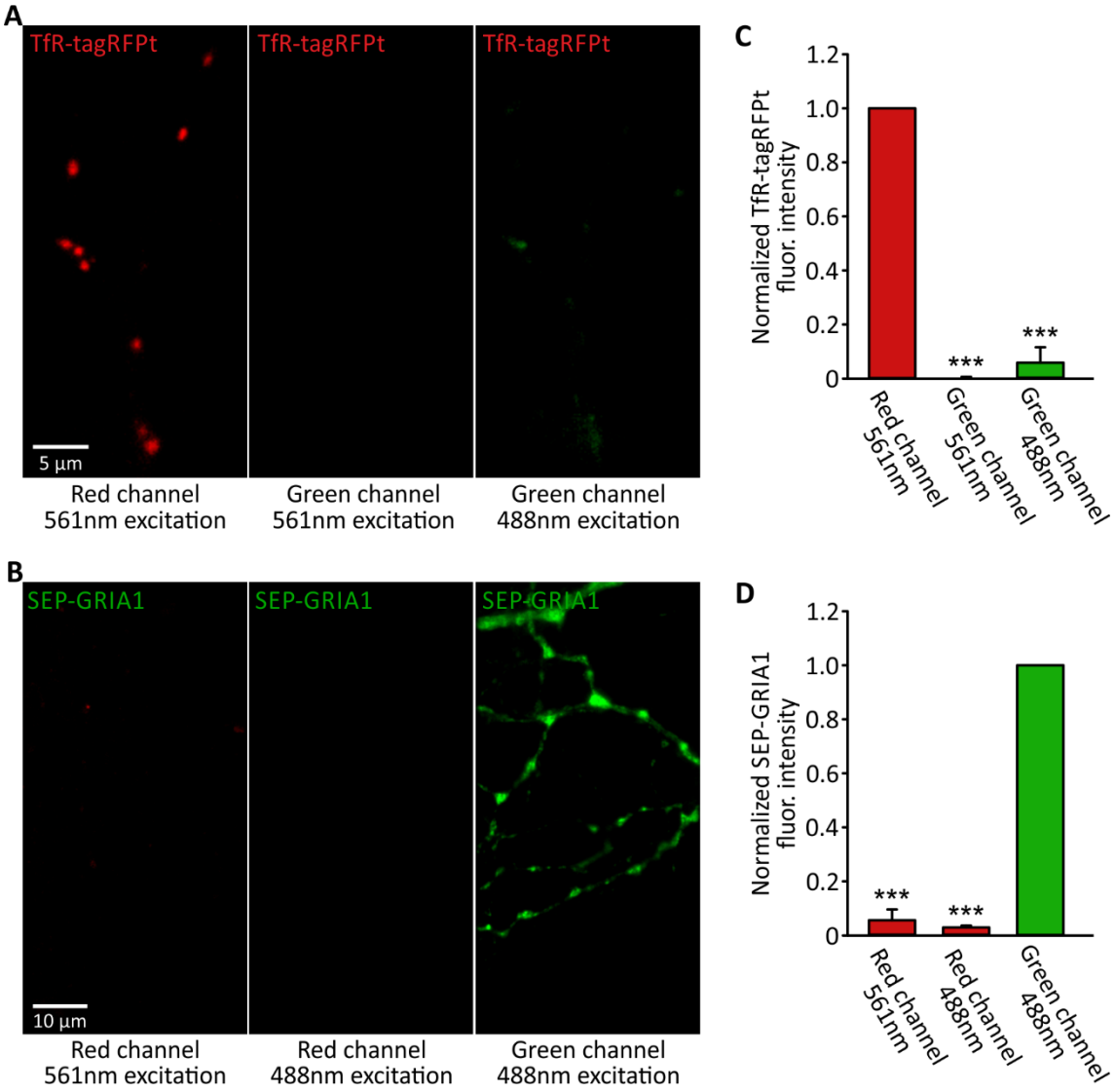


**Figure 33. TfR-tagRFPt and SEP-GRIA1 bleed-through is minimal in dual view imaging**
(**A**) Exemplary image of neurites of transfected hippocampal neuron (DIV 9) with TfR-tagRFPt shows red puncta in red channel when excited with 561 nm (**left**), no fluorescence in green channel when excited with 561 nm (**middle**), and also no fluorescence in green channel when excited with 488 nm (**right**). (**B**) Exemplary image of neurites of transfected hippocampal neuron (DIV 9) with SEP-GRIA1 shows green surface fluorescence in green channel when excited with 488 nm (**right**), no fluorescence in red channel when excited with 488 nm (**middle**), and also no fluorescence in red channel when excited with 561 nm (**right**). (**C**) Graph of averages of TfR-tagRFPt fluorescence intensities in red and green channel with 561 nm and 488 nm excitation. Fluorescence intensities were normalized to red fluorescence intensity in red channel. (**D**) Graph of averages of SEP-GRIA1 fluorescence intensities in red and green channel with 561 nm and 488 nm excitation. Fluorescence intensities were normalized to green fluorescence intensity in green channel. Data are mean ± SEM. n=3 in both conditions. Exposure time=100 ms. Statistical analysis was assessed with one way ANOVA followed by pairwise comparison with Student-Newman-Keuls test. (***p<0.001).

**C**). On the other hand, when SEP-GRIA1-transfected neurons were excited with 488 nm laser, maximal green fluorescence was seen in the green channel whereas minimal fluorescence was seen in the red channel (normalized fluorescence intensity: 0.0302±0.00376). Very low fluorescence intensity was also seen when the same neurons were excited with 561 nm laser in red channel (normalized fluorescence intensity: 0.0567±0.0229). Fluorescence intensities were normalized to the intensity captured in green channel with 488 nm excitation in case of SEP-GRIA1 transfected cells (**Figure 33B and D)**. This control experiment shows that negligible bleed through effect between red and green fluorescence emission exists when using dual view emission filters.

## 3.6 AMPAR insertion events occur near SEP-GRIA1-positive recycling endosomes

Having independently demonstrated the occurrence of AMPAR insertion events and SEP-GRIA1-loaded REs in dendrites of hippocampal neurons, we wondered whether we could also directly detect the fusion of AMPAR-containing REs with the surface membrane during real-time epifluorescence imaging. Therefore, we investigated the spatial relationship between insertion events and internal TFR-positive REs. Again, hippocampal neurons (DIV 8-11) were cotransfected with SEP-GRIA1 and TfR-tagRFPt for simultaneous live imaging of both, GRIA1 fusion events (green channel) and TfR-positive REs (red channel). To align the position of the fusion site with the localization of REs in the dendrites, we selected movie frames showing the peak fluorescence signal of each fusion event and analyzed the placements of surrounding tagRFPt-marked REs by line-scans (**Figure 34A and B**). Local maxima in longitudinal line scans through the dendrite were considered to really represent REs, if the red peak signal was higher than 5 SD of the baseline. RE and fusion event were considered colocalized, if the distance between RE signal peak and event fluorescence peak was less than 1.1 µm. Using this criteria, we found that 82 % of SEP-GRIA1 positive signals were colocalized with existing underlying TfR-tagRFPt-positive REs (**Figure 34C and D**).

We also investigated potential correlated changes of RE fluorescence during fusion events. An increase in local tagRFPt-fluorescence would in fact indicate dynamic alterations in the structure/size of REs (which might also affect the SEP-GRIA1 signal), while a decrease in tagRFPt-fluorescence reports the transition of TfRs from RE to the plasma membrane or even a collapse of the RE during fusion. However, no fluorescence increase in most red traces was

observed during green fluorescence increase of SEP-GRIA1 insertion (**Figure 34C and D**). The observation that the tagRFPt- signal persisted in most recordings indicates that REs persist after transient fusion, and that the fluorescence decay mostly reports re-acidification of the RE lumen after exocytosis.

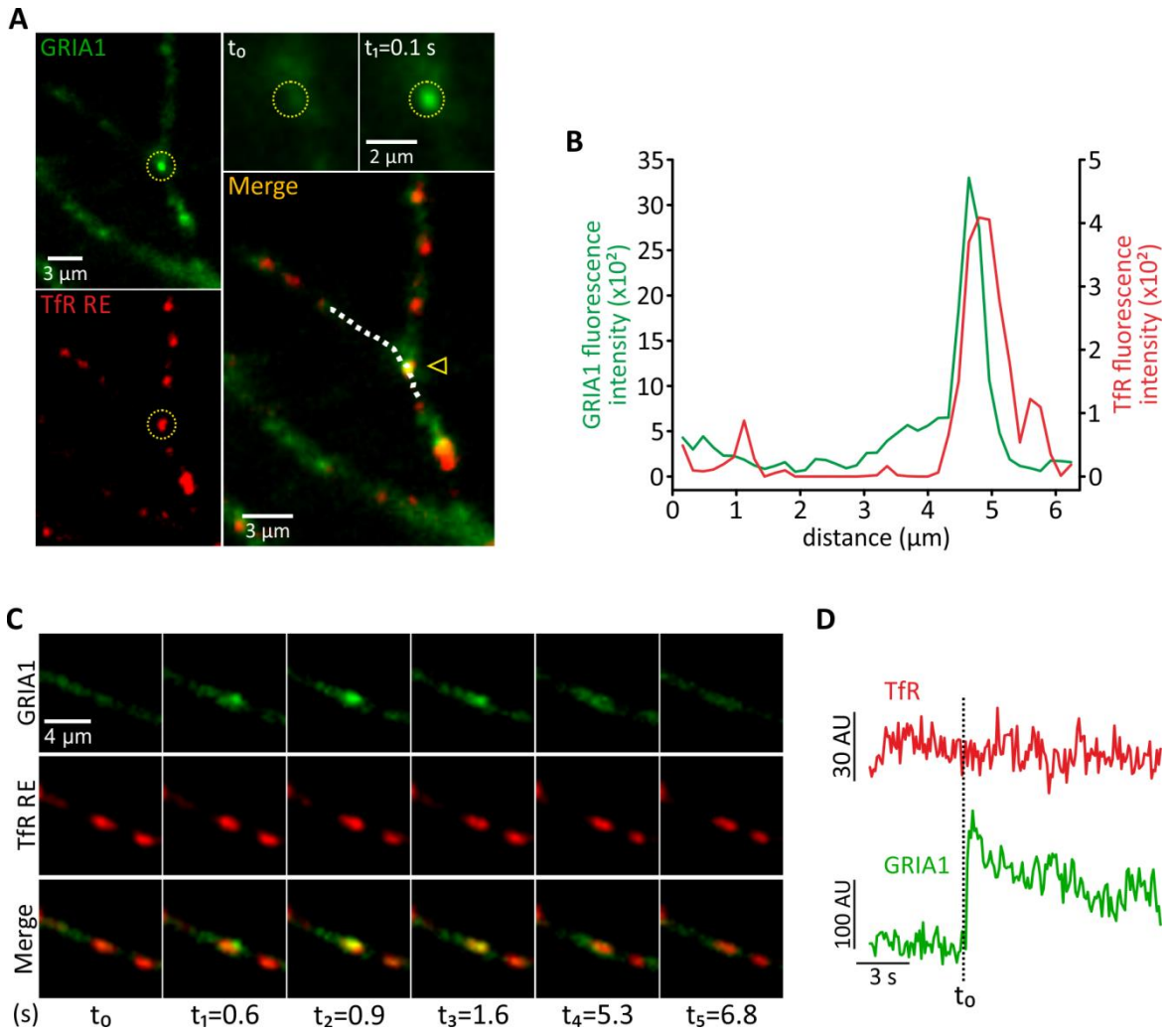


**Figure 34. AMPA receptor membrane insertion comes from local pre-existing recycling endosomes**
(**A**) Epifluorescence imaging of neurites of hippocampal neurons (DIV 11) cotransfected with SEP-GRIA1 (green) and TfR-tagRFPt (red). GRIA1 insertion event indicated by a yellow circle (**upper left**, green). Enlarged section of the upper left image at an instant before event occurrence (**$t_0$, upper middle**), and during an event (**$t_1$, upper right**). Lower right image (red) shows transferrin receptor recycling endosome indicated with a yellow circle corresponding to the region of the event in the upper left image. Lower right image corresponds to the merged image of green and red (**upper left** and **lower left**, respectively) with a white line (dotted) drawn over the region where the SEP-GRIA1 insertion event occurred in purpose for line intensity analysis. Yellow arrowhead indicates the event. (**B**) Line intensity analysis to show the colocalization between SEP-GRIA1 event and TfR-tagRFPt RE in **A** (merged image). Quantification presented in a graph where SEP-GRIA1 event is indicated in green and TfR-tagRFPt in red. (**C**) Time sequence of a SEP-GRIA1 (green) insertion event (**upper row**), and its corresponding TfRtagRFPt (red) recycling endosome (**middle row**). Lower row shows the merged time sequence of the green and red channel. (**D**) Exemplary traces of TfR-tagRFPt (red) and SEP-GRIA1 (green) during a SEP-GRIA1 insertion event. Images in (**A**) and (**C**) were smoothed for better presentation. Imaging frequency is 10 Hz in both channels with 100 ms exposure time.

## 3.7 Effect of auxiliary subunits on the surface expression of AMPARs

Our characterization of the AMPAR trafficking system showed that receptor surface insertion is a dynamic process. However, surface expression of AMPARs is highly regulated and involves several auxiliary and membrane associated proteins (Bredt and Nicoll, 2003).

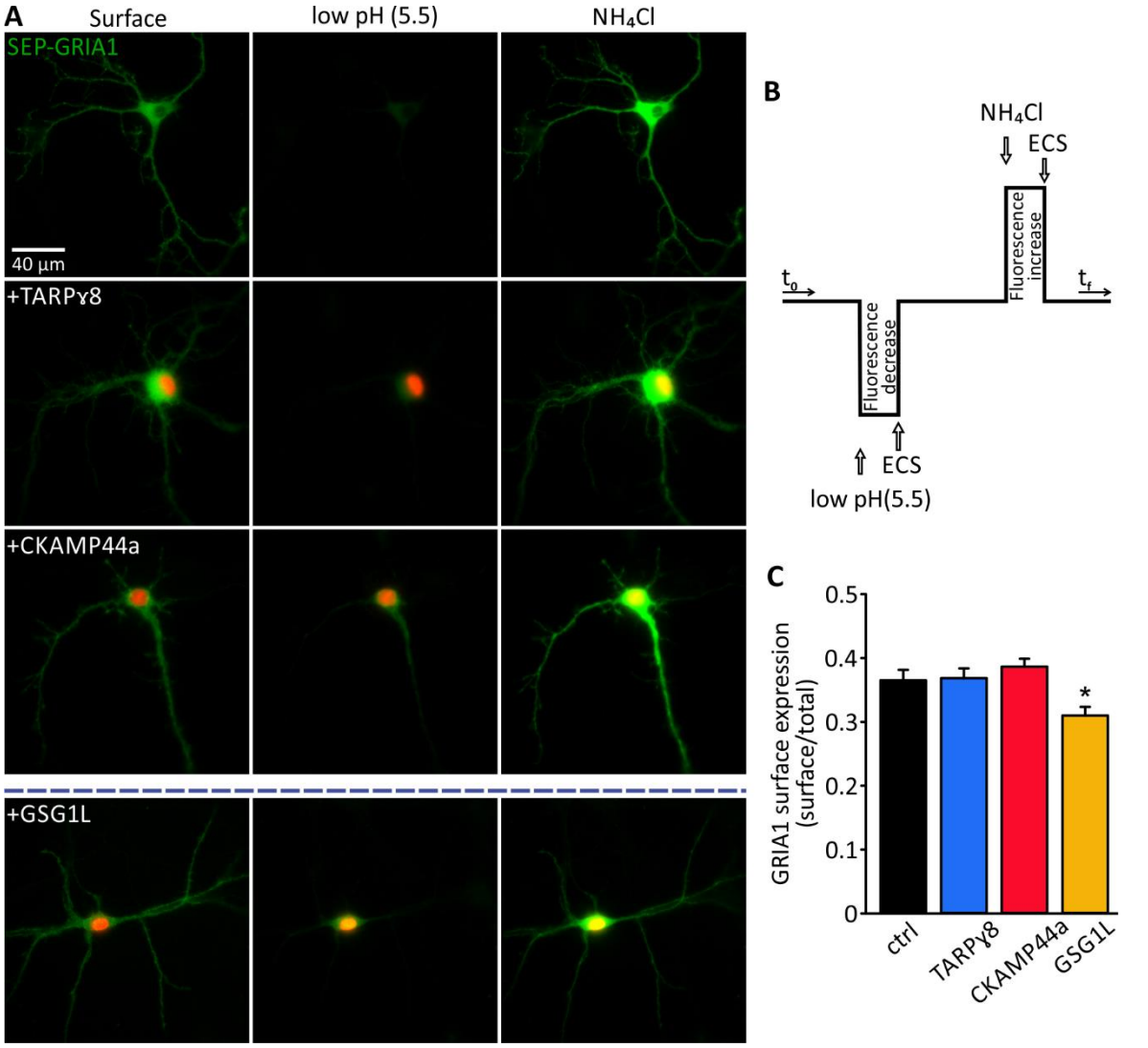


**Figure 35. Auxiliary subunits differentially regulate AMPAR surface expression in hippocampal neurons** (**A**) Exemplary epifluorescence images of hippocampal neurons (DIV 9-12) transfected with SEP-GRIA1 (green) (**first row**), cotransfected with SEP-GRIA1 (green) and either TARPγ8 IRES NLS-tdTomato (red nucleus) auxiliary subunit (**second row**), CKAMP44a IRES NLS-tdTomato (red nucleus) auxiliary subunit (**third raw**), or GSG1L IRES NLS-tdTomato (red nucleus) auxiliary subunit (**fourth raw**). Left column corresponds to SEP-GRIA1 surface fluorescence of neurons, middle column to neurons treated with low pH solution (pH=5.5) solution, and right column to neurons treated with $NH_4CL$ solution. (**B**) Schematic diagram illustrating the recording protocol with low pH (5.5) and $NH_4CL$ treatment. (**C**) Graph showing SEP-GRIA1 surface expression (surface to total ratio) in the different conditions. Data are mean ± SEM. Statistical analysis was assessed with one way ANOVA followed by pairwise comparison with Student-Newman-Keuls method test. *$p$<0.05. Imaging frequency is 10 Hz with 100 ms exposure time. Ctrl n=37 cells, TARPγ8 n=31 cells, CKAMP44a n=35 cells, GSG1L n=30 cells.

Obviously, auxiliary subunit-induced changes in the turnover of AMPARs affect the population of surface receptors (Greger et al., 2017; Jackson and Nicoll, 2011). Therefore, we investigated total AMPAR surface expression in hippocampal neurons overexpressing either TARPγ8, CKAMP44a, or GSG1L (Germ Cell-Specific Gene 1-Like) auxiliary subunits. Neurons were cotransfected (DIV 8-11) with SEP-GRIA1 and with each one of the auxiliary subunits, and the fluorescence signal of surface receptors was determined by application of a fluorescence-quenching acidic (pH 5.5) solution. The residual fluorescence of SEP-GRIA1, obtained upon treatment with the quenching solution (pH 5.5), was subtracted from the baseline fluorescence to yield pure surface fluorescence. Moreover, due to variability in neuron size, surface fluorescence was normalized to the total fluorescence, which was obtained by $NH_4Cl$ treatment (**Figure 35A and B**). Quantification of the fraction of surface receptors in neurons expressing TARPγ8 and CKAMP44a delivered comparable values, thus indicating that the availability of either auxiliary subunit is not limiting for the transport of receptors to the cell surface. On the other hand, we also expressed the newly identified auxiliary subunit GSG1L, which has been associated with facilitated endocytosis (Gu et al., 2016a), and observed that SEP-GRIA1 surface expression was significantly downregulated, as indicated by a reduced surface fluorescence fraction (ctrl: 0.365±0.016, TARPγ8: 0.369±0.015, CKAMP44a: 0.387±0.012, GSG1L: 0.31±0.013, and ctrl versus TARPγ8: $p$=0.867, ctrl versus CKAMP44a: $p$=0.523, ctrl versus GSG1L: $p$ value=0.007, **Figure 35C**).

## 3.8 TARPγ8 auxiliary subunit reduces the insertion rate of AMPARs

The auxiliary subunit TARPγ8, which is preferentially expressed in hippocampal neurons (Rouach et al., 2005), is an essential protein for AMPAR trafficking and regulation.

To examine the role of TARPγ8 in dendritic AMPAR trafficking, we coexpressed TARPγ8 with tdTomato reporter (pRK5 TARPγ8 IRES NLS-tdTomato) and SEP-GRIA1 in hippocampal neurons (DIV 8-11), which are used for imaging 24-48 h later. NLS-tdTomato (NLS: nuclear localizing sequence) is a red fluorescent protein that is localized in the nucleus due to NLS sequence and reports the presence of the TARPγ8-encoding vector in the transfected neuron.

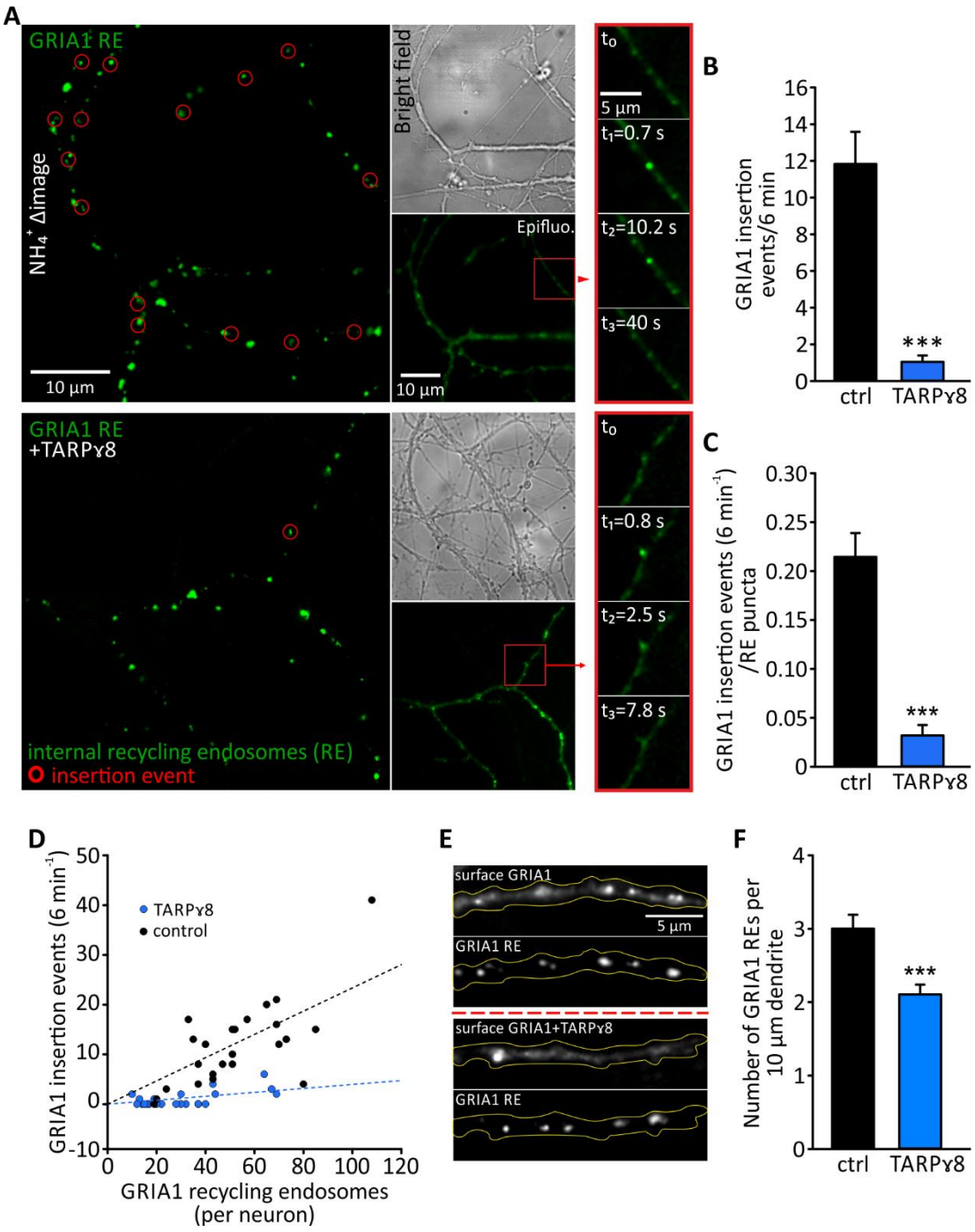


**Figure 36. TARPγ8 auxiliary subunit reduces AMPAR surface insertion**
(**A**) Exemplary images of SEP-GRIA1 with and without TARPγ8 IRES NLS-tdTomato transfected neurons (DIV9-12). Upper and lower left images represent subtracted images ($NH_4^+$ Δimage) indicating internal GRIA1 recycling endosomes (RE, green puncta) and GRIA1 insertion events indicated with red circles in neurites ($NH_4^+$ Δimage explained in **Figure 31**). Bright field images of neurites (**upper** and **third right**). Epifluorescence image showing surface SEP-GRIA1 (**second** and **fourth right**). Time series of SEP-GRIA insertion event (images in **upper** and **lower red rectangles**). (**B**) Average absolute number of insertion events of SEP-GRIA1 in 6 min. (**C**) Average normalized number of SEP-GRIA1 insertion events (in 6 min) to total RE count per field of view. ***$p$<0.001. (**D**) Scatter plot of number of SEP-GRIA1 insertion events versus number of SEP-GRIA1 REs per cell. (**E**) Exemplary image showing a dendritic segment (**first** and **third**) and the corresponding internal GRIA1 REs in control (SEP-GRIA1) and with TARPγ8 IRES NLS-tdTomato overexpression (**second** and **fourth**), respectively. (**F**) Quantification of average number of GRIA1 REs per 10 µm length of dendrite in control (SEP-GRIA1) and with TARPγ8 IRES NLS-tdTomato overexpression. ***$p$<0.001. Data are mean ± SEM. Statistical analysis was assessed with student t-test. Imaging frequency is 10 Hz with 100 ms exposure time. Ctrl n=24 cells, TARPγ8 n=22 cells

Constitutive exocytosis was studied in neurites using epifluorescence microscopy, assessing the frequency of SEP-GRIA1 insertion events. Intriguingly, we observed a significant reduction in the number of events per minute in cells with a high abundance of TARPγ8 in comparison with controls (mean frequency of insertion: ctrl: 11.833±1.75, TARPγ8: 1.045±0.345, $p<0.001$ **Figure 36B**). Arguing that the majority of exocytosis events originate from transient RE fusion, we also determined the number of SEP-GRIA1-positive REs in the field of view by application of $NH_4Cl$ and normalized the frequency of fusion events to this number (**Figure 36A**). Still, normalized SEP-GRIA1 insertion events were significantly reduced when coexpressed with TARPγ8 in comparison to controls (normalized mean frequency of insertion: ctrl: 0.214±0.024, TARPγ8: 0.031±0.01, $p<0.001$ **Figure 36C)**, excluding the possibility that TARPγ8 overexpression indirectly reduces the number of exocytotic events by decreasing the number of REs in dendrites.

To further emphasize that the existing REs putatively fuse with the plasma membrane with reduced probability in the presence of high amount of TARPγ8, we plotted the number of SEP-GRIA1 insertion events versus the number of REs for each neuron. Indeed, the slope of the regression line for TARPγ8 overexpression was clearly smaller than in controls (ctrl: 0.28, TARPγ8: 0.057, **Figure 36D**). In line with that, quantification of the number of GRIA1 REs per 10 µm dendrite showed that the RE number was significantly reduced in dendrites of neurons with TARPγ8-overexpression (average number of REs per 10 µm dendrite: ctrl: 0.3±0.0189, TARPγ8: 0.211±0.0133, $p<0.001$ **Figure 36E** and **F**). For the analysis, we chose dendrites of length > 20 µm, defined via scanlines, to quantify the number of REs.

The experiment above showed that TARPγ8 had an effect on AMPAR trafficking and the number of REs. We next tested whether AMPAR insertion events in TARPγ8-overexpressing cells possessed different fusion properties than in controls. Thus, we analyzed the kinetic parameters (amplitude, rise-time, and decay time constant) of the fusion events. In neurons overexpressing TARPγ8, the amplitude of insertion events was significantly reduced in comparison to controls (median of amplitude (AU): ctrl: 52.234, TARPγ8: 23.184, $p<0.001$). Onset and decay of insertion, however, were not significantly changed (median of onset (s): ctrl: 0.3, TARPγ8: 0.3, $p=0.914$; median of decay (s): ctrl: 9.182, TARPγ8: 8.118, $p=0.464$**, Figure 37A, B and C**). As the reduced fluorescence amplitude of fusion events suggests that dendritic storage organelles indeed contain a lower amount of AMPARs, if TARPγ8 abundance is high, we also analyzed the SEP-GRIA1-load in the intracellular dendritic structures previously visualized by $NH_4Cl$-unquenching. Indeed, fluorescence intensities of these SEP-GRIA1-positive puncta were significantly reduced in dendrites of TARPγ8-overexpressing

neurons (mean of median intensities of REs: ctrl: 1438.236±216.188, TARPγ8: 791.888±99.33, $p$= 0.011, **Figure 37D**). Thus, both results, the decreased amplitude of fusion events as well as the reduced AMPAR content of storage organelles consistently suggest that TARPγ8 association of receptors changes their recycling pathways.

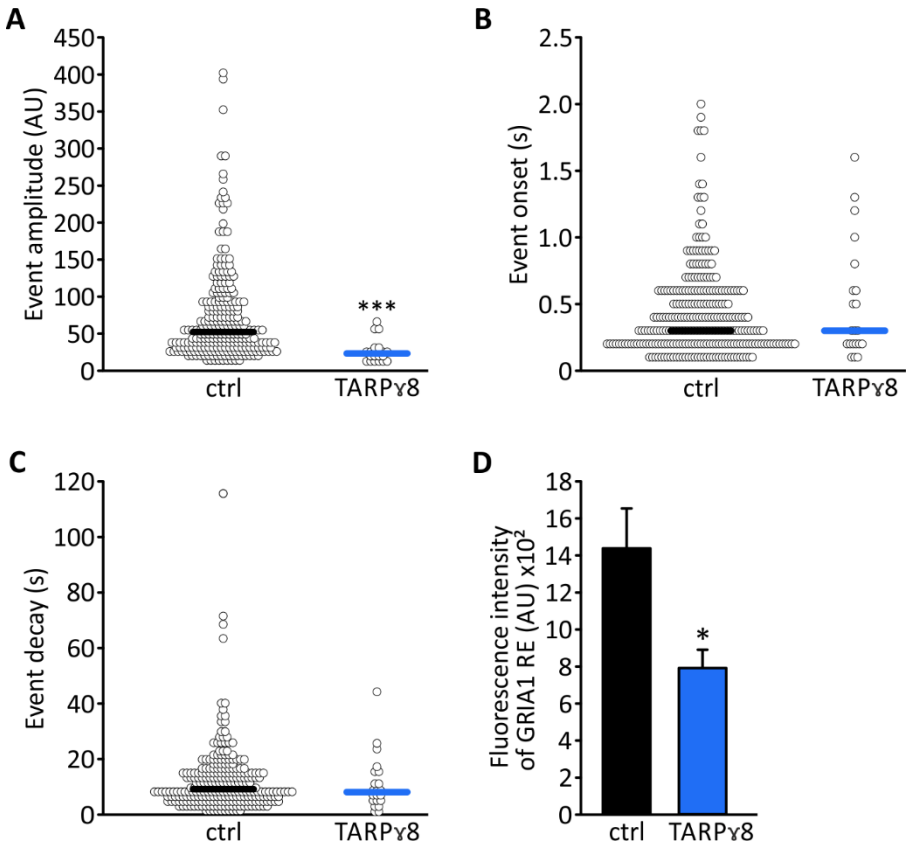


**Figure 37. TARPγ8 overexpression reduces AMPAR RE stores and amplitude of insertion events**
(**A**) Dot density plot illustrating distribution and median of amplitudes, onsets (**B**), and decays (**C**) of SEP-GRIA1 insertion events in control (SEP-GRIA1) and with TARPγ8 IRES NLS-tdTomato overexpression. (**D**) Quantification of SEP-GRIA1 recycling endosomes' fluorescence intensities. Graph shows the average of median intensities of REs. Ctrl: n=24 cells, TARPγ8: n=22 cells. Data are mean ± SEM. Statistical analysis was assessed with t-test using Mann-Whitney on ranks. *$p$<0.5.

While the reduced intracellular pool of SEP-GRIA1-containing receptor in cells overexpressing TARPγ8 may indicate specifically altered AMPAR trafficking, general effects on formation and function of REs cannot be excluded *a priori* based on above experiments. To test the specificity of the observed changes, we thus co-transfected neurons (DIV 8-11) with pCDNA3 CMV TfR-tagRFPt (red), pCI CMV SEP-GRIA1 (green), and pRK5 CMV TARPγ8

IRES NLS-tdTomato, in order to visualize the GRIA1-containing subset of endosomal compartments in conjunction with all TfR-positive REs. Control cultures were only transfected with TfR-tagRFPt and SEP-GRIA1 (**Figure 38A**). First, we analyzed the fluorescence of TfR-tagRFPt-positive puncta and found that the load of REs with TfR fluorescence was not altered by TARPγ8 overexpression (absolute fluorescence intensities of TfR-tagRFPt REs ($x10^5$): ctrl: 1.05±0.202, TARPγ8: 1.032±0.166, $p$=0.919, **Figure 38B**). Moreover, our analysis of the number of TfR REs per 10 µm dendrite (as previously described) also did not show a difference with increased amount of TARPγ8 (ctrl: 0.191±0.0197, TARPγ8: 0.173±0.0122, **Figure 38D and E**), unlike GRIA1 REs as we showed previously (**Figure 36F**). Therefore, it is unlikely that overexpression of TARPγ8 interferes with the formation or function of TfR REs. As previously shown, the vast majority of SEP-GRIA1-positive puncta colocalized with TFR-containing REs, and thus we calculated the fluorescence ratio unquenched SEP/tagRFPt for both conditions as a measure for the GRIA1-content of REs. In line with previous experiments, the fluorescence ratio was significantly smaller in the presence of increased amounts of TARPγ8 compared to the controls (ratio green/red fluorescence intensity: ctrl: 0.218±0.028, TARPγ8: 0.118±0.014, $p$=0.002, **Figure 38C**), which suggests that TARPγ8 specifically decreases content of SEP-GRIA1 in RE without affecting other types of receptor cargo.

Overall, our findings show that TARPγ8 abundance dramatically affects the dendritic trafficking of GRIA1-containing receptors, reducing the population of GRIA1-containing AMPAR in recycling endosomes and their insertion in the plasma membrane. Noteworthy, the reduced frequency of detectable RE fusion events might be a consequence of the reduced level of SEP-GRIA1 within the organelle.

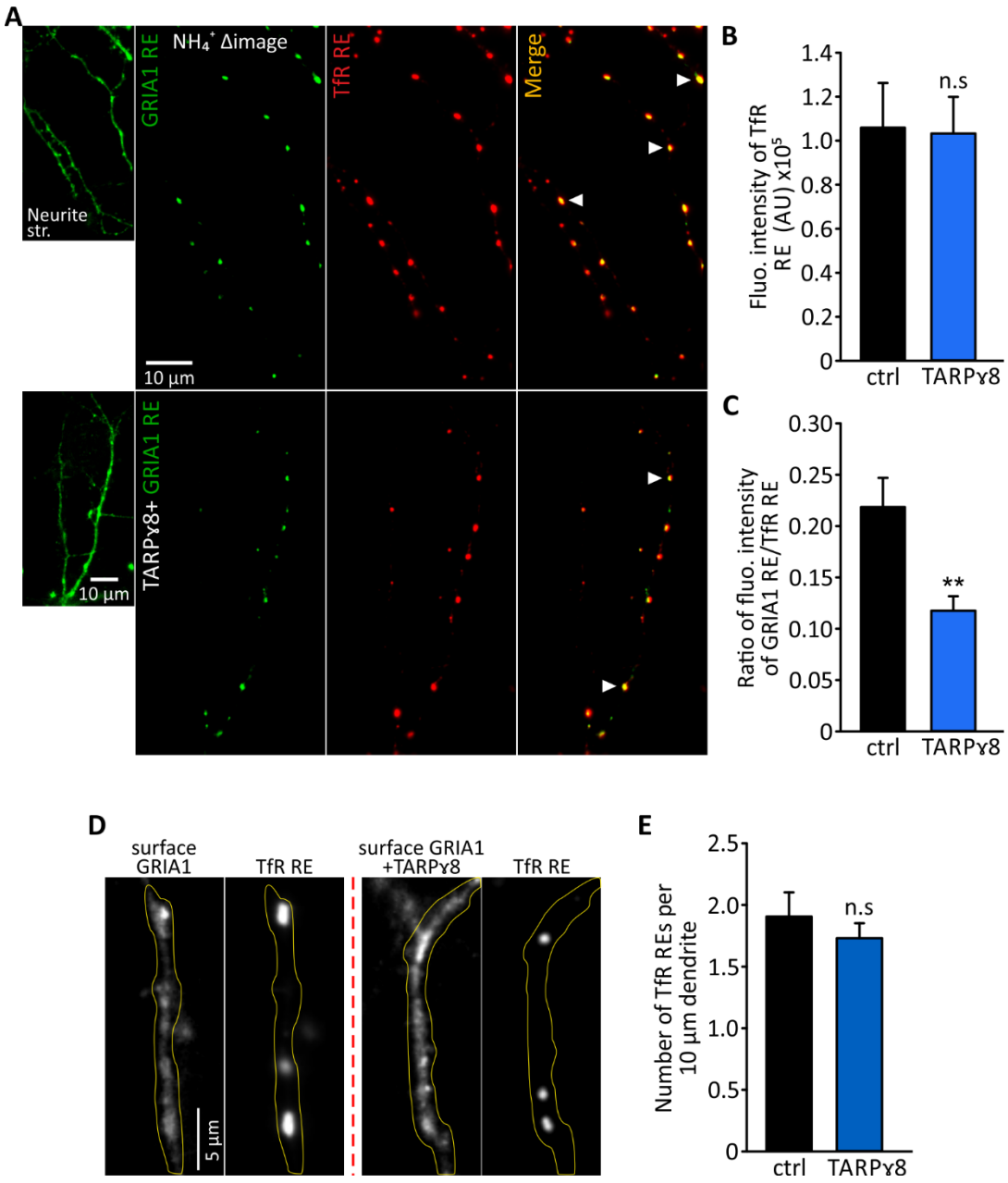


**Figure 38. TARPγ8 overexpression reduces AMPAR cargo in REs but not TfR**
(**A**) Epifluorescence image of SEP-GRIA1 and TfR-tagRFPt transfected hippocampal neurons (DIV 11) in control (**upper**) and with TARPγ8 IRES NLS-tdTomato overexpression (**lower**). Exemplary $NH_4^+$ Δimages with internal SEP-GRIA1 REs (green puncta) (**upper** and **lower second image**), internal TfR-tagRFPt REs (red puncta) (**upper** and **lower third image**), and merged images of green and red (**upper** and **lower fourth image**). Colocalized SEP-GRIA1 REs with TfR-tagRFPt REs are indicated with white arrowheads. Smaller images correspond to epifluorescence of dendrites (**upper** and **lower first image**) (**B**) Average of median fluorescence intensity of TfR-tagRFPt RE with and without TARPγ8. $p$=0.919. (**C**) Graph shows ratio of SEP-GRIA1 RE/TfR-tagRFPt RE fluorescence intensity. Data represents average medians of ratios of fluorescence intensities of each cell. **$p$<0.01. (**D**) Exemplary image showing a dendritic segment marked with SEP-GRIA1 (**first** and **third**) and the corresponding internal TfR REs in control (SEP-GRIA1 and TfR-tagRFPt) and with TARPγ8 IRES NLS-tdTomato overexpression (**second** and **fourth**), respectively. (**E**) Quantification of average number of TfR REs per 10 µm length of dendrite in control (SEP-GRIA1 and TfR-tagRFPt) and with TARPγ8 IRES NLS-tdTomato overexpression. Data are mean ± SEM. Ctrl: n=18 cells, TARPγ8: n=21 cells. Statistical analysis was assessed with student t-test.

## 3.9 The auxiliary subunit CKAMP44a affects dendritic AMPAR delivery

CKAMP44a has been recently identified as another AMPAR auxiliary subunit in the hippocampus, where it is most prominently expressed in the dentate gyrus granule cells (von Engelhardt et al., 2010). Given the observed effects of TARPγ8 overexpression on the fusion of AMPAR-containing dendritic REs, we wondered whether this unrelated auxiliary subunit also affects AMPAR turnover. To study the effect of CKAMP44a on basal AMPAR surface delivery, we cotransfected hippocampal neurons (DIV 8-11) with pRK5 CKAMP44a IRES::NLS-tdTomato and pCI SEP-GRIA1 and recorded movies of selected dendritic structures, as described above. Dendritic intracellular organelles containing SEP-GRIA1 were again visualized by application of $NH_4Cl$ and their number was used to normalize insertion frequency (**Figure 39A**). The absolute number as well as the normalized number of constitutive fusion events within the 6 min recording interval was significantly reduced in neurons overexpressing CKAMP44a compared to controls (ctrl: 7.273±0.914, CKAMP44a: 1.217±0.397; normalized mean frequency of insertion: ctrl: 0.226±0.043, CKAMP44a: 0.039±0.011,**Figure 39B and C)**. This strong 6-fold reduction in the delivery frequency for CKAMP44a-overexpressing cells is reminiscent of the decreased insertion rate observed for TARPγ8 overexpression, possibly indicating a similar impact on AMPAR dendritic trafficking.

To highlight the role of CKAMP44a in the SEP-GRIA1 insertion probability, we plotted the number of SEP-GRIA1 insertion events versus the number of REs for each neuron. In a similar fashion to TARPγ8, we observed a reduction in the SEP-GRIA1 insertion probability when the number of REs was reduced for CKAMP44a overexpression, as the slope of the regression line for CKAMP44a overexpression was clearly smaller than in controls (ctrl: 0.1675±0.0130, CKAMP44a**:** 0.068±0.0115**, Figure 39D)**. In line with that, quantification of the number of GRIA1 REs per 10 µm dendrite showed a significant reduction in RE number in dendrites of neurons with CKAMP44a-overexpression (ctrl: 0.259±0.0200, CKAMP44a**:** 0.167±0.0145, **Figure 39E and F**). The analysis was done as previously described in case of TARPγ8 overexpression.

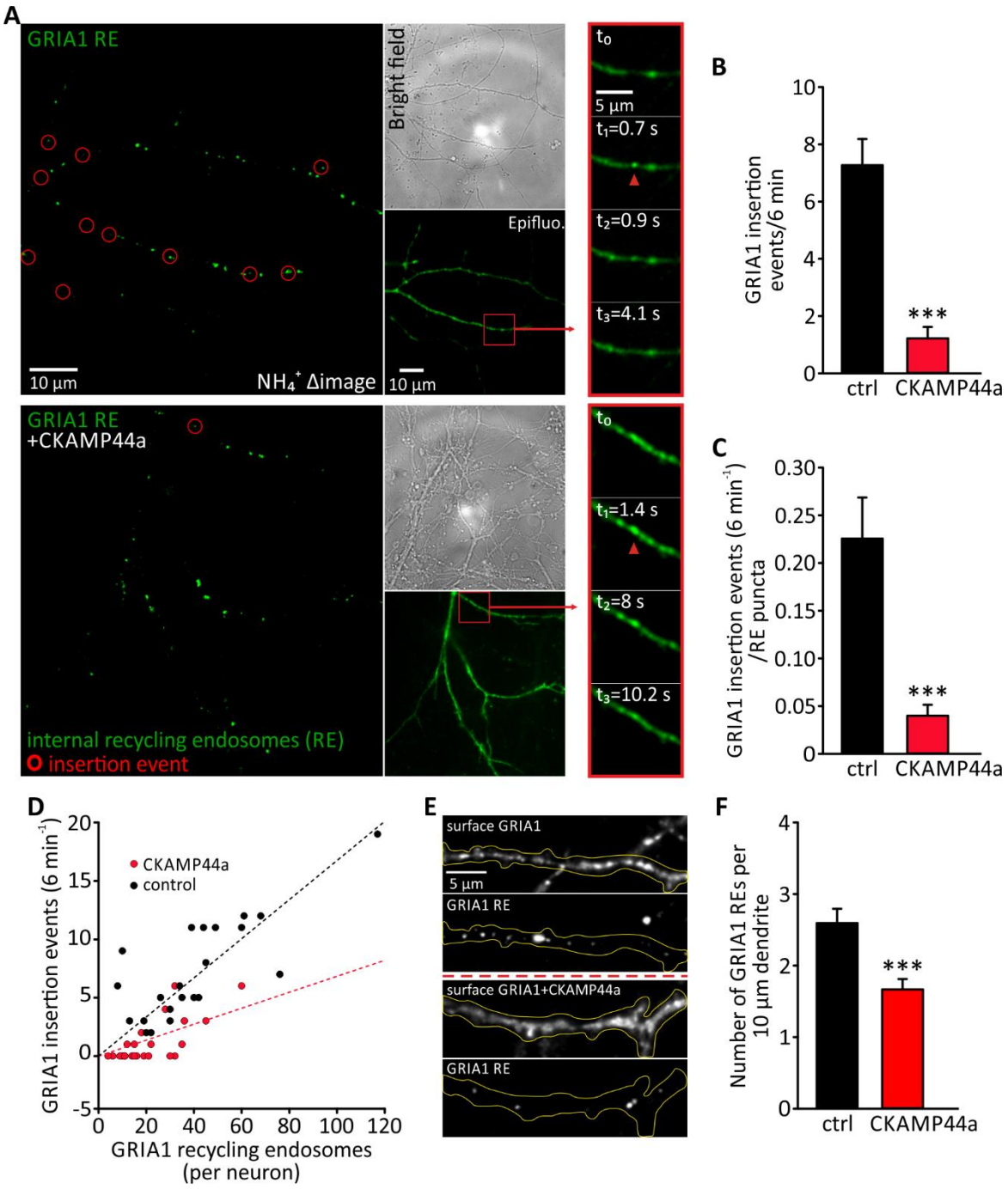


**Figure 39. CKAMP44a auxiliary subunit reduces AMPAR surface insertion**

(**A**) Exemplary images of SEP-GRIA1 with and without CKAMP44a IRES NLS-tdTomato transfected neurons (DIV 10-11). Upper and lower left images represent subtracted images ($NH_4^+$ Δimage) with internal GRIA1 recycling endosomes (RE, green puncta) in neurites. Bright field image of neurites (**upper** and **third right**). Epifluorescence images of SEP-GRIA1 (**second** and **lower right**). Time series of SEP-GRIA1 insertion event (images in **upper** and **lower red rectangles**). (**B**) Average of absolute number of insertion events of SEP-GRIA1 in 6 min. (**C**) Average number of SEP-GRIA1 insertion events (in 6 min) normalized to the total RE count per cell. **(D)** Scatter plot of number of SEP-GRIA1 insertion events per cell versus number of SEP-GRIA1 REs per cell. **(E)** Exemplary image showing a dendritic segment (**first** and **third**) and the corresponding internal GRIA1 REs in control (SEP-GRIA1) and with CKAMP44a IRES NLS-tdTomato overexpression (**second** and **fourth**), respectively. (**F**) Quantification of average number of GRIA1 REs per 10 µm length of dendrite in control (SEP-GRIA1) and with CKAMP44a IRES NLS-tdTomato overexpression. ***$p$< 0.001. Data are mean ± SEM. Statistical analysis was assessed with student t-test. Imaging frequency is 10 Hz with 100 ms exposure time.

Having noted a reduced fusion frequency, we wondered about potential alterations in the signal kinetics of the residual events. When CKAMP44a was overexpressed, a slight but not significant decrease in event amplitude was observed (median of amplitude (AU): ctrl: 37.243, CKAMP44a: 32.569, $p$=0.468, **Figure 40A**). Event decay time constant and rise-time were also not significantly different (median of rise-time (s): ctrl: 0.5, CKAMP44a: 0.6, $p$=0.148, median of decay time constant (s): ctrl: 10.807, CKAMP44a: 13.213, $p$= 0.661, **Figure 40B and C**). In addition, we quantified the absolute fluorescence intensities of the intracellular SEP-GRIA1-containing organelles identified by $NH_4Cl$ application and again found a slight tendency towards reduced AMPAR content, which was however not significant (ctrl: 693.801±71.201, CKAMP44a: 582.899±73.368, **Figure 40D**). These data show that CKAMP44a overexpression exerted a negative effect on the insertion rate of AMPARs from intracellular stores similar to the results of our previous experiments with TARPγ8, but that residual fusion events remained rather unaffected. That said, it should be considered that the kinetic analysis was based on a small number of fusion events and thus might correctly report potential changes.

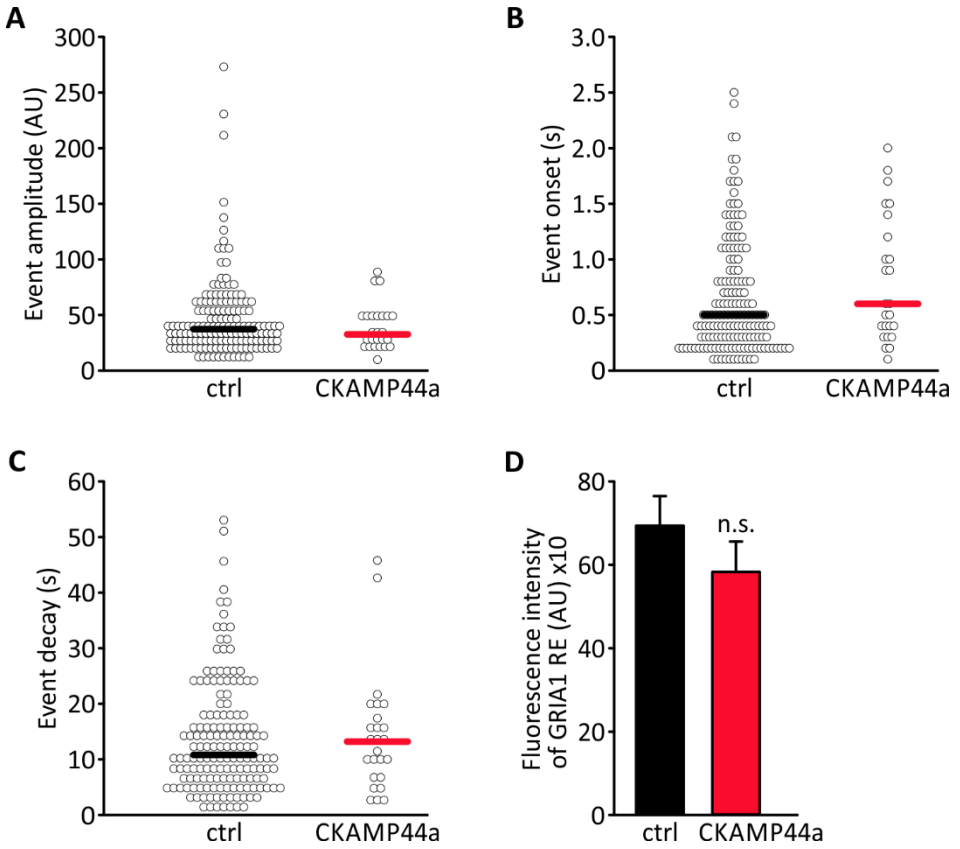


**Figure 40. SEP-GRIA1 fusion kinetics are not changed with CKAMP44a overexpression**
(**A**) Dot density plot illustrating the distribution and median of amplitudes, onsets (**B**), and decays (**C**) of SEP-GRIA1 insertion events. Ctrl n=22 cells, CKAMP44a n=23 cells. Statistical analysis was assessed with t-test using Mann-Whitney on ranks. (**D**) Quantification of SEP-GRIA1 recycling endosomes' fluorescence intensities. Graph shows average of median intensities of REs. Data are mean ± SEM. $p$=0.285, t-test.

In analogy to our experiments with TARPγ8, we also investigated cotransfected neurons (DIV 9-12) with pRK5 CKAMP44a IRES NLS-tdTomato, pCDNA3 TfR-tagRFPt,

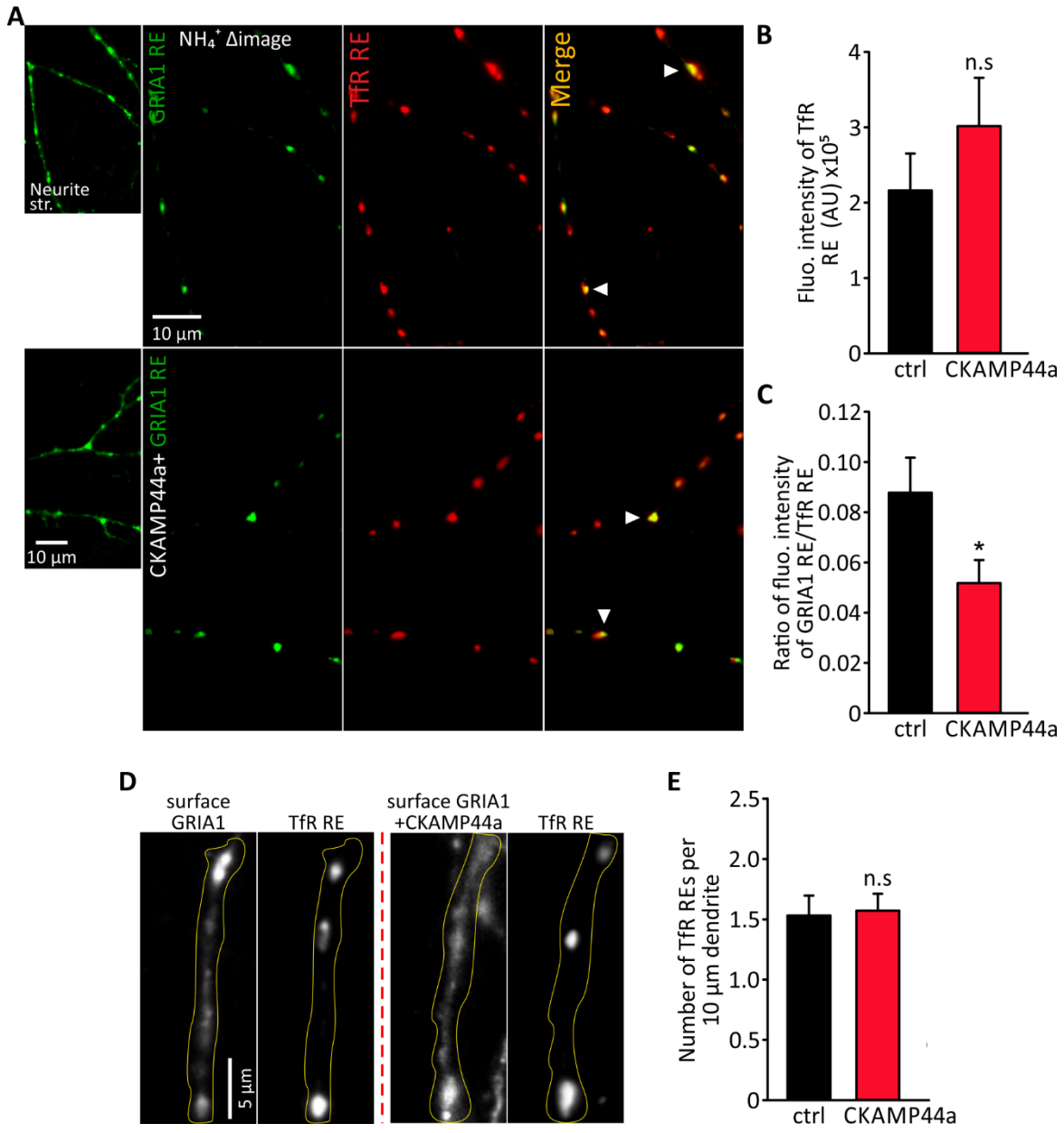


**Figure 41. CKAMP44a overexpression reduces AMPAR cargo in REs but not TfRs**
(**A**) Epifluorescence image of SEP-GRIA1 and TfR-tagRFPt transfected hippocampal neuron (DIV 10) in control (**upper**) and with CKAMP44a IRES NLSt-dTomato overexpression (**lower**). Exemplary $NH_4^+$ Δimages with internal SEP-GRIA1 REs (green puncta) (**upper and lower second image**), internal TfR-tagRFPt RE (red puncta) (**upper and lower third image**), and merged images of green and red (**upper and lower fourth image**). Colocalized SEP-GRIA1 with TfR-tagRFPt REs are indicated with white filled arrowheads. (**B**) Average fluorescence intensity of TfR-tagRFPt REs with CKAMP44a overexpression compared to controls. $p$=0.297. (**C**) Graph shows ratio of SEP-GRIA1 RE fluorescence intensity to TfR-tagRFPt RE fluorescence intensity. Data represents average medians of ratios of fluorescence intensities of each cell. *$p$<0.05. (**D**) Exemplary image showing a dendritic segment marked with SEP-GRIA1 (**first** and **third**) and the corresponding internal TfR REs in control (SEP-GRIA1 and TfRtagRFPt) and with CKAMP44a IRES NLS-tdTomato overexpression (**second** and **fourth**), respectively. (**E**) Quantification of average number of TfR REs per 10 µm length of dendrite in control (SEP-GRIA1 and TfR-tagRFPt) and with TARPγ8 IRES NLS-tdTomato overexpression. Data are mean ± SEM. Ctrl n=13 cells, CKAMP44a n=12 cells. Statistical analysis was assessed with student t-test.

and pCI SEP-GRIA1 to independently address the presence of AMPARs with the recycling endosomal compartment (**Figure 41A**). As before, we quantified the absolute fluorescence intensities of TfR-tagRFPt puncta to verify that REs were unchanged in size and density in neurons expressing CKAMP44a. Indeed, there was no significant difference between CKAMP44a-overexpressing cells and controls (value ($x10^5$): ctrl: 2.163±0.489, CKAMP44a: 3.016±0.641, **Figure 41B**). However, the fluorescence ratio SEP/tagRFPt for REs was significantly reduced for cells expressing CKAMP44a (ratio green/red fluorescence intensity: ctrl: 0.087±0.014, CKAMP44a: 0.051±0.009, $p$=0.045**, Figure 41C**), indicating that the pool of GRIA1-containing receptors in REs was reduced. Clearly, this result is not fully consistent with our previous finding that the intensity of the detected intracellular stores was not significantly changed (**Figure 40D)**, which might be attributed to a threshold problem in the absence of the TfR-marker. Moreover, our analysis of the number of TfR REs per 10 µm dendrite (as previously described) also did not show a difference with increased amount of CKAMP44a (ctrl: 0.153±0.0166, CKAMP44a: 0.157±0.0140, **Figure 41D and E**), unlike GRIA1 REs as we showed previously (**Figure 39F**).

In sum, our data show that CKAMP44a overexpression exerts an adverse effect on the intracellular AMPAR pool. This and other CKAMP44a-dependent mechanisms may reduce the apparent frequency of detectable AMPAR insertion events in dendrites.

## 3.10 Auxiliary subunits reduce endocytosis at extrasynaptic but not synaptic sites

AMPARs are known to be sorted in different trafficking organelles depending on whether they are taken up by constitutive or triggered endocytosis (Glebov et al., 2015). In order to study the general turnover of AMPAR in neurons expressing TARPγ8 or CKAMP44a auxiliary subunits, we used a GRIA1 variant marked with self-labelling *HaloTag*. The *HaloTag* sequence was fused to the N-terminus of GRIA1 subunit (HaloTag-GRIA1), replacing the SEP-fluorophore of the previously used constructs. *HaloTag* protein is an engineered version of a hydrolase whose catalytic function was altered. It catalyzes the formation of a covalent bond when a synthetic ligand containing a chloroalkane group is added. The catalytical reaction is specific, rapid, and irreversible. The ligand used in our experiments is cell membrane impermeable, and contains an "*Alexa Fluor 488*" fluorescent dye that once added to neurons renders HaloTag-GRIA1 receptors on the surface fluorescent (**Figure 42A**). Transient exposure

to the HaloTag-ligand can be used to selectively mark surface receptors and to follow their fate in pulse-chase experiments (**Figure 42B and C**). Staining of surface receptors was done at lowered temperature (15 °C) to suppress a premature onset of receptor endocytosis (Chanaday and Kavalali, 2018; de Figueiredo and Soares, 2000; Punnonen et al., 1998). Preparatory experiments showed that a saturating labelling of the surface pool can be accomplished by incubation times between 35 and 40 min, producing very little intracellular staining (**Figure 42B**).

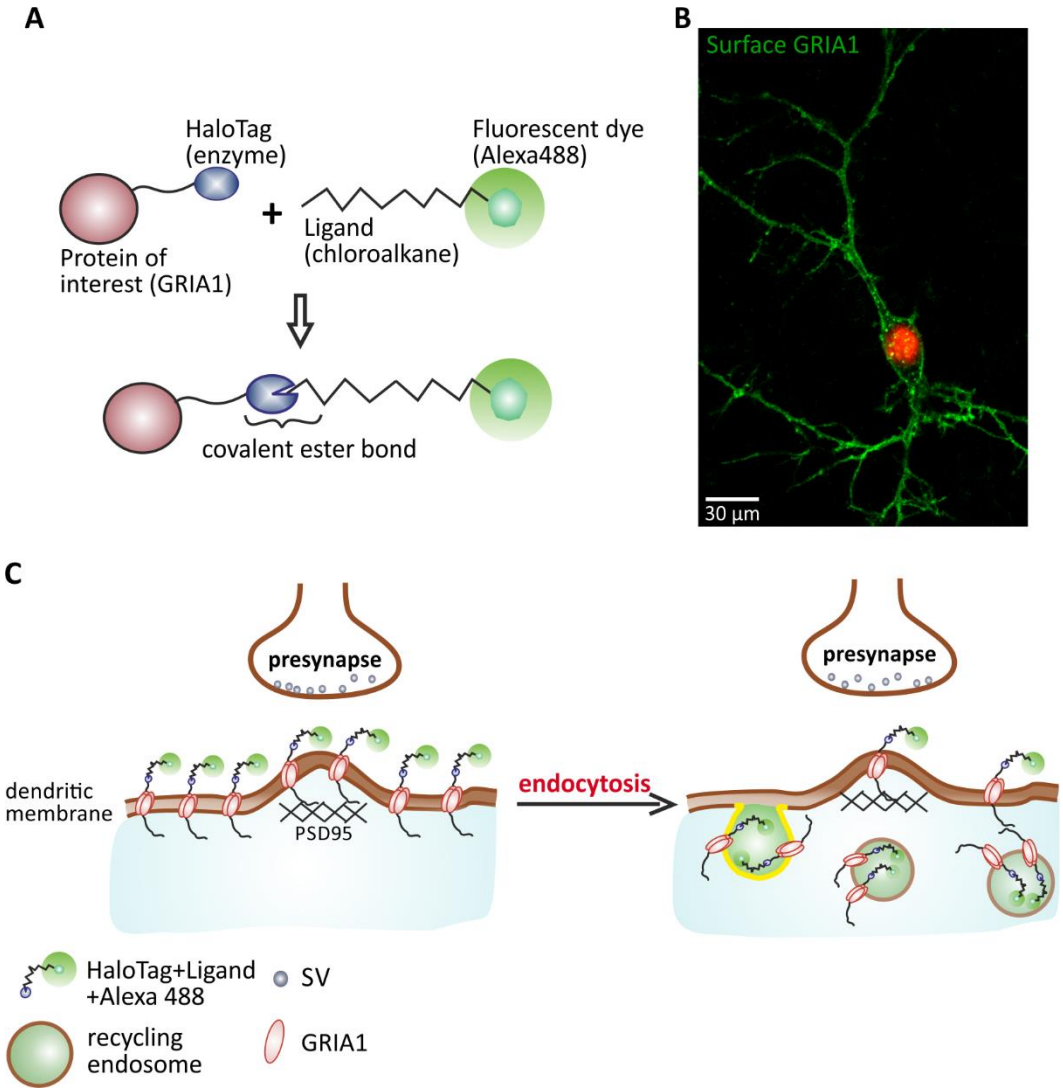


**Figure 42. Staining of self-labelling HaloTag to mark surface GRIA1 receptors**
(**A**) Diagram showing the binding of ligand to HaloTag fusion protein. HaloTag enzyme catalyzes an irreversible covalent ester bond with the ligand bound to the fluorescent dye Alexa Fluor 488. (**B**) Exemplary confocal image of a hippocampal neuron (DIV 9) expressing HaloTag-GRIA1 which surface is stained with the impermeable HaloTag ligand tagged to Alexa Fluor 488. (**C**) A dendritic membrane showing stained surface HaloTag-GRIA1 with the ligand-Alexa Fluor 488 (**left**), and HaloTag-GRIA1-ligand-Alexa Fluor 488 complex in recycling endosomes after endocytosis (**right**).

Since postsynaptic AMPAR anchorage has been in part attributed to MAGUK-interactions of auxiliary subunits (Bats et al., 2007; Nicoll et al., 2006; Stein et al., 2003), we were interested to study receptor uptake at synaptic as well as at extrasynaptic sites with TARPγ8 or CKAMP44a overexpression under basal conditions. To distinguish between extrasynaptic and synaptic domains, we used PSD95-tagRFPt as a synaptic marker in pulse chase experiments with HaloTag-GRIA1 (**Figure 43A**). Accordingly, hippocampal neurons (DIV 8-11) were transfected with pCI CMV HaloTag-GRIA1 as well as with pCDNA CMV PSD95-tagRFPt, and alternatively also with pRK5 CMV TARPγ8 IRES NLS-tdTomato or pRK5 CMV CKAMP44a IRES NLS-tdTomato to investigate the influence of auxiliary subunits. As for controls, neurons were cotransfected with pCI CMV HaloTag-GRIA1 and pCDNA CMV PSD95-tagRFPt, or transfected with pCI CMV HaloTag-GRIA1 IRES NLS-tdTomato only. Using confocal laser-scanning microscopy (LSM), we observed fluorescent "strands" outlining the dendritic membrane in confocal slices of 1 µm (**Figure 43A**). The same region was scanned every 4 minutes for a total duration of 24 min, and during each time point, three slices were acquired. Imaging was performed at 37 °C and with 5 % $CO_2$. We noticed a clear colocalization between HaloTag-GRIA1-positive puncta on the surface and the intracellular PSD95-tagRFPt signal, allowing us to easily identify synaptic receptor accumulations (**Figure 43A**). To separately quantify the internalization of extrasynaptic and synaptic receptors, we either set regions of interest (ROIs) at PSD95-tagRFPt-marked synaptic sites or placed scanlines at PSD95-tagRFPt free extrasynaptic membrane sections using *"ImageJ"* software (**Figure 43A**). As for the synaptic site, to generate ROIs corresponding to individual synapses, we summed up all three slices in red channel for each time point, and thresholded the summed red image to obtain individual ROIs. These ROIs were then overlayed on the summed green image of every time point and fluorescence intensity was quantified. On the other hand, to quantify receptor internalization at extrasynaptic sites, every confocal slice was separately analyzed over the 24 min. A scanline of length >3.2 µm was set along the extrasynaptic membrane, and the region was straightened (**Figure 43A and B**) to get uniform intensity traces through the membrane (**Figure 43C**). All obtained traces corresponding to the region under the scanline were averaged, and the peak value was taken for the analysis (**Figure 43C**). Eventually, fluorescence intensity of every chosen region was normalized to the first time point, and normalized intensities of all regions for every neuron were averaged.

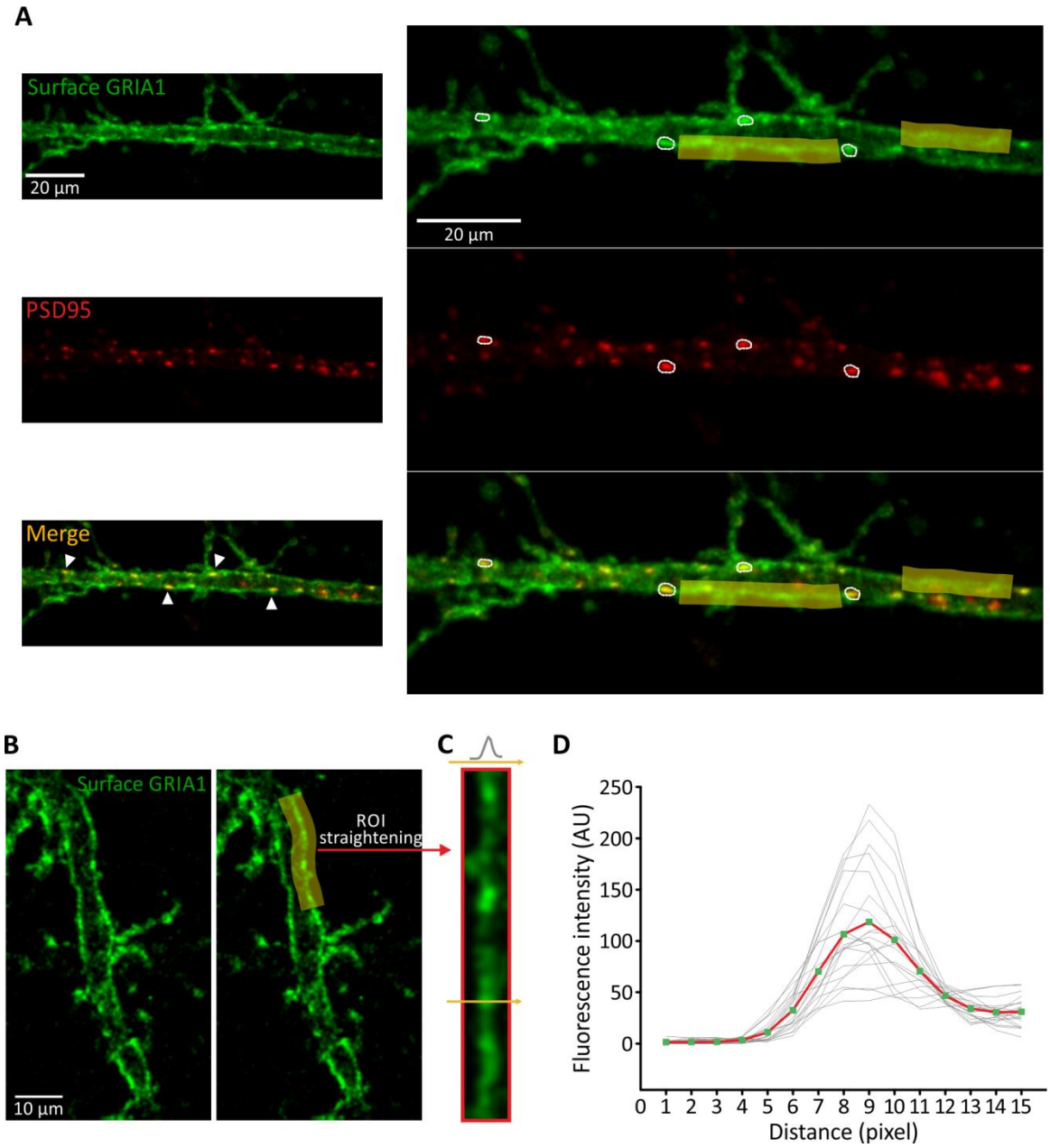


**Figure 43. Analysis of membrane fluorescence intensity of HaloTag-GRIA1 at synaptic and extrasynaptic site**

(**A**) Confocal image of a dendrite from a neuron (DIV 11) transfected with HaloTag-GRIA1 (green) and the synaptic marker PSD95-tagRFPt (red). Membrane HaloTag-GRIA1 stained with its ligand tagged to Alexa Fluor 488. Quantification of HaloTag-GRIA1 fluorescence intensity on synaptic membrane using circle like ROIs (white) obtained from the red PSD95-tagRFPt image by thresholding (second and third row). Quantification of HaloTag-GRIA1 fluorescence intensity on extrasynaptic membrane using scanline (yellow) along non-punctate regions (first and third row). White arrowheads indicate synaptic regions in the merged image (lower left). Images were interpolated for better presentation. (**B**, **C**, and **D**) Show a detailed procedure of the analysis and quantification of the extrasynaptic fluorescence intensity. (**B**) Exemplary confocal image of a stained dendrite from a neuron (DIV 9) transfected with HaloTag-GRIA1 (ligand-Alexa Fluor 488). After drawing a scanline (**B**, right), membrane under the ROI is straitened (**C**) to obtain uniform intensity traces along the whole region (**D**). Red trace indicates the average intensity of all traces along the membrane (**D**). Pixel size: 0.18-0.21 µm. Confocal imaging is done with green laser of 8 % power. Images were interpolated for better presentation.

In controls, we observed a progressive fluorescence reduction in membrane sections over time, which was more pronounced than the bleaching effects of continuous imaging and thus reflecting a putative removal of surface receptors via endocytosis. Comparing images at the beginning of a measurement ($t_0$) and after 24 min, an uptake of labelled HaloTag-GRIA1-containing AMPARs was observed in all four conditions (both controls, TARPγ8, and CKAMP44a) especially in the extrasynaptic domains of neurons (**Figure 44**). With a monoexponential fit, we obtained a reduced rate of receptor endocytosis with TARPγ8 and CKAMP44a overexpression in the extrasynaptic site (mean of endocytosis rate ($min^{-1}$): ctrl: 0.0235±0.00150, ctrl+PSD95-tagRFPt: 0.0256±0.00167, TARPγ8+PSD95-tagRFPt: 0.0128±0.00161, CKAMP44a+PSD95-tagRFPt: 0.0130±0.00271; and ctrl versus TARPγ8+PSD95-tagRFPt: $p$=0.004, ctrl+PSD95-tagRFPt versus TARPγ8+PSD95-tagRFPt: $p$<0.001, ctrl versus CKAMP44a+PSD95-tagRFPt: $p$=0.005, ctrl+PSD95-tagRFPt versus CKAMP44a+PSD95-tagRFPt: $p$<0.001, **Figure 45A and D**). This indicates that the internalization rate of GRIA1-containing AMPARs was reduced in TARPγ8 and CKAMP44a-overexpressing neurons than in control conditions.

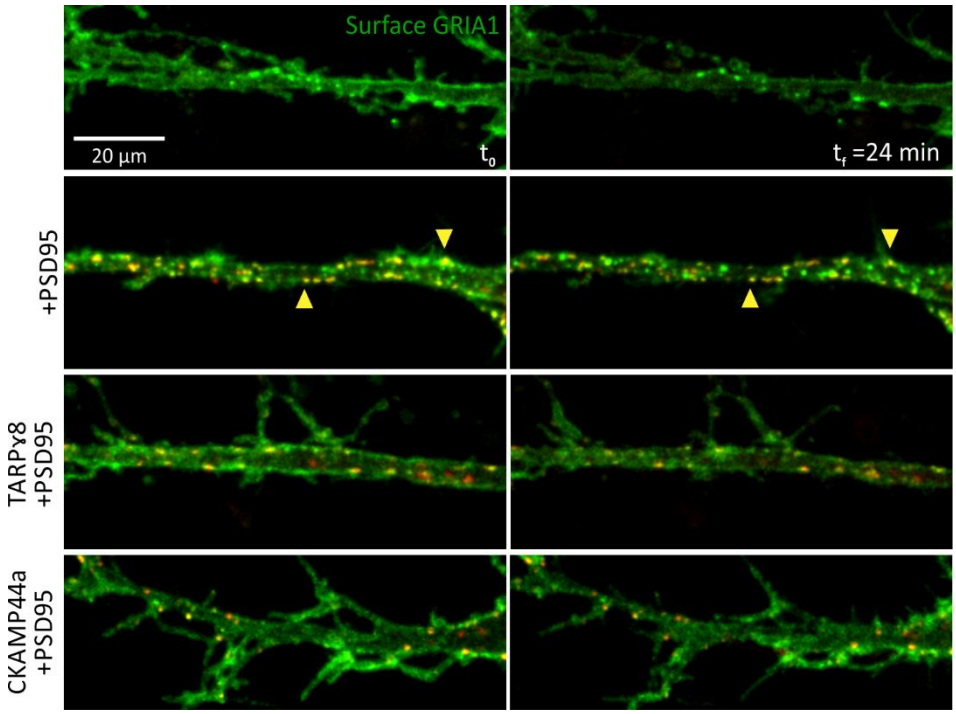


**Figure 44. Auxiliary subunit overexpression reduces HaloTag-GRIA1 endocytosis visually assessed through fluorescence uptake**
Exemplary confocal image of dendrites from neurons (DIV 10-11) transfected with HaloTag-GRIA1 IRES NLS-tdTomato (**first row**), HaloTag-GRIA1 and PSD95-tagRFPt (**second row**), HaloTag-GRIA1 with PSD95-tagRFPt and alternatively with TARPγ8 IRES NLS-tdTomato (**third row**) or CKAMP44a IRES NLS-tdTomato (**fourth row**). Left column corresponds to time zero ($t_0$), and right column corresponds to images after 24 min. In all fourth conditions fluorescence intensity uptake in observed but with different levels. Filled yellow arrowheads indicate synaptic regions. Images were interpolated for better presentation.

We then quantified the Alexa Fluor 488 fluorescence intensities of identified synaptic puncta of the same neurons, and also saw a gradual decrease in intensities. Comparing the fluorescence decay profiles, there was no difference in fluorescence intensities observed among TARPγ8 and CKAMP44a overexpressed neurons and controls (HaloTag-GRIA1 and PSD95-tagRFPt) conditions. With a monoexponential fit, we also did not obtain a difference in endocytosis rate in the synaptic site among the three different conditions (mean of endocytosis rate ($min^{-1}$): ctrl+PSD95-tagRFPt: 0.0127±0.00210, TARPγ8+PSD95-tagRFPt: 0.0141±0.00175, CKAMP44a+PSD95-tagRFPt: 0.00987±0.00170, $p$=0.333, **Figure 45B and E**).

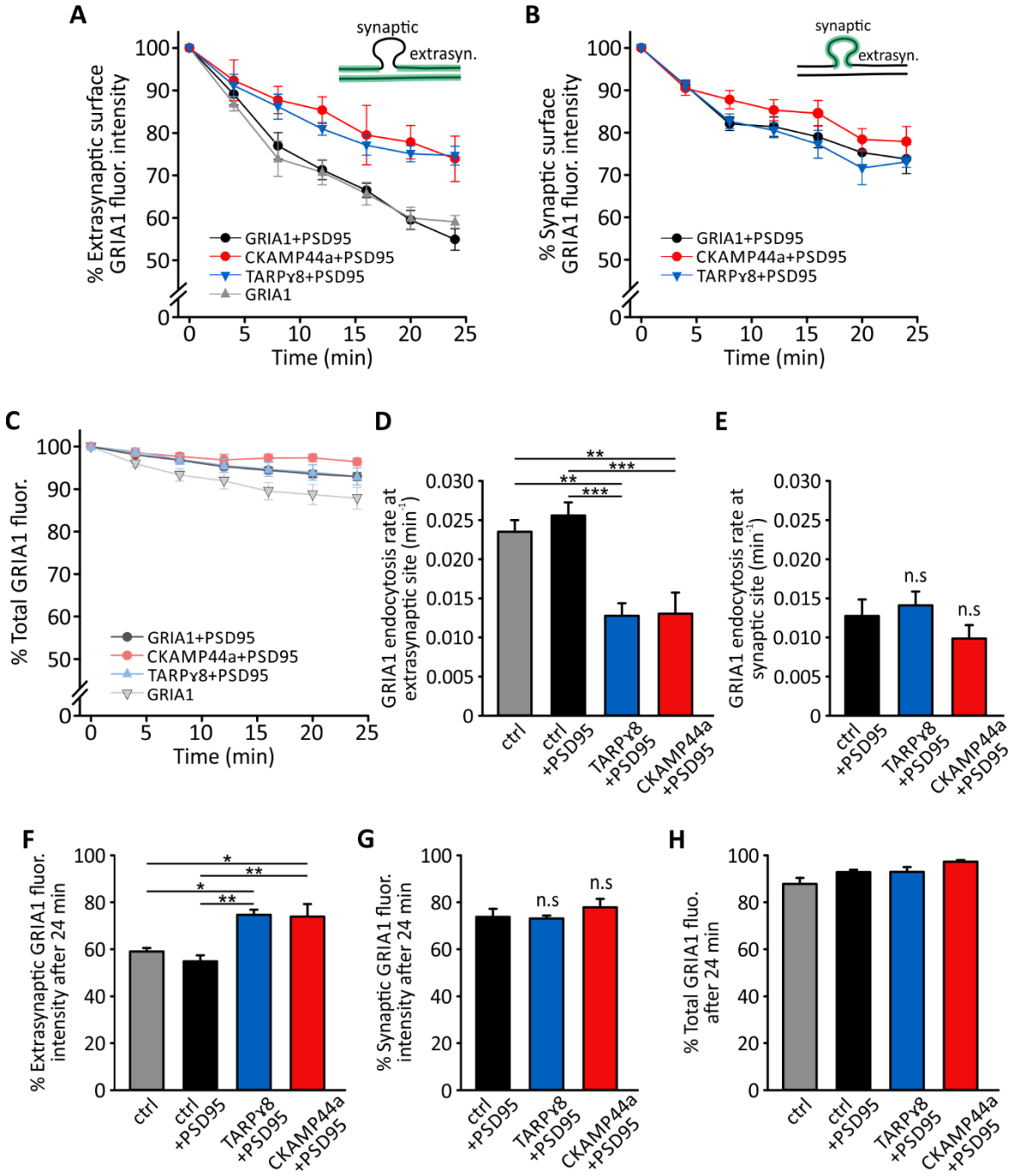

**Figure 45. TARPγ8 and CKAMP44a auxiliary subunits decrease GRIA1 endocytosis at extrasynaptic but not at synaptic sites**
**(A**) Time course of HaloTag-GRIA1 fluorescence change at extrasynaptic site in control (black and grey) and with auxiliary subunit overexpression (blue and red). (**B**) Time course of HaloTag-GRIA1 fluorescence change at synaptic site in control (black) and with auxiliary subunit overexpression (blue and red). (**C**) Traces of total HaloTag-GRIA1 fluorescence change during 24 min. (**D**) Average rate of HaloTag-GRIA1 endocytosis at the extrasynaptic site in higher in controls (black and grey) compared with TARPγ8 or CKAMP44a overexpression conditions (blue and red). (**E**) Average rate of HaloTag-GRIA1 endocytosis at the synaptic site in similar in control (black) to TARPγ8 or CKAMP44a overexpression conditions (blue and red). (**F**) Bar graph shows total HaloTag-GRIA1 fluorescence intensity at extrasynaptic sites after 24 min (in %). Ctrl: 59.1±1.47, ctrl+PSD95: 54.9±2.54, TARPγ8+PSD95: 74.7±2.21, CKAMP44a+PSD95: 73.9±5.34. Ctrl vs ctrl+PSD95: $p$=0.360, ctrl vs TARPγ8+PSD95: **$p$=0.007, ctrl vs CKAMP44a+PSD95: **$p$=0.004, ctrl+PSD95 vs TARPγ8+PSD95: **$p$=0.001, ctrl+PSD95 vs CKAMP44a+PSD95: ***$p$<0.001. (**G**) Bar graph shows total HaloTag-GRIA1 fluorescence intensity at synaptic sites after 24 min (in %). Ctrl+PSD95: 73.8±3.45, TARPγ8+PSD95: 73.1±1.29, CKAMP44a+PSD95: 77.9±3.58. (**H**) Percentage of total HaloTag-GRIA1 fluorescence change after 24 min. Data are mean ± SEM. Ctrl n=7 cells, ctrl+PSD95 n=8, TARP+PSD95 n=7, CKAMP44a+PSD95 n=7 (n=6 for synaptic intensity). Statistical analysis was assessed with one way ANOVA and with Student-Newman-Keuls pairwise comparison test.

We also compared the decay of the GRIA1-signal in the control conditions (without CKAMP44a and TARPγ8 overexpression) at extrasynaptic and synaptic domains, and noticed that endocytosis was higher at extrasynaptic than synaptic domains (mean of endocytosis rate ($min^{-1}$): ctrl+PSD95-tagRFPt (extrasynaptic): 0.0256±0.00167, ctrl+PSD95-tagRFPt (synaptic): 0.0127±0.00210, **Figure 45D and E**).

Overall, these findings show that TARPγ8 and CKAMP44a primarily modulated internalization of extrasynaptic, GRIA1-containing AMPARs. In contrast, the turnover of synaptic receptors is not directly dependent on the abundance of auxiliary subunits and is clearly delayed in comparison to extrasynaptic receptors, which possibly indicates that the rate-limiting step for transport and internalization of these receptors is their dissociation from the postsynaptic cluster, but not endocytosis itself.

## 3.11 Induced endocytosis of surface AMPARs is reduced with TARPγ8 overexpression

The density of AMPAR on the dendritic surface depends on the dynamic delivery and reuptake of receptors by exocytosis and endocytosis, respectively. Our previous experiment demonstrated a reduced receptor reuptake under basal conditions, if TARPγ8 was overexpressed. To test whether stimulated endocytosis is also affected by the presence of high amounts of auxiliary subunits, we studied AMPAR endocytosis in hippocampal neurons by acute application of insulin and analyzed the progressive reduction in surface SEP-GRIA1

fluorescence. Neurons (DIV 8-11) were cotransfected with PCI SEP-GRIA1 and pRK5 TARPγ8 IRES NLS-tdTomato, and live-cell imaging of dendritic structures was done as described above. After recording an initial baseline image series of about 2 min, insulin (50 µM) was at least 4 min continously applied to the neurons using a local superfusion system (17 µl/s) until the whole extracellular solution was exchanged with insulin solution. Recording was done in the presence of insulin for the rest of the imaging period after application (~10 min) (**Figure 46A and B**). Insulin has been previously shown to induce fast AMPAR endocytosis within ~10-15 min (Man et al., 2000). In controls, treatment with insulin led to an exponential decay of surface fluorescence, resulting in a 19.5% ± 1.61% reduction of fluorescence within 10 min. In contrast, TARPγ8 overexpression significantly limited the extent of endocytosis to 13.7% ± 1.45% (**Figure 46C and D**). Note that, the rate of endocytosis (monoexponential fit) was not significantly changed (rate of endocytosis ($s^{-1}$): ctrl: 0.152±0.034, TARPγ8: 0.142±0.021, **Figure 46E**), which indicates that a larger fraction of the surface pool is protected against induced endocytosis, while mobile receptors are taken up at normal speed. Thus, TARPγ8 association may actively shield receptors from triggered endocytosis.

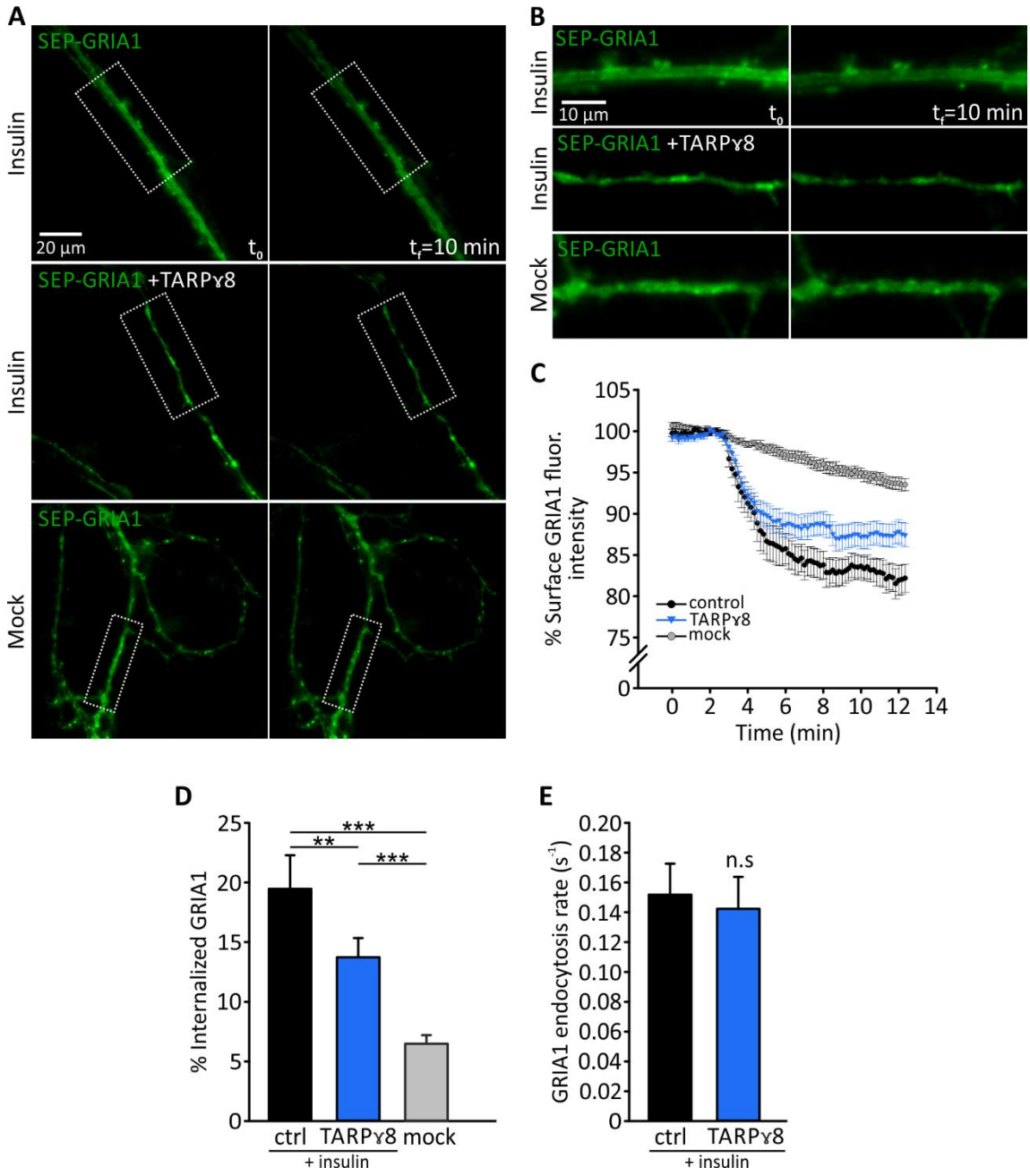


**Figure 46. Insulin induced AMPAR endocytosis is reduced with TARPγ8 overexpression in hippocampal neurons**

(**A**) Exemplary image showing surface SEP-GRIA1 in dendrites from hippocampal neurons (DIV 10) transfected with SEP-GRIA1 (ctrl) (**upper and lower panel**) or cotransfected with TARPγ8 IRES NLS-tdTomato (**middle panel**). Application of insulin solution (50 µM) (**upper and middle panel**) or with normal extracellular solution (mock, **lower panel**). Left column shows dendrites before treatment ($t_0$=0 min) and right column at the end of treatment ($t_f$=10 min). (**B**) Enlarged section of dendrite from (**A**) before and after treatment in the different conditions. (**C**) Traces of SEP-GRIA1 fluorescence change during insulin and normal extracellular solution application. (**D**) Graph showing percentage of internalized SEP-GRIA1 after 10 min. $^{**}p<0.01$, $^{***}p<0.001$. Statistical analysis was assessed with one way ANOVA followed by pairwise comparison with Student-Newman-Keuls. (**E**) Graph showing rate of SEP-GRIA1 endocytosis ($s^{-1}$). $p$=0.811. Statistical analysis was assessed with two-tailed student t-test. Data are mean ± SEM. Ctrl n=18 cells, TARPγ8 n=21 cells, mock n=20 cells. Imaging frequency is 0.1 Hz with 100 ms exposure time. Images were interpolated for better presentation.

# 4. Discussion

Trafficking of AMPARs in neurons can be investigated by several experimental approaches, including biochemistry, immunocytochemistry, and live-cell imaging. In contrast to most antibody-based staining techniques, live-cell imaging allows for a continuous observation of the transport of tagged receptors in individual neurons. Here, we used different, genetically encoded tags in order to study glutamate receptor transfer from intracellular stores to the plasma membrane and in reverse direction. Employing SEP-GRIA1, plasma membrane delivery of GRIA1-containing receptors could be detected as local fluorescence increases, which report the transition of the pH from the acidic lumen of the secretory organelle to the neutral extracellular space. We first used TIRF microscopy to directly visualize receptor insertion of SEP-GRIA1 receptors with high resolution in somatic membrane areas, but soon realized that epifluorescence microscopy is sufficient to follow insertion events in dendrites due to their small dimensions. TIRF and epifluorescence microscopy indeed showed insertion events whose accompanying fluorescence signals were qualitatively nearly identical. Generally, exocytotic events exhibited a fast onset, but varied in their decay properties, possibly not only mirroring receptor dispersion but also reacidification after transient fusion.

Synaptic receptor accumulation is believed to be dynamically altered by neuronal activity, either in a homeostatic fashion to ensure sufficient network activity or to selectively change the efficiency of individual synaptic connections in synaptic plasticity (Henley et al., 2011; Luscher et al., 1999; Malinow and Malenka, 2002). Here, we tested the effects of a chronic depression of neuronal activity by addition of TTX or in consequence of disabled exocytotic machinery (*Snap25*$^{-/-}$ neurons). In both cases, we indeed observed that AMPAR trafficking at the soma was reduced compared to the control condition, indicating that global receptor turnover reacts very sensitive to changes in activity. Given that the majority of synapses are localized on dendrites, we focused in most experiments on trafficking AMPARs in dendritic/neuritic structures in hippocampal neurons. Intracellular AMPARs in dendrites mainly reside in TfR-positive REs, and their mobilization seems to be regulated by different factors and proteins. We show here that two prominent auxiliary subunits influence AMPAR trafficking in the hippocampus: TARPγ8 and CKAMP44a overexpression significantly reduced AMPAR delivery to the dendritic surface. Interestingly, the decrease in exocytosis was accompanied by a reduction in the intracellular pool of AMPAR within RE, which at least in part may also account for a reduced frequency of detectable events. Total surface expression was however not significantly changed, when TARPγ8 and CKAMP44a were overexpressed,

pointing to a general slowdown of receptor turnover in the presence of associated auxiliary subunits. To address correlated changes in endocytosis, we used a GRIA1-variant fused to self-labelling HaloTag, which can be used to follow surface receptors in pulse-chase experiments. We found that TARPγ8 and CKAMP44a overexpression significantly reduced the uptake of receptors at extrasynaptic sites but not at the synaptic site. Promotion of endocytosis by application of insulin affected a smaller fraction of surface AMPAR in cells with high TARPγ8 content. Thus, our data point to a mechanism, in which the presence of auxiliary subunits increases the surface lifetime of AMPARs.

## 4.1 Analysis of AMPA receptor delivery in live-cell imaging experiments with a pH-dependent fluorophore tag

It is well established that AMPARs are dynamically trafficked between intracellular organelles and the surface of neurons (Ehlers*, 2000; Hirling, 2009). While antibody-feeding experiments in combination with biochemical assays were very successful in delineating the general kinetics of AMPAR turnover (Sans et al., 2003), live-cell imaging experiments allow for a more detailed view of individual transport events, especially with respect to incorporation of new AMPARs into the plasma membrane (Roth et al., 2017). Using SEP-tagged GRIA1-subunits in combination with TIRF microscopy, we could observe local fluorescence transients, which represent *bona fide* receptor delivery events to the plasma membrane. While the spatially restricted sample illumination in TIRF microscopy allows for resolving small fluorescence signals near or on the plasma membrane of cultured hippocampal neurons, imaging is largely restricted to membrane sections tightly adhering to the glass coverslip. However, due to the small dimensions of dendrites, we could observe SEP signals in dendrites using conventional epifluorescence illumination, thus allowing us to extend our view to the dendritic compartment, where most of the synapses reside. The fluorescence signals for both experimental approaches were qualitatively very similar, as previously noted by Yudowski et al. (2007). This implies that the same exocytotic mechanism of receptor insertion is employed throughout soma and dendritic compartments. The observed kinetics of putative receptor delivery events is also consistent with the results of several other studies that used SEP-tagged glutamate receptor subunits (Araki et al., 2010; Lin et al., 2009).

However, when comparing the frequency of SEP-GRIA1 delivery events in our experiments with previous published data, it is notable that the number of exocytotic events per

minute was dramatically lower in our TIRF microscopy experiments than in other studies (Yudowski et al., 2007). The up to tenfold difference in fusion event frequency might be explained by different factors: (1) experimental differences that affect event detection. For example, several studies (Araki et al., 2010; Yudowski et al., 2007) used a pre-bleaching protocol to increase sensitivity, which was not regularly employed in our recordings. Moreover, differences in threshold settings and analysis algorithms may contribute to the overall lower count of fusion events in our experiments. (2) Culture conditions and expression levels of SEP-GRIA1 may also influence the apparent rate of receptor delivery. We used cultures around DIV 10 for most experiments, while other studies performed experiments on slightly older cultures (18-19 DIV (Araki et al., 2010); 12-15 DIV (Lin et al., 2009); 15-20 DIV (Yudowski et al., 2007)). It might be speculated that older neurons that entertain a large number of synaptic contacts, require a more developed recycling infrastructure and thus could exhibit higher steady-state delivery rates. In concert with the longer cultivation times also SEP-GRIA1 expression levels were likely also higher in some studies, especially in the experiments of Yudowski et al. (2007) who transfected neurons as early as 5 DIV and performed experiments 10 days later.

Independently of the microscopic technique, experiments with SEP-GRIA1-subunits showed two principle types of fluorescence signals accompanying putative AMPAR delivery events: (1) In the case of "short burst events", the fluorescence signal rapidly decayed in less than one second after an initial fast onset. (2) In contrast, fluorescence signals with a total decay time of ~ 2 s and variable kinetics were classified as "long display events". Both event types have been reported in virtually all studies that use pH-dependent fluorophore-tags (Jullie et al., 2014; Yudowski et al., 2007), although the criteria for classification slightly varied. For example, Yudowski et al. (2007) categorized AMPAR delivery within ~ 1 s as "transient events" and signals lasting 5-10 s as "persistent events". In agreement with that, our experiments showed event decay times typically ranging between 0.5 and 25 s, according to what was published before included so-called transient (short burst) and persistent (long display) events (Yudowski et al., 2007). It stands to reason that the duality of kinetic profiles indicates the existence of different delivery pathways or fusion modes. Interestingly, different types of receptor cargo (e.g. GRIA1, TfR, and β2 adrenergic receptor) have been observed to exhibit similar kinetic profiles in neurons, while long display events were rarely seen in astrocytes and fibroblasts (Jullie et al., 2014). That said, there is also a relationship between the type of cargo and event kinetics in neurons, as for example, different GPCRs exhibited different signal shapes (Yudowski and von Zastrow, 2011). The decay kinetics of fast fusion

events may represent a rapid dispersion of AMPARs on the neuronal surface after the transport organelle has collapsed into the plasma membrane. Indeed, we could observe several events (**Figure 25B**), in which a clear broadening of the fluorescent signal was found in consecutive images, pointing to a lateral diffusion of the freshly inserted receptors as the prime reason for the fluorescence decrease at the fusion site. Similar observations have been previously made by Yudowski et al. (2007), who estimated the portion of dendritic delivery events that increased the fluorescence of neighboring spines to be around 25 % of transient signals. Noteworthy, they also report that longer lasting persistent events did not produce a fluorescence increase in their experiments. Assuming that the transport organelles can also engage in kiss-and-run fusion instead of full fusion (Alabi and Tsien, 2013), a fluorescence decay might alternatively reflect the reacidification of the resealed intracellular structures. A systematic analysis by Jullie et al. (2014) indeed showed that repeated variation of extracellular pH does not result in correlated changes in the long-lasting fluorescence transients accompanying the putative delivery of SEP-marked receptors from REs, indicating that the compartment has already fully resealed. In line with this idea, we show here that TfR-tagRFPt-positive REs persisted after fusion reported by SEP-GRIA1 cargo. Thus, it seems that only limited amounts of the receptor cargo are indeed delivered to the surface by kiss-and-run fusion.

It is interesting to note that recent work on large dense core vesicle (LDCV) fusion in neuroendocrine chromaffin cells suggested a tight coupling between exocytotic and endocytotic processes. Respectively, they allow for a dynamic shrinking and expansion of the organelle in the fusion pore ("Ω") stage, resulting either in the loss of the vesicle or its recovery at unchanged or altered size (Chiang et al., 2014). A similar dynamic membrane and cargo flow through a dynamic fusion pore may also underlie the delivery of AMPAR via transport vesicles and recycling endosomes, thereby explaining the varying kinetic profiles of fusion events.

### 4.1.1 Activity dependent AMPAR surface insertion

While AMPAR exocytosis occurs constitutively, a wealth of experimental evidence has suggested that the trafficking of AMPARs onto the plasma membrane and into the postsynaptic density is regulated by neuronal activity (Ehlers*, 2000), and may be critical for synaptic plasticity (Malinow and Malenka, 2002). By chronically depressing the activity of neurons using TTX or utilizing *Snap25*$^{-/-}$ neurons that have a disabled exocytotic machinery (Sollner et al., 1993), we could show that AMPAR trafficking is significantly reduced. Unlike GRIA2

subunit which has been often attributed to constitutive surface trafficking, GRIA1 trafficking is activity dependent and considered the driving force of receptors to the surface (Passafaro et al., 2001). By using SEP-GRIA1 in combination with TIRF microscopy, we could show that the number of transient exocytotic events was dramatically reduced in both conditions. Our result agrees with what was shown before when neurons were treated with a cocktail of inhibitors suppressing neuronal activity to study GRIA1 surface insertion (Lin et al., 2009). Considering the stronger effect of $SNAP25^{-/-}$ on GRIA1 surface insertion as compared to that of TTX, it is possible that SNAP25 SNARE protein plays an additional role in the fusion machinery of AMPAR organelles and does not only impair neuronal activity. Indeed, SNARE proteins, like Syntaxin-4 and SNAP-23, have been proven to interfere in glutamate receptor trafficking in dendrites, and SNAP-25 has been related particularly to NMDA receptor trafficking (Kennedy et al., 2010; Lau et al., 2010; Suh et al., 2010). These findings support our hypothesis that SNAP25 is involved in the fusion of GRIA1 receptor to the surface membrane.

In addition to the frequency of exocytosis, we tested whether reduced activity of neurons influences the fusion kinetics of SEP-GRIA1. We analyzed the different parameters of SEP-GRIA1 membrane fusion and saw that the event amplitude was clearly smaller with depressed neuronal activity. This suggests a reduced receptor content in the trafficking organelle probably due to a lower recycling rate. However, Yudowski et al. (2007) showed that when LTP was induced chemically, the receptor content per vesicle was not increased although the exocytotic rate was raised. According to this study, we should not observe a difference in RE content when exocytotic events decrease. The discrepancy of analysis and interpretation may be a result of the different experimental setup compared to Yudowski's et al. (2007) study, where they used older neurons (DIV 15-20) than we did (DIV 9-12). Moreover, the type of analysis done to quantify the different kinetic parameters, like setting thresholds for example, may also play a role in the variable outcome. Regardless of the effect on the RE content, the change in frequency of exocytosis events upon low activity of neurons in our experiments agrees with the published data. Overall, our results reveal that trafficking of AMPAR organelles is regulated by neuronal activity.

## 4.2 AMPAR delivery events in dendrites primarily constitute transient fusion of recycling endosomes

The population of surface AMPARs is complemented by a pool of receptors residing in different intracellular stores, which are shifted to the plasma membrane in an activity-

dependent fashion. There is still considerable debate about the specific delivery pathways and relative contributions of newly synthesized receptors versus recycled receptors under different physiological conditions (Bowen et al., 2017; Hangen et al., 2018; Ju et al., 2004). Indeed, recent work by Hangen et al. (2018) demonstrated considerable intracellular vesicular transport and surface insertion of freshly synthesized AMPARs in dendrites, which could be modulated by chemical induction of LTP and receptor phosphorylation. Fusion of recycling endosomes might as well contribute to the receptor delivery process, with recent evidence even pointing to direct transport of locally synthesized receptors to this compartment without intermittent GOLGI processing (Bowen et al., 2017). As the frequency of dendritic fusion events is meaningless without information about the abundance of intracellular stores, we specifically visualized AMPAR-containing intracellular compartments taking advantage of the locally existing organelles, where synthesized AMPAR might directly represent another "source" of AMPAR-containing transport vesicles for the replenishment of the surface pool (Hangen et al., 2018). While discrete AMPAR organelles were previously detected by antibody labeling followed by biochemical permeabilization and fixation (Carroll et al., 1999), we were able to visualize local AMPAR intracellular organelles using SEP-GRIA1 in combination with live epifluorescence imaging of fine dendritic structures. Plenty of studies have shown that membrane trafficking of AMPAR is accomplished through REs in dendrites and triggered by synaptic activity to replenish the surface membrane (Brown et al., 2007; Park et al., 2004). Specifically, Rab11-dependent REs and Rab8 have been shown to dominate the population in the dendritic shaft and spine region for surface delivery and final insertion of receptors (Brown et al., 2007; Cooney et al., 2002; Park et al., 2004), although AMPARs may be contained in different endocytic compartments in the neuron (Hausser and Schlett, 2017). In agreement with the published data, we could show through live dual view imaging that almost all visualized intracellular SEP-GRIA1 organelles in dendrites were located in reservoirs of REs that were marked with the TfR-tagRFPt recycling endosome marker. However, we cannot rule out that other trafficking organelles (newly synthesized AMPARs) and endosomes (early and sorting endosomes) exist in the dendrite that we did not mark to visualize (Cooney et al., 2002; Ehlers*, 2000; Hangen et al., 2018; Hausser and Schlett, 2017). Unlike dendrites, using TIRF microscopy to visualize individual REs in soma was not possible due to the crowdedness of endosomes and spatial limitation of the imaging technique. As for dendrites, we further showed that SEP-GRIA1 exocytosis events occurred locally at regions of RE stores. We could almost correlate all SEP-GRIA1 events (~82 %) to existing REs marked with TfR-tagRFPt. Depending on a previous study showing through electron microscopy that several spines share common

REs, it can be assumed that AMPAR containing REs are in a continuous dynamic movement to locally deliver receptors to the neighboring surface membrane (Cooney et al., 2002). Moreover, our result supports recent findings showing that induced release of AMPAR-containing REs from dendritic ER by chemical means accumulate locally before surface delivery (Bowen et al., 2017). Thus, AMPARs stored in dendritic REs undergo local trafficking and subsequently release receptors in the neighboring surface membrane.

## 4.3 Impact of TARPγ8 on transient AMPAR exocytosis and intracellular trafficking

Auxiliary subunits have been proposed to interact with AMPARs promoting their trafficking and regulating the channel properties (Haering et al., 2014). Transmembrane AMPA receptor regulatory proteins (TARPs) were the first auxiliary proteins to be identified (Burgess et al., 2001; Chen et al., 2000). Predominantly present in the hippocampus, TARPγ8 has been shown to occupy important roles in the surface expression of AMPAR in addition to regulating the channel function (Fukaya et al., 2006; Rouach et al., 2005; Tomita et al., 2003; Zheng et al., 2015a). Previously published data showed an increase in AMPAR surface expression without affecting the total protein expression when TARPγ8 was overexpressed suggesting a shift between surface and total receptor levels (Rouach et al., 2005). We could not reproduce this finding by quantifying the surface fluorescence of SEP-GRIA1. In other words, we did not obtain increased GRIA1 surface expression with overexpressed TARPγ8. The difference with previous result is not due to a mislocalization of SEP-GRIA1 because control experiments in which we measured miniEPSC showed a clear increase in spontaneous currents when SEP-GRIA1 was overexpressed indicating correctly localized receptors on the surface membrane. However, the difference in outcome may be assigned to the difference in quantification of surface receptors or to the experimental setup. Rouach et al. (2005) used immunofluorescent labelling to assess AMPAR surface expression whereas we obtained surface fluorescence by direct subtraction of internal fluorescence in live imaging of SEP-GRIA1 in hippocampal neurons. It is noteworthy to mention that AMPAR surface level as well as total expression was severely reduced when TARPγ8 was knocked out indicating that TARPγ8 indeed is involved in AMPAR surface delivery (Fukaya et al., 2006; Rouach et al., 2005). Interestingly, our negative control, GSG1L overexpression, reduced GRIA1 surface expression, which goes in line with previously published studies showing a suppressive role of

GSG1L on AMPAR surface delivery (Gu et al., 2016a). Hence, we are confident that our method to assess GRIA1 surface expression is correct. In addition, the discrepancy between GSG1L and TARPγ8 effect confirms the differential regulation of AMPARs by auxiliary subunits (Greger et al., 2017; Haering et al., 2014). Furthermore, to highlight the role of TARPγ8 on AMPAR surface delivery, we studied the rate of transient GRIA1 exocytotic events in TARPγ8 overexpressing neurons under basal conditions by using SEP-GRIA1 variant as previously explained. The primary effect seen through TARPγ8 overexpression was a dramatic reduction in GRIA1 exocytosis. To further interpret this result, we quantified the dendritic GRIA1 RE stores with TARPγ8 overexpression. Indeed, our detailed quantification of GRIA1 intracellular stores showed a strong correlation with the number of GRIA1 exocytotic events. High amounts of TARPγ8 went hand in hand with the decreased GRIA1 RE content together with the reduced GRIA1 exocytosis rate. Indeed, this result is in agreement with previous data showing that impairing TARPγ8 function leads to an increased intracellular accumulation of AMPARs (Zheng et al., 2015a), which may explain why with intact TARPγ8 overexpression we obtain less AMPARs in REs. However, one cannot exclude the possibility that the reduction in GRIA1 RE content may influence the detectability of the GRIA1 transient fusion events with less intense signals. In other words, SEP-GRIA1 may have fluorescence intensities during membrane fusion that lay under the threshold of detection. Therefore, in case of TARPγ8 overexpression, some SEP-GRIA1 fusion events may be missed due to smaller fluorescence intensity of the RE. Thus, TARPγ8 clearly reduces GRIA1 exocytosis, but the technical limitation should be taken into consideration to what extent TARPγ8 affects exocytosis.

In agreement with the decreased GRIA1 RE stores, GRIA1 RE count was also reduced in the dendrites when TARPγ8 was overexpressed. Moreover, the number of GRIA1 exocytosis events were correlated to the number of REs, explaining why we saw reduced GRIA1 exocytotic rate with TARPγ8 overexpression.

The decreased GRIA1 exocytosis and intracellular stores when TARPγ8 is overexpressed can be attributed to the reduced recycling of GRIA1 receptors. One reasonable explanation for the low recycling rate is the stabilization of GRIA1 receptors by TARPγ8 on the dendritic membrane. A similar function on AMPAR stabilization has been recently identified for the canonical TARP stargazin/TARPγ2 subunit via cryo-electron microscopy (Twomey et al., 2016). Since AMPAR trafficking in REs is important for the replenishment of the synaptic site in a constitutive and activity-dependent manner (Gerges et al., 2004; Park et

al., 2004), it might be possible that a stabilization of AMPARs on the membrane counteracts the forward trafficking of the receptors.

Intensive studies have shown a direct role of PSD95 protein in stabilizing AMPARs on the postsynaptic membrane through the interaction with TARP proteins at their C-terminal domain. Whereas a direct binding between PSD95 and AMPAR is not possible because the AMPAR does not have a PDZ binding motifs (Bats et al., 2007; Nicoll et al., 2006; Stein et al., 2003), a direct assembly between TARP protein and AMPAR has been proven to exist and intermediate between PSD95 and AMPAR in several studies (Bats et al., 2007; Kim et al., 2010; Shi et al., 2009). Accordingly, an increase in TARPγ8 levels would enhance the molecular linking between available AMPARs and PSD95, thus leading to more stability of receptors on the surface membrane.

Previous published data shows that TARPγ8 is required for basal AMPAR trafficking and neurotransmission (Rouach et al., 2005; Sumioka et al., 2011). In line with that, the prominent effect of TARPγ8 on AMPARs we saw in our experiments was also under basal condition of neurons. However, TARP proteins, including TARPγ8, are also thought to regulate AMPAR trafficking for LTP and neuronal plasticity (Khodosevich et al., 2014; Rouach et al., 2005; Tomita, 2010). As with TARPγ8$^{-/-}$ neurons, LTP was impaired in these neurons (Rouach et al., 2005). Obviously, TARPγ8 regulates AMPAR trafficking under basal and activity-dependent condition but which details still have to be clarified.

## 4.4 AMPAR endocytosis

AMPAR surface expression is dynamically regulated by continuous removal of receptors through endocytosis and subsequent insertion of new ones (Carroll et al., 1999; Mukherjee et al., 1997; Turrigiano, 2000). While antibody feeding assays and western blots were successful in characterizing the endocytosis of AMPARs (Carroll et al., 1999; Zheng et al., 2015b), live imaging has added new details to follow the process of endocytosis in real time. Using a GRIA1-variant tagged to a self labelling HaloTag sequence (Urh and Rosenberg, 2012), we were able to stain exclusively the surface membrane of hippocampal neurons with an impermeable ligand tagged to Alexa Fluor 488. Confocal imaging allowed us to observe a gradual decrease in fluorescence intensity of defined membranous structures indicating consequent receptor endocytosis. Employing this technique, we studied basal GRIA1 endocytosis in dendrites and by using the well-known postsynaptic marker, PSD95 tagged to –

tagRFPt, we were able to differentiate between synaptic and extrasynaptic receptor endocytosis. Although AMPARs are present along the dendrite, our investigation showed that receptor uptake by endocytosis was clearly higher in the extrasynaptic site. Our data goes in line with a wealth of studies showing that AMPARs become internalized at hot spots of extrasynaptic or perisynaptic sites rather than at synapses sites (Ashby et al., 2004; Blanpied et al., 2002; Petrini et al., 2009; Tao-Cheng et al., 2011). The exact site of endocytosis is debatable. Whereas experiments using electron microscopy show that AMPARs are internalized at regions of the dendritic shaft and spine neck (Cooney et al., 2002), single particle tracking indicate that AMPARs can be endocytosed from regions laterally near the postsynaptic density (PSD) called endocytic zones (EZs) (Petrini et al., 2009; Rosendale et al., 2017). However, our quantification of surface fluorescence at the synaptic site still showed a considerable percentage of GRIA1 uptake (~27 %). Indeed, synaptic AMPARs are also cycled in and out, but rather by lateral diffusion to neighboring endocytic sites of the extrasynaptic domain for internalization as shown in many studies (Ashby et al., 2004; Ashby et al., 2006). Published data shows that AMPAR rapid internalization at extrasynaptic site precedes slow removal from the synapse (Ashby et al., 2004), which was also later confirmed by detailed studies characterizing the sites of AMPAR endocytosis post-lateral diffusion from the synapse for recycling (Petrini et al., 2009; Rosendale et al., 2017). However, we cannot exclude completely that AMPARs may be recycled from the synapse, as one study showed that AMPARs are inserted in the spine upon LTP (Patterson et al., 2010). Together these results show that AMPAR is dynamically recycled on the dendritic membrane with a differential endocytic rate between extrasynaptic and synaptic receptors.

## 4.5 Effect of TARPγ8 on basal AMPAR endocytosis

TARPγ8 regulates forward trafficking of AMPARs in hippocampal neurons (Rouach et al., 2005; Tomita et al., 2003); however, its role in AMPAR reuptake and endocytosis has not been investigated yet. Therefore, to follow up our finding that TARPγ8 reduces GRIA1 membrane recycling in dendrites, we intended to examine the effect of TARPγ8 overexpression on AMPAR endocytosis by using HaloTag-GRIA1 variant to stain the dendritic surface of neurons. Moreover, we differentiated between extrasynaptic and synaptic GRIA1 endocytosis by using PSD95-tagRFPt synaptic marker as mentioned before. TARPγ8 overexpression did not show any additional effect on synaptic GRIA1 endocytosis although we are suggesting that

TARPγ8 stabilizes AMPARs on the surface membrane. As discussed earlier, synaptic AMPARs are protected from endocytosis and are rather removed from the postsynaptic density by lateral diffusion (Ashby et al., 2004). Therefore, the absence of TARPγ8 effect on synaptic GRIA1 reuptake can be due to the difficulty to distinguish minor fluorescence changes arising from lateral migration of receptors towards the extrasynaptic site. We indeed could assume that synaptic AMPAR reuptake should be reduced with TARPγ8 overexpression, knowing that TARP protein interacts with the AMPAR and forms an intermediate (TARP/AMPAR) for the binding with PSD95 for receptor stabilization (Bats et al., 2007; Nicoll et al., 2006). A study supporting this idea showed that disrupting the binding between stargazin/TARPγ2 and PSD95 increases surface diffusion of AMPARs and impairs synaptic accumulation of receptors (Bats et al., 2007). In fact, AMPARs, and unlike NMDARs (Niethammer et al., 1996), do not have a PDZ binding motif to bind PSD95. Therefore, an increase in TARPγ8, as a binding intermediate, should enhance AMPAR stability. Interestingly, this stabilization was shown to occur mainly under basal condition (Bats et al., 2007; Nicoll et al., 2006), which was the case in our experiments too, but we did not see a reduced endocytic effect on the synaptic level. Furthermore, TARPγ8 plays a role in synaptic potentiation as its absence impaired LTP (Khodosevich et al., 2014; Park et al., 2016; Rouach et al., 2005) suggesting that we may find a more obvious modulation of synaptic AMPAR internalization if tested under synaptic potentiation. In other words, we may have a stronger reduction in AMPAR internalization rate when TARPγ8 is overexpressed and neurons are stimulated for LTP. Another possibility could be that AMPARs are supposed to be naturally stabilized on the synaptic membrane through postsynaptic proteins, including auxiliary subunits, which makes it redundant if TARPγ8 is overexpressed especially that we were working with wild type background neurons (Bats et al., 2007; Nicoll et al., 2006; Stein et al., 2003). Intriguingly, a wealth of studies showed the involvement of other proteins in regulating the synaptic anchoring of AMPARs. Among others, GRIP1, PICK1, MAGUK proteins, and other AMPAR auxiliary proteins modulate the receptor stability on the synaptic membrane (Dong et al., 1997; Greger et al., 2017; Lin and Huganir, 2007; Xu, 2011). GRIP1 for instance, binds directly and enhances AMPAR accumulation at the synapse whereas PICK1 is the antagonist that enhances AMPAR internalization (Dong et al., 1997; Lin and Huganir, 2007). Obviously, AMPAR stabilization in the synaptic site involves several proteins making it complicated to observe the effect of TARPγ8 only especially that receptor endocytosis occurs post-lateral diffusion to extrasynaptic sites.

On the other hand, our findings show a clear reduction in extrasynaptic GRIA1 endocytosis under basal activity when TARPγ8 was overexpressed. Taking into account that

AMPARs are endocytosed in the extrasynaptic domain (Ashby et al., 2004; Blanpied et al., 2002) and that TARPγ8 is distributed on the dendritic membrane including the extrasynaptic site (Fukaya et al., 2006), GRIA1 receptors are presumably stabilized at the extrasynaptic membrane upon excessive numbers of TARPγ8. Studies supporting our assumption showed a consequent and drastic reduction in extrasynaptic AMPARs as well as in AMPAR mediated responses (~90 %) in TARPγ8$^{-/-}$ neurons (Fukaya et al., 2006; Rouach et al., 2005). Moreover, the studies emphasizing the notion that internalization of AMPARs mainly occurs in extrasynaptic and endocytic zones (EZs) and maintain a mobile pool of receptors (Ashby et al., 2004; Borgdorff and Choquet, 2002; Petrini et al., 2009) supports our assumption that TARPγ8 overexpression in our experiment has slowed down receptor mobility thus reducing GRIA1 endocytosis. The immobilization and accumulation of AMPARs at synapses is a characteristic of potentiation to enhance synaptic transmission (Petrini et al., 2009), which may be a role also played by TARPγ8 to enhance synaptic activity. Our findings imply that TARPγ8 stabilizes AMPARs on the extrasynaptic membrane by shielding their endocytosis.

Overall, our results demonstrate that TARPγ8 exclusively modulates the stability of inserted AMPARs in the extrasynaptic site by reducing endocytosis without showing a clear effect on the synaptic AMPARs under basal conditions. Thus, TARPγ8 effect on AMPAR endocytosis generally complements the results obtained with AMPAR exocytosis and intracellular stores all referring to a role in stabilization on the surface membrane by the auxiliary protein.

### 4.5.1 TARPγ8 reduces stimulated AMPAR endocytosis in hippocampal neurons

TARPγ8 role in AMPAR surface expression is prominent under basal activity although it has been shown to contribute in an activity dependent manner (Park et al., 2016; Rouach et al., 2005; Sumioka et al., 2011). We discussed previously that TARPγ8 reduces AMPAR endocytosis under basal activity. In the present study, using SEP-tagged GRIA1-subunits to visualize surface fluorescence and inducing GRIA1 endocytosis via insulin treatment in hippocampal neurons, we examined the effect of TARPγ8 overexpression on stimulated GRIA1 endocytosis. Insulin was shown to accelerate AMPAR endocytosis and induce LTD in the past (Man et al., 2000). Indeed, when we acutely applied insulin, we saw an increased endocytosis rate of GRIA1 receptors. However, it is important to mention that constitutive and regulated endocytosis of AMPARs pass through different pathways and involve different

proteins (Man et al., 2000; Rosendale et al., 2017; Zheng et al., 2015b). Activity dependent endocytosis of AMPARs involves the classical clathrin-mediated pathway that had been generally accepted before (Ehlers*, 2000; Man et al., 2000; Merrifield et al., 2005). Later, a clathrin-independent pathway of endocytosis was identified to dominate during basal activity (Glebov et al., 2015; Zheng et al., 2015b). According to published data, constitutive AMPAR endocytosis is either mediated through two GTPases Arf6 (ADP-ribosylation factor 6) and TC10 proteins (Zheng et al., 2015b) or through Rac1 and a pool of F-actin (Glebov et al., 2015). Interestingly, when we overexpressed TARPγ8, induced SEP-GRIA1 endocytosis by insulin was strongly reduced. Our finding indicates that TARPγ8 regulates GRIA1 endocytosis in an activity dependent manner as well as under basal activity as we showed before. Although our results for GRIA1 constitutive and stimulated endocytosis are similar with TARPγ8 overexpression indicating reduced endocytosis, the way of endocytosis may be different. According to our hypothesis, TARPγ8 stabilizes AMPARs on the surface membrane consequently reducing endocytosis. However, TARPγ8 presumably protects AMPARs from clathrin mediated endocytosis upon regulated activity (Man et al., 2000) and from clathrin independent endocytosis under basal activity (Glebov et al., 2015; Zheng et al., 2015b). Interestingly, clathrin dependent AMPAR endocytosis takes place during LTD and is suggested to occur during synaptic potentiation (Zheng et al., 2015b). Therefore, TARPγ8 may increase AMPAR stabilization upon increased synaptic activity to enhance synaptic transmission. In conclusion, our findings reveal that TARPγ8 reduces AMPAR endocytosis upon stimulation as well as under basal activity to stabilize receptors on the surface membrane.

## 4.6 Impact of CKAMP44a on AMPAR transient exocytosis and intracellular trafficking

Recent studies have identified several AMPAR auxiliary proteins of prominent roles in AMPAR channel regulation and surface expression (Greger et al., 2017). The novel CKAMP44 auxiliary protein, with its “a” and “b” variants, was recently identified as a prominent auxiliary subunit that modulates AMPAR trafficking and function in dentate gyrus (DG) granule cells and hippocampal neurons (von Engelhardt et al., 2010). Although not expressed in high amounts in the hippocampus, CKAMP44 was shown to increase AMPAR surface expression in these types of neurons (Khodosevich et al., 2014). However, our data disagrees with this outcome, as quantifying the surface fluorescence using SEP-GRIA1 variant we did not obtain

increased GRIA1 surface expression when CKAMP44a isoform was overexpressed. As we suggested for TARPγ8 auxiliary subunit previously, the difference in outcome may be referred to the difference in quantification of surface receptors or to the experimental setup. Khodosevich et al. (2014) used impermeable antibody feeding assay to label and assess AMPAR surface expression whereas we obtained surface fluorescence by direct subtraction of internal fluorescence in live imaging of SEP-GRIA1 in hippocampal neurons. It is not clear how CKAMP44 regulates AMPAR surface trafficking, but it is proposed to regulate AMPAR delivery through controlling ER exit, which is a known function for the *Shisa* protein family (Nagano et al., 2006; Yamamoto et al., 2005). For example, CKAMP44 overexpression increased surface AMPARs in heterologous cells (Khodosevich et al., 2014) thus indicating a role in AMPAR surface expression but which details have still to be resolved (von Engelhardt, 2019). Interestingly, the negative control GSG1L overexpression, compared to CKAMP44a, reduced GRIA1 surface expression in our experiments, which agrees with the recent study showing a suppressive role of GSG1L auxiliary subunit on AMPAR surface delivery (Gu et al., 2016a) as we discussed earlier. Our finding about the effect of GSG1L, TARPγ8, and now CKAMP44a on GRIA1 surface expression again confirms that auxiliary subunits differentially regulate AMPAR trafficking supporting previous studies (Greger et al., 2017; Haering et al., 2014). Furthermore, to highlight the role of CKAMP44a on AMPAR surface delivery, we studied the rate of transient GRIA1 exocytotic events in CKAMP44a overexpressed neurons under basal conditions by using SEP-GRIA1 similar to what we did in case of TARPγ8 overexpression. GRIA1 exocytosis rate was dramatically reduced with CKAMP44a overexpression indicating a decreased GRIA1 delivery to the surface membrane. To further interpret this result, we quantified the dendritic GRIA1 intracellular RE stores with CKAMP44a overexpression. Indeed, our quantification of GRIA1 intracellular stores showed a strong correlation to the number of GRIA1 exocytotic events. As with high amounts of CKAMP44a, GRIA1 RE content went hand in hand with the reduction of GRIA1 exocytosis rate. However, the assumption that the reduction in GRIA1 RE content may influence the detectability of the GRIA1 transient fusion events that have less intense signals should also be considered in case of CKAMP44a overexpression since we used the same experimental setup as in case of TARPγ8. In other words, SEP-GRIA1 may have fluorescence intensities during membrane fusion that lay under the threshold of detection. Therefore, in case of CKAMP44a overexpression, some SEP-GRIA1 fusion events may be missed due to smaller fluorescence intensity exerted by the RE upon exocytosis. Thus, the technical limitation should be taken into consideration when interpreting the strong effect of CKAMP44a on GRIA1 exocytosis as we

interpreted also for TARPγ8. Moreover, GRIA1 RE number was also reduced with CKAMP44a overexpression going in line with the reduction in GRIA1 exocytosis and RE content as it was the case for TARPγ8 overexpression. Overall, the overlapping phenotype of CKAMP44a overexpression to that of TARPγ8 suggests a similar role in modulating the recycling of AMPAR on the surface membrane thus stabilizing them. Previous data supporting this idea shows that CKAMP44 deletion reduces surface AMPARs in dendrites, precisely in the extrasynaptic and synaptic sites (Khodosevich et al., 2014). However, CKAMP44 is involved in short-term plasticity (Khodosevich et al., 2014) whereas TARPγ8 in LTP (Park et al., 2016; Rouach et al., 2005) suggesting that both stabilize AMPARs on the surface membrane but differentially regulate neuronal activity. Indeed, CKAMP44 modulates the gating of AMPAR channel differently from TARPγ8. While TARPγ8 increases the desensitization period and decreases the recovery period, CKAMP44 does the opposite (Khodosevich et al., 2014). In fact, coimmunoprecipitation experiments show that CKAMP44 associates with TARPγ8 indicating that they may exist in the same AMPAR receptor complex to differentially modulate its function (Khodosevich et al., 2014). Our findings reveal that CKAMP44a reduces AMPAR surface delivery and consequently decreases receptor turnover in purpose to stabilize them as it is also attributed for TARPγ8 (Rouach et al., 2005).

## 4.7 Effect of CKAMP44a on AMPAR endocytosis

CKAMP44a was shown to promote the surface expression of AMPARs in the hippocampus (Khodosevich et al., 2014). Moreover, our assumption that CKAMP44a presumably stabilizes AMPARs on the surface membrane following the strong impact of CKAMP44a on AMPAR exocytosis and intracellular stores led us to study its effect on AMPAR endocytosis to further confirm this hypothesis. By using HaloTag-GRIA1 variant to stain the dendritic surface of neurons with an impermeable ligand tagged to a fluorescent dye and PSD95-tagRFPt synaptic marker to differentiate between synaptic and extrasynaptic GRIA1 receptors as we did for TARPγ8 overexpression, we examined the impact of CKAMP44a overexpression on basal GRIA1 endocytosis. The absence of CKAMP44a effect on synaptic GRIA1 endocytosis was similar to the observed result of TARPγ8 suggesting the same interpretation that synaptic AMPAR endocytosis does not occur. Synaptic AMPARs are protected from endocytosis through postsynaptic proteins, and any minor receptor reuptake at the synaptic site would be difficult to recognize through small fluorescence changes. Indeed, CKAMP44 has a preserved PDZ type II binding motif (EVTV) at its C-terminal domain that

serves as a binding site for PDZ proteins, like PSD95, to intermediate the stabilization of AMPARs (Farrow et al., 2015; Karataeva et al., 2014; Khodosevich et al., 2014; Kunde et al., 2017; von Engelhardt, 2019) thus preventing reuptake of receptors. In line with that, deleting CKAMP44 (CKAMP44$^{-/-}$) reduces synaptic AMPARs indicating that CKAMP44 enhances receptor accumulation on synapses (Khodosevich et al., 2014; von Engelhardt, 2019). Therefore, a more detailed analysis using more accurate detection tools to resolve small fluorescence changes may indicate a pronounced effect of CKAMP44a on the synaptic AMPAR reuptake. As we mentioned earlier, synaptic AMPAR removal occurs through lateral diffusion upon release from PSD95 binding (Ashby et al., 2004; Ashby et al., 2006; Bats et al., 2007), which rate should perhaps decrease with CKAMP44a overexpression. Another possibility would be the redundancy of overexpressed CKAMP44a among the existence of all other scaffold proteins on the synapse as we also suggested for TARPγ8 overexpression.

While synaptic AMPAR internalization was absent, extrasynaptic AMPAR endocytosis was strongly reduced under basal activity with CKAMP44a overexpression. Interestingly, CKAMP44$^{-/-}$ showed a reduction in extrasynaptic and synaptic AMPARs in hippocampal neurons (Khodosevich et al., 2014), which suggests that CKAMP44 somehow plays a role in extrasynaptic AMPAR expression. However, in contrary to TARPγ8 that localizes on synaptic and extrasynaptic site (Fukaya et al., 2006), CKAMP44 has yet only been shown to localize at the synaptic site (von Engelhardt et al., 2010), which raises the question how it regulates extrasynaptic GRIA1 expression and reduces endocytosis as we obtained. Interestingly, CKAMP44 and CKAMP52 have been found to associate with AMPAR complexes containing TARPγ8 subunit (Khodosevich et al., 2014; Klaassen et al., 2016). Therefore, it is very plausible that CKAMP44 also localizes on the extrasynaptic membrane to stabilize AMPARs by reducing their mobility but which has still to be proven. Moreover, the fact that internalization of AMPARs mainly occurs in extrasynaptic sites that maintain a mobile pool of receptors (Ashby et al., 2004; Borgdorff and Choquet, 2002; Petrini et al., 2009), supports our assumption that CKAMP44a overexpression in our experiment has slowed down receptor mobility leading to reduced GRIA1 endocytosis similar to TARPγ8 overexpression. The immobilization and accumulation of AMPARs at synapses is a characteristic of potentiation to enhance synaptic transmission (Petrini et al., 2009), which may be a role also played by CKAMP44a to enhance synaptic activity as we also suggested for TARPγ8. However, CKAMP44 was shown to enhance short term plasticity (Khodosevich et al., 2014) and not LTP as TARPγ8 (Khodosevich et al., 2014; Park et al., 2016; Rouach et al., 2005) thus playing a differential role in stabilization of AMPARs.

Overall, our results show that CKAMP44a modulates AMPAR recycling by shielding endocytosis on the extrasynaptic membrane suggesting a stabilization role without affecting synaptic AMPAR endocytosis. Therefore, CKAMP44a regulation of endocytosis, exocytosis, and intracellular stores refer to a stabilization effect on the surface membrane as suggested for the TARPγ8 auxiliary protein.

## 4.8 Conclusion and Perspective

AMPARs are dynamic receptors that continuously migrate in and out of the plasma membrane to maintain the balance between intracellular and surface receptors for regulated synaptic activity. Overall, our study demonstrates some of the properties of AMPAR trafficking and the role of prominent auxiliary proteins in the regulation of this trafficking. We have first characterized the AMPAR trafficking system in soma and dendrites by examining the rate of exocytosis and its kinetics. In addition, we showed in dendrites that AMPARs are predominantly stored and delivered in recycling endosomes.

Later, we studied the regulation of AMPAR trafficking and recycling by AMPAR auxiliary proteins. Two prominent auxiliary proteins, TARPγ8 and CKAMP44a, showed a regulatory effect on the recycling of AMPARs under basal condition and in an activity dependent manner. While surface expression of AMPARs was unchanged with excessive amount of TARPγ8 or CKAMP44a, surface delivery of AMPARs under basal conditions was strongly reduced indicating decreased exocytosis. Interestingly, the downsized exocytosis rate was accompanied with reduced intracellular RE stores implicating a reduced turnover of AMPARs with the plasma membrane. Furthermore, AMPAR endocytosis was also decelerated upon overexpression of auxiliary subunits in dendrites, precisely at the extrasynaptic site. Overall, our findings showed a reduced exocytosis and endocytosis of AMPARs hand in hand with the reduced intracellular stores but without affecting the surface expression of receptors upon overexpression of auxiliary subunits. Thus, auxiliary subunits presumably stabilize AMPARs on the surface membrane by reducing the recycling and consequently leading to a prolonged lifetime of surface receptors that regulate neuronal activity (**Figure 47)**.

Our experiments were done with wild type background neurons to test the effect of TARPγ8 and CKAMP44a subunits on AMPAR recycling. It would be interesting to test in the future AMPAR exocytosis and endocytosis using our same live imaging methods with either TARPγ8 or CKAMP44a knockout neurons. We can also examine the AMPAR intracellular stores as well. According to our data, we would expect the opposite in case of auxiliary subunit

knockout. In other words, AMPAR endocytosis and exocytosis may increase due to increased turnover rate because receptors are then less stabilized on the surface membrane in the absence of a prominent auxiliary subunit, which consequently would also increase the intracellular AMPAR stores in recycling endosomes. Moreover, to understand the underlying mechanisms of the regulation of AMPAR trafficking by auxiliary subunits, it is necessary to mutate the domains that constitute the binding sites of TARPγ8 or CKAMP44a with AMPARs. Unmasking the details of AMPAR regulation by auxiliary subunits may be important to understand central nervous system (CNS) linked disorders. TARPs, for example, have been attributed to many diseases like epilepsy, schizophrenia, and neuropathic pain, but it is not clear what effect TARPγ8 causes in case of loss or mutation in the hippocampus (Knight et al., 2008). Therefore, understanding the mechanisms on the molecular level may be helpful to understand and treat brain disorders.

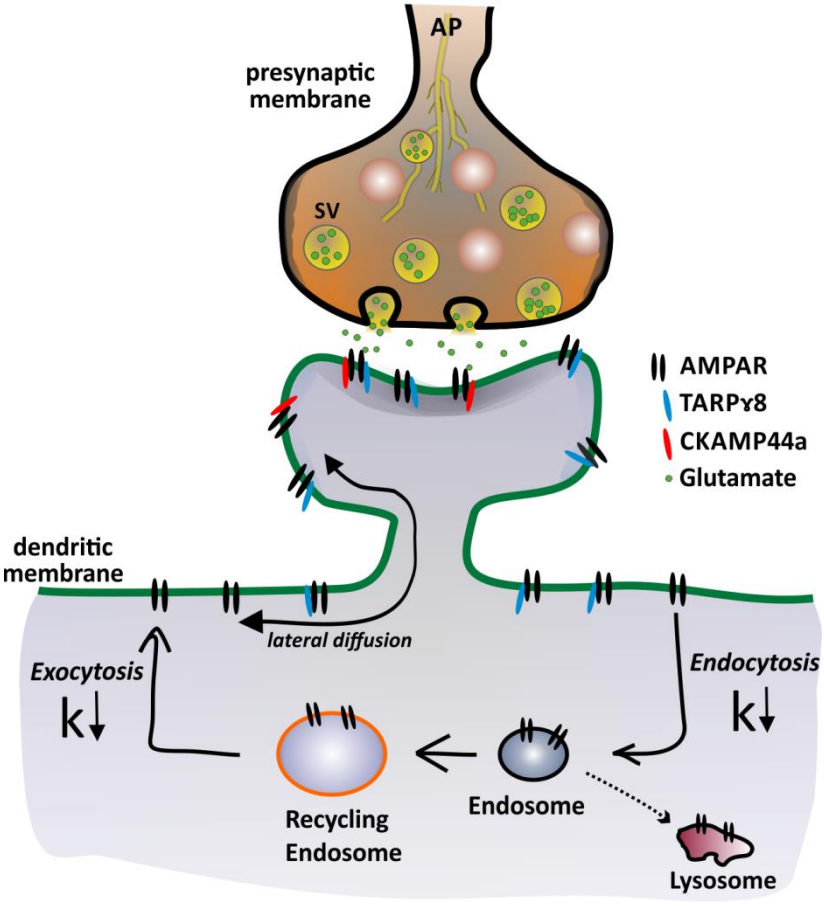


**Figure 47. Downregulation of AMPAR recycling by auxiliary subunits**
Schematic figure illustrating the downregulation of AMPAR exocytosis and endocytosis by TARPγ8 and CKAMP44a auxiliary subunits. It also shows that AMPARs are trafficked to and from the surface membrane by REs.

# References

Adesnik, H., Nicoll, R.A., and England, P.M. (2005). Photoinactivation of native AMPA receptors reveals their real-time trafficking. Neuron *48*, 977-985.

Alabi, A.A., and Tsien, R.W. (2013). Perspectives on kiss-and-run: role in exocytosis, endocytosis, and neurotransmission. Annual review of physiology *75*, 393-422.

Andersen, B.B., Korbo, L., and Pakkenberg, B. (1992). A quantitative study of the human cerebellum with unbiased stereological techniques. The Journal of comparative neurology *326*, 549-560.

Anggono, V., and Huganir, R.L. (2012). Regulation of AMPA receptor trafficking and synaptic plasticity. Current opinion in neurobiology *22*, 461-469.

Anwyl, R. (1999). Metabotropic glutamate receptors: electrophysiological properties and role in plasticity. Brain research Brain research reviews *29*, 83-120.

Araki, Y., Lin, D.T., and Huganir, R.L. (2010). Plasma membrane insertion of the AMPA receptor GluA2 subunit is regulated by NSF binding and Q/R editing of the ion pore. Proc Natl Acad Sci U S A *107*, 11080-11085.

Armstrong, N., and Gouaux, E. (2000). Mechanisms for activation and antagonism of an AMPA-sensitive glutamate receptor: crystal structures of the GluR2 ligand binding core. Neuron *28*, 165-181.

Ashby, M.C., De La Rue, S.A., Ralph, G.S., Uney, J., Collingridge, G.L., and Henley, J.M. (2004). Removal of AMPA receptors (AMPARs) from synapses is preceded by transient endocytosis of extrasynaptic AMPARs. J Neurosci *24*, 5172-5176.

Ashby, M.C., Maier, S.R., Nishimune, A., and Henley, J.M. (2006). Lateral diffusion drives constitutive exchange of AMPA receptors at dendritic spines and is regulated by spine morphology. J Neurosci *26*, 7046-7055.

Banke, T.G., Bowie, D., Lee, H., Huganir, R.L., Schousboe, A., and Traynelis, S.F. (2000). Control of GluR1 AMPA receptor function by cAMP-dependent protein kinase. J Neurosci *20*, 89-102.

Bats, C., Groc, L., and Choquet, D. (2007). The interaction between Stargazin and PSD-95 regulates AMPA receptor surface trafficking. Neuron *53*, 719-734.

Benke, T.A., Luthi, A., Isaac, J.T., and Collingridge, G.L. (1998). Modulation of AMPA receptor unitary conductance by synaptic activity. Nature *393*, 793-797.

Blanpied, T.A., Scott, D.B., and Ehlers, M.D. (2002). Dynamics and regulation of clathrin coats at specialized endocytic zones of dendrites and spines. Neuron *36*, 435-449.

Bliss, T.V., and Collingridge, G.L. (1993). A synaptic model of memory: long-term potentiation in the hippocampus. Nature *361*, 31-39.

Bliss, T.V., and Lomo, T. (1973). Long-lasting potentiation of synaptic transmission in the dentate area of the anaesthetized rabbit following stimulation of the perforant path. The Journal of physiology *232*, 331-356.

Boehm, J., Kang, M.G., Johnson, R.C., Esteban, J., Huganir, R.L., and Malinow, R. (2006). Synaptic incorporation of AMPA receptors during LTP is controlled by a PKC phosphorylation site on GluR1. Neuron *51*, 213-225.

Bokel, C., Dass, S., Wilsch-Brauninger, M., and Roth, S. (2006). Drosophila Cornichon acts as cargo receptor for ER export of the TGFalpha-like growth factor Gurken. Development *133*, 459-470.

Borgdorff, A.J., and Choquet, D. (2002). Regulation of AMPA receptor lateral movements. Nature *417*, 649-653.

Boulter, J., Hollmann, M., O'Shea-Greenfield, A., Hartley, M., Deneris, E., Maron, C., and Heinemann, S. (1990). Molecular cloning and functional expression of glutamate receptor subunit genes. Science *249*, 1033-1037.

Bowen, A.B., Bourke, A.M., Hiester, B.G., Hanus, C., and Kennedy, M.J. (2017). Golgi-independent secretory trafficking through recycling endosomes in neuronal dendrites and spines. eLife *6*.

Bredt, D.S., and Nicoll, R.A. (2003). AMPA receptor trafficking at excitatory synapses. Neuron *40*, 361-379.

Brockie, P.J., Jensen, M., Mellem, J.E., Jensen, E., Yamasaki, T., Wang, R., Maxfield, D., Thacker, C., Hoerndli, F., Dunn, P.J., *et al.* (2013). Cornichons control ER export of AMPA receptors to regulate synaptic excitability. Neuron *80*, 129-142.

Brown, T.C., Correia, S.S., Petrok, C.N., and Esteban, J.A. (2007). Functional compartmentalization of endosomal trafficking for the synaptic delivery of AMPA receptors during long-term potentiation. J Neurosci *27*, 13311-13315.

Brown, T.C., Tran, I.C., Backos, D.S., and Esteban, J.A. (2005). NMDA receptor-dependent activation of the small GTPase Rab5 drives the removal of synaptic AMPA receptors during hippocampal LTD. Neuron *45*, 81-94.

Brusa, R., Zimmermann, F., Koh, D.S., Feldmeyer, D., Gass, P., Seeburg, P.H., and Sprengel, R. (1995). Early-onset epilepsy and postnatal lethality associated with an editing-deficient GluR-B allele in mice. Science *270*, 1677-1680.

Buonarati, O.R., Hammes, E.A., Watson, J.F., Greger, I.H., and Hell, J.W. (2019). Mechanisms of postsynaptic localization of AMPA-type glutamate receptors and their regulation during long-term potentiation. Science signaling *12*.

Burgess, D.L., Gefrides, L.A., Foreman, P.J., and Noebels, J.L. (2001). A cluster of three novel Ca2+ channel gamma subunit genes on chromosome 19q13.4: evolution and expression profile of the gamma subunit gene family. Genomics *71*, 339-350.

Cais, O., Herguedas, B., Krol, K., Cull-Candy, S.G., Farrant, M., and Greger, I.H. (2014). Mapping the interaction sites between AMPA receptors and TARPs reveals a role for the receptor N-terminal domain in channel gating. Cell reports *9*, 728-740.

Cajal, S.R.y. (1899, 1904). Textura del Sistema Nervioso del Hombre y de los Vertebrados. Madrid, Moya, 2 Vols in 3.

Carroll, R.C., Beattie, E.C., Xia, H., Luscher, C., Altschuler, Y., Nicoll, R.A., Malenka, R.C., and von Zastrow, M. (1999). Dynamin-dependent endocytosis of ionotropic glutamate receptors. Proc Natl Acad Sci U S A *96*, 14112-14117.

Cartmell, J., and Schoepp, D.D. (2000). Regulation of neurotransmitter release by metabotropic glutamate receptors. Journal of neurochemistry *75*, 889-907.

Chanaday, N.L., and Kavalali, E.T. (2018). Time course and temperature dependence of synaptic vesicle endocytosis. FEBS letters *592*, 3606-3614.

Chen, L., Chetkovich, D.M., Petralia, R.S., Sweeney, N.T., Kawasaki, Y., Wenthold, R.J., Bredt, D.S., and Nicoll, R.A. (2000). Stargazin regulates synaptic targeting of AMPA receptors by two distinct mechanisms. Nature *408*, 936-943.

Chen, X., Levy, J.M., Hou, A., Winters, C., Azzam, R., Sousa, A.A., Leapman, R.D., Nicoll, R.A., and Reese, T.S. (2015). PSD-95 family MAGUKs are essential for anchoring AMPA and NMDA receptor complexes at the postsynaptic density. Proc Natl Acad Sci U S A *112*, E6983-6992.

Chen, X., Vinade, L., Leapman, R.D., Petersen, J.D., Nakagawa, T., Phillips, T.M., Sheng, M., and Reese, T.S. (2005). Mass of the postsynaptic density and enumeration of three key molecules. Proc Natl Acad Sci U S A *102*, 11551-11556.

Chen, Y.A., Scales, S.J., Patel, S.M., Doung, Y.C., and Scheller, R.H. (1999). SNARE complex formation is triggered by Ca2+ and drives membrane fusion. Cell *97*, 165-174.

Chiang, H.C., Shin, W., Zhao, W.D., Hamid, E., Sheng, J., Baydyuk, M., Wen, P.J., Jin, A., Momboisse, F., and Wu, L.G. (2014). Post-fusion structural changes and their roles in exocytosis and endocytosis of dense-core vesicles. Nature communications *5*, 3356.

Cho, C.H., St-Gelais, F., Zhang, W., Tomita, S., and Howe, J.R. (2007). Two families of TARP isoforms that have distinct effects on the kinetic properties of AMPA receptors and synaptic currents. Neuron *55*, 890-904.

Chu, P.J., Robertson, H.M., and Best, P.M. (2001). Calcium channel gamma subunits provide insights into the evolution of this gene family. Gene *280*, 37-48.

Coleman, S.K., Moykkynen, T., Cai, C., von Ossowski, L., Kuismanen, E., Korpi, E.R., and Keinanen, K. (2006). Isoform-specific early trafficking of AMPA receptor flip and flop variants. J Neurosci *26*, 11220-11229.

Collingridge, G.L., Kehl, S.J., and McLennan, H. (1983). Excitatory amino acids in synaptic transmission in the Schaffer collateral-commissural pathway of the rat hippocampus. The Journal of physiology *334*, 33-46.

Collingridge, G.L., and Lester, R.A. (1989). Excitatory amino acid receptors in the vertebrate central nervous system. Pharmacological reviews *41*, 143-210.

Cooney, J.R., Hurlburt, J.L., Selig, D.K., Harris, K.M., and Fiala, J.C. (2002). Endosomal compartments serve multiple hippocampal dendritic spines from a widespread rather than a local store of recycling membrane. J Neurosci *22*, 2215-2224.

Cosker, K.E., and Segal, R.A. (2014). Neuronal signaling through endocytosis. Cold Spring Harbor perspectives in biology *6*.

Cui-Wang, T., Hanus, C., Cui, T., Helton, T., Bourne, J., Watson, D., Harris, K.M., and Ehlers, M.D. (2012). Local zones of endoplasmic reticulum complexity confine cargo in neuronal dendrites. Cell *148*, 309-321.

Curtis, D.R., Phillis, J.W., and Watkins, J.C. (1960). The chemical excitation of spinal neurones by certain acidic amino acids. The Journal of physiology *150*, 656-682.

Curtis, D.R., and Watkins, J.C. (1960). The excitation and depression of spinal neurones by structurally related amino acids. Journal of neurochemistry *6*, 117-141.

Davidson, E.M., and Carlton, S.M. (1998). Intraplantar injection of dextrorphan, ketamine or memantine attenuates formalin-induced behaviors. Brain research *785*, 136-142.

Daw, M.I., Chittajallu, R., Bortolotto, Z.A., Dev, K.K., Duprat, F., Henley, J.M., Collingridge, G.L., and Isaac, J.T. (2000). PDZ proteins interacting with C-terminal GluR2/3 are involved in a PKC-dependent regulation of AMPA receptors at hippocampal synapses. Neuron *28*, 873-886.

de Figueiredo, R.C., and Soares, M.J. (2000). Low temperature blocks fluid-phase pinocytosis and receptor-mediated endocytosis in Trypanosoma cruzi epimastigotes. Parasitology research *86*, 413-418.

Delgado-Martinez, I., Nehring, R.B., and Sorensen, J.B. (2007). Differential abilities of SNAP-25 homologs to support neuronal function. J Neurosci *27*, 9380-9391.

Derkach, V., Barria, A., and Soderling, T.R. (1999). Ca2+/calmodulin-kinase II enhances channel conductance of alpha-amino-3-hydroxy-5-methyl-4-isoxazolepropionate type glutamate receptors. Proc Natl Acad Sci U S A *96*, 3269-3274.

Diaz, E. (2010). SynDIG1 regulation of synaptic AMPA receptor targeting. Communicative & integrative biology *3*, 347-349.

Dingledine, R., Borges, K., Bowie, D., and Traynelis, S.F. (1999). The glutamate receptor ion channels. Pharmacological reviews *51*, 7-61.

Dong, H., O'Brien, R.J., Fung, E.T., Lanahan, A.A., Worley, P.F., and Huganir, R.L. (1997). GRIP: a synaptic PDZ domain-containing protein that interacts with AMPA receptors. Nature *386*, 279-284.

Dong, H., Zhang, P., Song, I., Petralia, R.S., Liao, D., and Huganir, R.L. (1999). Characterization of the glutamate receptor-interacting proteins GRIP1 and GRIP2. J Neurosci *19*, 6930-6941.

Doyle, D.A., Lee, A., Lewis, J., Kim, E., Sheng, M., and MacKinnon, R. (1996). Crystal structures of a complexed and peptide-free membrane protein-binding domain: molecular basis of peptide recognition by PDZ. Cell *85*, 1067-1076.

Ehlers, M.D., Heine, M., Groc, L., Lee, M.C., and Choquet, D. (2007). Diffusional trapping of GluR1 AMPA receptors by input-specific synaptic activity. Neuron *54*, 447-460.

Ehlers*, M.D. (2000). Reinsertion or Degradation of AMPA Receptors Determined by Activity-Dependent Endocytic Sorting Neuron *Vol. 28, 511–525*.

El-Husseini, A.E., Schnell, E., Chetkovich, D.M., Nicoll, R.A., and Bredt, D.S. (2000). PSD-95 involvement in maturation of excitatory synapses. Science *290*, 1364-1368.

Esteban, J.A., Shi, S.H., Wilson, C., Nuriya, M., Huganir, R.L., and Malinow, R. (2003). PKA phosphorylation of AMPA receptor subunits controls synaptic trafficking underlying plasticity. Nat Neurosci *6*, 136-143.

Farrow, P., Khodosevich, K., Sapir, Y., Schulmann, A., Aslam, M., Stern-Bach, Y., Monyer, H., and von Engelhardt, J. (2015). Auxiliary subunits of the CKAMP family differentially modulate AMPA receptor properties. eLife *4*, e09693.

Fernandez-Monreal, M., Brown, T.C., Royo, M., and Esteban, J.A. (2012). The balance between receptor recycling and trafficking toward lysosomes determines synaptic strength during long-term depression. J Neurosci *32*, 13200-13205.

Foster, M., and Sherrington, C.S. (1887). Text-book of Physiol., iii. London.

Fukaya, M., Tsujita, M., Yamazaki, M., Kushiya, E., Abe, M., Akashi, K., Natsume, R., Kano, M., Kamiya, H., Watanabe, M., *et al.* (2006). Abundant distribution of TARP gamma-8 in synaptic and extrasynaptic surface of hippocampal neurons and its major role in AMPA receptor expression on spines and dendrites. The European journal of neuroscience *24*, 2177-2190.

Fukaya, M., Yamazaki, M., Sakimura, K., and Watanabe, M. (2005). Spatial diversity in gene expression for VDCCgamma subunit family in developing and adult mouse brains. Neuroscience research *53*, 376-383.

Funatsu, T., Harada, Y., Tokunaga, M., Saito, K., and Yanagida, T. (1995). Imaging of single fluorescent molecules and individual ATP turnovers by single myosin molecules in aqueous solution. Nature *374*, 555-559.

Furukawa, H., Singh, S.K., Mancusso, R., and Gouaux, E. (2005). Subunit arrangement and function in NMDA receptors. Nature *438*, 185-192.

Gainey, M.A., Tatavarty, V., Nahmani, M., Lin, H., and Turrigiano, G.G. (2015). Activity-dependent synaptic GRIP1 accumulation drives synaptic scaling up in response to action potential blockade. Proc Natl Acad Sci U S A *112*, E3590-3599.

Gan, Q., Salussolia, C.L., and Wollmuth, L.P. (2015). Assembly of AMPA receptors: mechanisms and regulation. The Journal of physiology *593*, 39-48.

Gaullier, J.M., Ronning, E., Gillooly, D.J., and Stenmark, H. (2000). Interaction of the EEA1 FYVE finger with phosphatidylinositol 3-phosphate and early endosomes. Role of conserved residues. The Journal of biological chemistry *275*, 24595-24600.

Gerges, N.Z., Backos, D.S., and Esteban, J.A. (2004). Local control of AMPA receptor trafficking at the postsynaptic terminal by a small GTPase of the Rab family. The Journal of biological chemistry *279*, 43870-43878.

Gerges, N.Z., Backos, D.S., Rupasinghe, C.N., Spaller, M.R., and Esteban, J.A. (2006). Dual role of the exocyst in AMPA receptor targeting and insertion into the postsynaptic membrane. The EMBO journal *25*, 1623-1634.

Gill, M.B., Kato, A.S., Roberts, M.F., Yu, H., Wang, H., Tomita, S., and Bredt, D.S. (2011). Cornichon-2 modulates AMPA receptor-transmembrane AMPA receptor regulatory protein assembly to dictate gating and pharmacology. J Neurosci *31*, 6928-6938.

Glebov, O.O., Tigaret, C.M., Mellor, J.R., and Henley, J.M. (2015). Clathrin-independent trafficking of AMPA receptors. J Neurosci *35*, 4830-4836.

Graham, M.E., Washbourne, P., Wilson, M.C., and Burgoyne, R.D. (2002). Molecular analysis of SNAP-25 function in exocytosis. Annals of the New York Academy of Sciences *971*, 210-221.

Granger, A.J., Shi, Y., Lu, W., Cerpas, M., and Nicoll, R.A. (2013). LTP requires a reserve pool of glutamate receptors independent of subunit type. Nature *493*, 495-500.

Greger, I.H., Khatri, L., and Ziff, E.B. (2002). RNA editing at arg607 controls AMPA receptor exit from the endoplasmic reticulum. Neuron *34*, 759-772.

Greger, I.H., Watson, J.F., and Cull-Candy, S.G. (2017). Structural and Functional Architecture of AMPA-Type Glutamate Receptors and Their Auxiliary Proteins. Neuron *94*, 713-730.

Grooms, S.Y., Noh, K.M., Regis, R., Bassell, G.J., Bryan, M.K., Carroll, R.C., and Zukin, R.S. (2006). Activity bidirectionally regulates AMPA receptor mRNA abundance in dendrites of hippocampal neurons. J Neurosci *26*, 8339-8351.

Gu, X., Mao, X., Lussier, M.P., Hutchison, M.A., Zhou, L., Hamra, F.K., Roche, K.W., and Lu, W. (2016a). GSG1L suppresses AMPA receptor-mediated synaptic transmission and uniquely modulates AMPA receptor kinetics in hippocampal neurons. Nature communications *7*, 10873.

Gu, Y., Chiu, S.L., Liu, B., Wu, P.H., Delannoy, M., Lin, D.T., Wirtz, D., and Huganir, R.L. (2016b). Differential vesicular sorting of AMPA and GABAA receptors. Proc Natl Acad Sci U S A *113*, E922-931.

Haering, S.C., Tapken, D., Pahl, S., and Hollmann, M. (2014). Auxiliary subunits: shepherding AMPA receptors to the plasma membrane. Membranes *4*, 469-490.

Hangen, E., Cordelieres, F.P., Petersen, J.D., Choquet, D., and Coussen, F. (2018). Neuronal Activity and Intracellular Calcium Levels Regulate Intracellular Transport of Newly Synthesized AMPAR. Cell reports *24*, 1001-1012 e1003.

Hanley, J.G., and Henley, J.M. (2005). PICK1 is a calcium-sensor for NMDA-induced AMPA receptor trafficking. The EMBO journal *24*, 3266-3278.

Hanley, J.G., Khatri, L., Hanson, P.I., and Ziff, E.B. (2002). NSF ATPase and alpha-/beta-SNAPs disassemble the AMPA receptor-PICK1 complex. Neuron *34*, 53-67.

Hanus, C., and Ehlers, M.D. (2008). Secretory outposts for the local processing of membrane cargo in neuronal dendrites. Traffic *9*, 1437-1445.

Harvey, C.D., and Svoboda, K. (2007). Locally dynamic synaptic learning rules in pyramidal neuron dendrites. Nature *450*, 1195-1200.

Hashimoto, K., Fukaya, M., Qiao, X., Sakimura, K., Watanabe, M., and Kano, M. (1999). Impairment of AMPA receptor function in cerebellar granule cells of ataxic mutant mouse stargazer. J Neurosci *19*, 6027-6036.

Hausser, A., and Schlett, K. (2017). Coordination of AMPA receptor trafficking by Rab GTPases. Small GTPases, 1-14.

Heine, M., Groc, L., Frischknecht, R., Beique, J.C., Lounis, B., Rumbaugh, G., Huganir, R.L., Cognet, L., and Choquet, D. (2008). Surface mobility of postsynaptic AMPARs tunes synaptic transmission. Science *320*, 201-205.

Henley, J.M., Barker, E.A., and Glebov, O.O. (2011). Routes, destinations and delays: recent advances in AMPA receptor trafficking. Trends in neurosciences *34*, 258-268.

Herguedas, B., Garcia-Nafria, J., Cais, O., Fernandez-Leiro, R., Krieger, J., Ho, H., and Greger, I.H. (2016). Structure and organization of heteromeric AMPA-type glutamate receptors. Science *352*, aad3873.

Herring, B.E., Shi, Y., Suh, Y.H., Zheng, C.Y., Blankenship, S.M., Roche, K.W., and Nicoll, R.A. (2013). Cornichon proteins determine the subunit composition of synaptic AMPA receptors. Neuron *77*, 1083-1096.

Hirling, H. (2009). Endosomal trafficking of AMPA-type glutamate receptors. Neuroscience *158*, 36-44.

Hollmann, M., and Heinemann, S. (1994). Cloned glutamate receptors. Annual review of neuroscience *17*, 31-108.

Horton, A.C., and Ehlers, M.D. (2003). Dual modes of endoplasmic reticulum-to-Golgi transport in dendrites revealed by live-cell imaging. J Neurosci *23*, 6188-6199.

Horton, A.C., Racz, B., Monson, E.E., Lin, A.L., Weinberg, R.J., and Ehlers, M.D. (2005). Polarized secretory trafficking directs cargo for asymmetric dendrite growth and morphogenesis. Neuron *48*, 757-771.

Hosokawa, T., Mitsushima, D., Kaneko, R., and Hayashi, Y. (2015). Stoichiometry and phosphoisotypes of hippocampal AMPA-type glutamate receptor phosphorylation. Neuron *85*, 60-67.

Hu, Y.B., Dammer, E.B., Ren, R.J., and Wang, G. (2015). The endosomal-lysosomal system: from acidification and cargo sorting to neurodegeneration. Translational neurodegeneration *4*, 18.

Jackson, A.C., and Nicoll, R.A. (2011). The expanding social network of ionotropic glutamate receptors: TARPs and other transmembrane auxiliary subunits. Neuron *70*, 178-199.

Jin, R., Singh, S.K., Gu, S., Furukawa, H., Sobolevsky, A.I., Zhou, J., Jin, Y., and Gouaux, E. (2009). Crystal structure and association behaviour of the GluR2 amino-terminal domain. The EMBO journal *28*, 1812-1823.

Johnson, J.W., and Ascher, P. (1987). Glycine potentiates the NMDA response in cultured mouse brain neurons. Nature *325*, 529-531.

Johnson, K.A., Conn, P.J., and Niswender, C.M. (2009). Glutamate receptors as therapeutic targets for Parkinson's disease. CNS & neurological disorders drug targets *8*, 475-491.

Ju, W., Morishita, W., Tsui, J., Gaietta, G., Deerinck, T.J., Adams, S.R., Garner, C.C., Tsien, R.Y., Ellisman, M.H., and Malenka, R.C. (2004). Activity-dependent regulation of dendritic synthesis and trafficking of AMPA receptors. Nat Neurosci *7*, 244-253.

Jullie, D., Choquet, D., and Perrais, D. (2014). Recycling endosomes undergo rapid closure of a fusion pore on exocytosis in neuronal dendrites. J Neurosci *34*, 11106-11118.

Kalashnikova, E., Lorca, R.A., Kaur, I., Barisone, G.A., Li, B., Ishimaru, T., Trimmer, J.S., Mohapatra, D.P., and Diaz, E. (2010). SynDIG1: an activity-regulated, AMPA- receptor-interacting transmembrane protein that regulates excitatory synapse development. Neuron *65*, 80-93.

Karataeva, A.R., Klaassen, R.V., Stroder, J., Ruiperez-Alonso, M., Hjorth, J.J., van Nierop, P., Spijker, S., Mansvelder, H.D., and Smit, A.B. (2014). C-terminal interactors of the AMPA receptor auxiliary subunit Shisa9. PloS one *9*, e87360.

Kato, A.S., Gill, M.B., Yu, H., Nisenbaum, E.S., and Bredt, D.S. (2010). TARPs differentially decorate AMPA receptors to specify neuropharmacology. Trends in neurosciences *33*, 241-248.

Kato, A.S., Siuda, E.R., Nisenbaum, E.S., and Bredt, D.S. (2008). AMPA receptor subunit-specific regulation by a distinct family of type II TARPs. Neuron *59*, 986-996.

Kato, A.S., Zhou, W., Milstein, A.D., Knierman, M.D., Siuda, E.R., Dotzlaf, J.E., Yu, H., Hale, J.E., Nisenbaum, E.S., Nicoll, R.A., *et al.* (2007). New transmembrane AMPA receptor regulatory protein isoform, gamma-7, differentially regulates AMPA receptors. J Neurosci *27*, 4969-4977.

Kennedy, M.J., Davison, I.G., Robinson, C.G., and Ehlers, M.D. (2010). Syntaxin-4 defines a domain for activity-dependent exocytosis in dendritic spines. Cell *141*, 524-535.

Kessels, H.W., and Malinow, R. (2009). Synaptic AMPA receptor plasticity and behavior. Neuron *61*, 340-350.

Khodosevich, K., Jacobi, E., Farrow, P., Schulmann, A., Rusu, A., Zhang, L., Sprengel, R., Monyer, H., and von Engelhardt, J. (2014). Coexpressed auxiliary subunits exhibit distinct modulatory profiles on AMPA receptor function. Neuron *83*, 601-615.

Kim, C.H., Chung, H.J., Lee, H.K., and Huganir, R.L. (2001). Interaction of the AMPA receptor subunit GluR2/3 with PDZ domains regulates hippocampal long-term depression. Proc Natl Acad Sci U S A *98*, 11725-11730.

Kim, K.S., Yan, D., and Tomita, S. (2010). Assembly and stoichiometry of the AMPA receptor and transmembrane AMPA receptor regulatory protein complex. J Neurosci *30*, 1064-1072.

Klaassen, R.V., Stroeder, J., Coussen, F., Hafner, A.S., Petersen, J.D., Renancio, C., Schmitz, L.J., Normand, E., Lodder, J.C., Rotaru, D.C., *et al.* (2016). Shisa6 traps AMPA receptors at postsynaptic sites and prevents their desensitization during synaptic activity. Nature communications *7*, 10682.

Klugbauer, N., Dai, S., Specht, V., Lacinova, L., Marais, E., Bohn, G., and Hofmann, F. (2000). A family of gamma-like calcium channel subunits. FEBS letters *470*, 189-197.

Knight, H.M., Maclean, A., Irfan, M., Naeem, F., Cass, S., Pickard, B.S., Muir, W.J., Blackwood, D.H., and Ayub, M. (2008). Homozygosity mapping in a family presenting with schizophrenia, epilepsy and hearing impairment. European journal of human genetics : EJHG *16*, 750-758.

Kopec, C.D., Li, B., Wei, W., Boehm, J., and Malinow, R. (2006). Glutamate receptor exocytosis and spine enlargement during chemically induced long-term potentiation. J Neurosci *26*, 2000-2009.

Kott, S., Werner, M., Korber, C., and Hollmann, M. (2007). Electrophysiological properties of AMPA receptors are differentially modulated depending on the associated member of the TARP family. J Neurosci *27*, 3780-3789.

Kunde, S.A., Rademacher, N., Zieger, H., and Shoichet, S.A. (2017). Protein kinase C regulates AMPA receptor auxiliary protein Shisa9/CKAMP44 through interactions with neuronal scaffold PICK1. FEBS open bio *7*, 1234-1245.

Lau, C.G., Takayasu, Y., Rodenas-Ruano, A., Paternain, A.V., Lerma, J., Bennett, M.V., and Zukin, R.S. (2010). SNAP-25 is a target of protein kinase C phosphorylation critical to NMDA receptor trafficking. J Neurosci *30*, 242-254.

Lee, H.K., Takamiya, K., Han, J.S., Man, H., Kim, C.H., Rumbaugh, G., Yu, S., Ding, L., He, C., Petralia, R.S., *et al.* (2003). Phosphorylation of the AMPA receptor GluR1 subunit is required for synaptic plasticity and retention of spatial memory. Cell *112*, 631-643.

Leonard, A.S., Davare, M.A., Horne, M.C., Garner, C.C., and Hell, J.W. (1998). SAP97 is associated with the alpha-amino-3-hydroxy-5-methylisoxazole-4-propionic acid receptor GluR1 subunit. The Journal of biological chemistry *273*, 19518-19524.

Lerma, J. (2006). Kainate receptor physiology. Current opinion in pharmacology *6*, 89-97.

Lin, D.T., and Huganir, R.L. (2007). PICK1 and phosphorylation of the glutamate receptor 2 (GluR2) AMPA receptor subunit regulates GluR2 recycling after NMDA receptor-induced internalization. J Neurosci *27*, 13903-13908.

Lin, D.T., Makino, Y., Sharma, K., Hayashi, T., Neve, R., Takamiya, K., and Huganir, R.L. (2009). Regulation of AMPA receptor extrasynaptic insertion by 4.1N, phosphorylation and palmitoylation. Nat Neurosci *12*, 879-887.

Lovero, K.L., Blankenship, S.M., Shi, Y., and Nicoll, R.A. (2013). SynDIG1 promotes excitatory synaptogenesis independent of AMPA receptor trafficking and biophysical regulation. PloS one *8*, e66171.

Lu, W., Shi, Y., Jackson, A.C., Bjorgan, K., During, M.J., Sprengel, R., Seeburg, P.H., and Nicoll, R.A. (2009). Subunit composition of synaptic AMPA receptors revealed by a single-cell genetic approach. Neuron *62*, 254-268.

Luscher, C., Xia, H., Beattie, E.C., Carroll, R.C., von Zastrow, M., Malenka, R.C., and Nicoll, R.A. (1999). Role of AMPA receptor cycling in synaptic transmission and plasticity. Neuron *24*, 649-658.

Makino, H., and Malinow, R. (2009). AMPA receptor incorporation into synapses during LTP: the role of lateral movement and exocytosis. Neuron *64*, 381-390.

Malinow, R., and Malenka, R.C. (2002). AMPA receptor trafficking and synaptic plasticity. Annual review of neuroscience *25*, 103-126.

Man, H.Y., Lin, J.W., Ju, W.H., Ahmadian, G., Liu, L., Becker, L.E., Sheng, M., and Wang, Y.T. (2000). Regulation of AMPA receptor-mediated synaptic transmission by clathrin-dependent receptor internalization. Neuron *25*, 649-662.

Mao, X., Gu, X., and Lu, W. (2017). GSG1L regulates the strength of AMPA receptor-mediated synaptic transmission but not AMPA receptor kinetics in hippocampal dentate granule neurons. Journal of neurophysiology *117*, 28-35.

Matt, L., Kirk, L.M., Chenaux, G., Speca, D.J., Puhger, K.R., Pride, M.C., Qneibi, M., Haham, T., Plambeck, K.E., Stern-Bach, Y., *et al.* (2018). SynDIG4/Prrt1 Is Required for Excitatory Synapse Development and Plasticity Underlying Cognitive Function. Cell reports *22*, 2246-2253.

Mattson, M.P., Cheng, B., Davis, D., Bryant, K., Lieberburg, I., and Rydel, R.E. (1992). beta-Amyloid peptides destabilize calcium homeostasis and render human cortical neurons vulnerable to excitotoxicity. J Neurosci *12*, 376-389.

McGee, T.P., Bats, C., Farrant, M., and Cull-Candy, S.G. (2015). Auxiliary Subunit GSG1L Acts to Suppress Calcium-Permeable AMPA Receptor Function. J Neurosci *35*, 16171-16179.

Merrifield, C.J., Perrais, D., and Zenisek, D. (2005). Coupling between clathrin-coated-pit invagination, cortactin recruitment, and membrane scission observed in live cells. Cell *121*, 593-606.

Miesenbock, G., De Angelis, D.A., and Rothman, J.E. (1998). Visualizing secretion and synaptic transmission with pH-sensitive green fluorescent proteins. Nature *394*, 192-195.

Milstein, A.D., and Nicoll, R.A. (2009). TARP modulation of synaptic AMPA receptor trafficking and gating depends on multiple intracellular domains. Proc Natl Acad Sci U S A *106*, 11348-11351.

Milstein, A.D., Zhou, W., Karimzadegan, S., Bredt, D.S., and Nicoll, R.A. (2007). TARP subtypes differentially and dose-dependently control synaptic AMPA receptor gating. Neuron *55*, 905-918.

Monaghan, D.T., Bridges, R.J., and Cotman, C.W. (1989). The excitatory amino acid receptors: their classes, pharmacology, and distinct properties in the function of the central nervous system. Annual review of pharmacology and toxicology *29*, 365-402.

Monyer, H., Sprengel, R., Schoepfer, R., Herb, A., Higuchi, M., Lomeli, H., Burnashev, N., Sakmann, B., and Seeburg, P.H. (1992). Heteromeric NMDA receptors: molecular and functional distinction of subtypes. Science *256*, 1217-1221.

Morita, K., Furuse, M., Fujimoto, K., and Tsukita, S. (1999). Claudin multigene family encoding four-transmembrane domain protein components of tight junction strands. Proc Natl Acad Sci U S A *96*, 511-516.

Mukherjee, S., Ghosh, R.N., and Maxfield, F.R. (1997). Endocytosis. Physiological reviews *77*, 759-803.

Muller, B.M., Kistner, U., Kindler, S., Chung, W.J., Kuhlendahl, S., Fenster, S.D., Lau, L.F., Veh, R.W., Huganir, R.L., Gundelfinger, E.D., *et al.* (1996). SAP102, a novel postsynaptic protein that interacts with NMDA receptor complexes in vivo. Neuron *17*, 255-265.

Murray, D.H., Jahnel, M., Lauer, J., Avellaneda, M.J., Brouilly, N., Cezanne, A., Morales-Navarrete, H., Perini, E.D., Ferguson, C., Lupas, A.N., *et al.* (2016). An endosomal tether undergoes an entropic collapse to bring vesicles together. Nature *537*, 107-111.

Nagano, T., Takehara, S., Takahashi, M., Aizawa, S., and Yamamoto, A. (2006). Shisa2 promotes the maturation of somitic precursors and transition to the segmental fate in Xenopus embryos. Development *133*, 4643-4654.

Nakanishi, S. (1994). Metabotropic glutamate receptors: synaptic transmission, modulation, and plasticity. Neuron *13*, 1031-1037.

Nicoll, R.A., Tomita, S., and Bredt, D.S. (2006). Auxiliary subunits assist AMPA-type glutamate receptors. Science *311*, 1253-1256.

Niethammer, M., Kim, E., and Sheng, M. (1996). Interaction between the C terminus of NMDA receptor subunits and multiple members of the PSD-95 family of membrane-associated guanylate kinases. J Neurosci *16*, 2157-2163.

Noebels, J.L., Qiao, X., Bronson, R.T., Spencer, C., and Davisson, M.T. (1990). Stargazer: a new neurological mutant on chromosome 15 in the mouse with prolonged cortical seizures. Epilepsy research *7*, 129-135.

O'Brien, R.J., Xu, D., Petralia, R.S., Steward, O., Huganir, R.L., and Worley, P. (1999). Synaptic clustering of AMPA receptors by the extracellular immediate-early gene product Narp. Neuron *23*, 309-323.

Olsen, R.W., and Sieghart, W. (2008). International Union of Pharmacology. LXX. Subtypes of gamma-aminobutyric acid(A) receptors: classification on the basis of subunit composition, pharmacology, and function. Update. Pharmacological reviews *60*, 243-260.

Park, J., Chavez, A.E., Mineur, Y.S., Morimoto-Tomita, M., Lutzu, S., Kim, K.S., Picciotto, M.R., Castillo, P.E., and Tomita, S. (2016). CaMKII Phosphorylation of TARPgamma-8 Is a Mediator of LTP and Learning and Memory. Neuron *92*, 75-83.

Park, M., Penick, E.C., Edwards, J.G., Kauer, J.A., and Ehlers, M.D. (2004). Recycling endosomes supply AMPA receptors for LTP. Science *305*, 1972-1975.

Parker, M.J., Zhao, S., Bredt, D.S., Sanes, J.R., and Feng, G. (2004). PSD93 regulates synaptic stability at neuronal cholinergic synapses. J Neurosci *24*, 378-388.

Parkinson, G.T., and Hanley, J.G. (2018). Mechanisms of AMPA Receptor Endosomal Sorting. Frontiers in molecular neuroscience *11*, 440.

Passafaro, M., Piech, V., and Sheng, M. (2001). Subunit-specific temporal and spatial patterns of AMPA receptor exocytosis in hippocampal neurons. Nat Neurosci *4*, 917-926.

Patterson, M.A., Szatmari, E.M., and Yasuda, R. (2010). AMPA receptors are exocytosed in stimulated spines and adjacent dendrites in a Ras-ERK-dependent manner during long-term potentiation. Proc Natl Acad Sci U S A *107*, 15951-15956.

Pei, J., and Grishin, N.V. (2012). Unexpected diversity in Shisa-like proteins suggests the importance of their roles as transmembrane adaptors. Cellular signalling *24*, 758-769.

Perrais, D., Veran, J., and Mulle, C. (2010). Gating and permeation of kainate receptors: differences unveiled. Trends in pharmacological sciences *31*, 516-522.

Petrini, E.M., Lu, J., Cognet, L., Lounis, B., Ehlers, M.D., and Choquet, D. (2009). Endocytic trafficking and recycling maintain a pool of mobile surface AMPA receptors required for synaptic potentiation. Neuron *63*, 92-105.

Pierce, J.P., Mayer, T., and McCarthy, J.B. (2001). Evidence for a satellite secretory pathway in neuronal dendritic spines. Current biology : CB *11*, 351-355.

Punnonen, E.-L., Ryhänen, K., and Marjomi, V.S. (1998). At reduced temperature, endocytic membrane traffic is blocked in multivesicular carrier endosomes in rat cardiac myocytes. European Journal of Cell Biology *75*, 344-352.

Rebola, N., Sachidhanandam, S., Perrais, D., Cunha, R.A., and Mulle, C. (2007). Short-term plasticity of kainate receptor-mediated EPSCs induced by NMDA receptors at hippocampal mossy fiber synapses. J Neurosci *27*, 3987-3993.

Reymann, K.G., and Frey, J.U. (2007). The late maintenance of hippocampal LTP: requirements, phases, 'synaptic tagging', 'late-associativity' and implications. Neuropharmacology *52*, 24-40.

Roche, K.W., O'Brien, R.J., Mammen, A.L., Bernhardt, J., and Huganir, R.L. (1996). Characterization of multiple phosphorylation sites on the AMPA receptor GluR1 subunit. Neuron *16*, 1179-1188.

Rodriguez-Moreno, A., Herreras, O., and Lerma, J. (1997). Kainate receptors presynaptically downregulate GABAergic inhibition in the rat hippocampus. Neuron *19*, 893-901.

Roman-Vendrell, C., Chevalier, M., Acevedo-Canabal, A.M., Delgado-Peraza, F., Flores-Otero, J., and Yudowski, G.A. (2014). Imaging of kiss-and-run exocytosis of surface receptors in neuronal cultures. Frontiers in cellular neuroscience *8*, 363.

Roos, A., and Boron, W.F. (1981). Intracellular pH. Physiological reviews *61*, 296-434.

Rosendale, M., Jullie, D., Choquet, D., and Perrais, D. (2017). Spatial and Temporal Regulation of Receptor Endocytosis in Neuronal Dendrites Revealed by Imaging of Single Vesicle Formation. Cell reports *18*, 1840-1847.

Roth, R.H., Zhang, Y., and Huganir, R.L. (2017). Dynamic imaging of AMPA receptor trafficking in vitro and in vivo. Current opinion in neurobiology *45*, 51-58.

Rouach, N., Byrd, K., Petralia, R.S., Elias, G.M., Adesnik, H., Tomita, S., Karimzadegan, S., Kealey, C., Bredt, D.S., and Nicoll, R.A. (2005). TARP gamma-8 controls hippocampal AMPA receptor number, distribution and synaptic plasticity. Nat Neurosci *8*, 1525-1533.

Rubio, M.E., and Wenthold, R.J. (1999). Calnexin and the immunoglobulin binding protein (BiP) coimmunoprecipitate with AMPA receptors. Journal of neurochemistry *73*, 942-948.

Russo, I., Bonini, D., Via, L.L., Barlati, S., and Barbon, A. (2013). AMPA receptor properties are modulated in the early stages following pilocarpine-induced status epilepticus. Neuromolecular medicine *15*, 324-338.

Safferling, M., Tichelaar, W., Kummerle, G., Jouppila, A., Kuusinen, A., Keinanen, K., and Madden, D.R. (2001). First images of a glutamate receptor ion channel: oligomeric state and molecular dimensions of GluRB homomers. Biochemistry *40*, 13948-13953.

Sans, N., Vissel, B., Petralia, R.S., Wang, Y.X., Chang, K., Royle, G.A., Wang, C.Y., O'Gorman, S., Heinemann, S.F., and Wenthold, R.J. (2003). Aberrant formation of glutamate receptor complexes in hippocampal neurons of mice lacking the GluR2 AMPA receptor subunit. J Neurosci *23*, 9367-9373.

Schmitz, L.J.M., Klaassen, R.V., Ruiperez-Alonso, M., Zamri, A.E., Stroeder, J., Rao-Ruiz, P., Lodder, J.C., van der Loo, R.J., Mansvelder, H.D., Smit, A.B., *et al.* (2017). The AMPA receptor-associated protein Shisa7 regulates hippocampal synaptic function and contextual memory. eLife *6*.

Schnell, E., Sizemore, M., Karimzadegan, S., Chen, L., Bredt, D.S., and Nicoll, R.A. (2002). Direct interactions between PSD-95 and stargazin control synaptic AMPA receptor number. Proc Natl Acad Sci U S A *99*, 13902-13907.

Schwenk, J., Harmel, N., Brechet, A., Zolles, G., Berkefeld, H., Muller, C.S., Bildl, W., Baehrens, D., Huber, B., Kulik, A., *et al.* (2012). High-resolution proteomics unravel architecture and molecular diversity of native AMPA receptor complexes. Neuron *74*, 621-633.

Schwenk, J., Harmel, N., Zolles, G., Bildl, W., Kulik, A., Heimrich, B., Chisaka, O., Jonas, P., Schulte, U., Fakler, B., *et al.* (2009). Functional proteomics identify cornichon proteins as auxiliary subunits of AMPA receptors. Science *323*, 1313-1319.

Shaib, A.H., Staudt, A., Harb, A., Klose, M., Shaaban, A., Schirra, C., Mohrmann, R., Rettig, J., and Becherer, U. (2018). Paralogs of the Calcium-Dependent Activator Protein for Secretion Differentially Regulate Synaptic Transmission and Peptide Secretion in Sensory Neurons. Frontiers in cellular neuroscience *12*, 304.

Shanks, N.F., Savas, J.N., Maruo, T., Cais, O., Hirao, A., Oe, S., Ghosh, A., Noda, Y., Greger, I.H., Yates, J.R., 3rd, *et al.* (2012). Differences in AMPA and kainate receptor interactomes facilitate identification of AMPA receptor auxiliary subunit GSG1L. Cell reports *1*, 590-598.

Shi, S.H., Hayashi, Y., Petralia, R.S., Zaman, S.H., Wenthold, R.J., Svoboda, K., and Malinow, R. (1999). Rapid spine delivery and redistribution of AMPA receptors after synaptic NMDA receptor activation. Science *284*, 1811-1816.

Shi, Y., Lu, W., Milstein, A.D., and Nicoll, R.A. (2009). The stoichiometry of AMPA receptors and TARPs varies by neuronal cell type. Neuron *62*, 633-640.

Sobolevsky, A.I., Rosconi, M.P., and Gouaux, E. (2009). X-ray structure, symmetry and mechanism of an AMPA-subtype glutamate receptor. Nature *462*, 745-756.

Sollner, T., Whiteheart, S.W., Brunner, M., Erdjument-Bromage, H., Geromanos, S., Tempst, P., and Rothman, J.E. (1993). SNAP receptors implicated in vesicle targeting and fusion. Nature *362*, 318-324.

Sommer, B., Kohler, M., Sprengel, R., and Seeburg, P.H. (1991). RNA editing in brain controls a determinant of ion flow in glutamate-gated channels. Cell *67*, 11-19.

Srivastava, S., Osten, P., Vilim, F.S., Khatri, L., Inman, G., States, B., Daly, C., DeSouza, S., Abagyan, R., Valtschanoff, J.G., *et al.* (1998). Novel anchorage of GluR2/3 to the postsynaptic density by the AMPA receptor-binding protein ABP. Neuron *21*, 581-591.

Stein, V., House, D.R., Bredt, D.S., and Nicoll, R.A. (2003). Postsynaptic density-95 mimics and occludes hippocampal long-term potentiation and enhances long-term depression. J Neurosci *23*, 5503-5506.

Sugiyama, H., Ito, I., and Hirono, C. (1987). A new type of glutamate receptor linked to inositol phospholipid metabolism. Nature *325*, 531-533.

Suh, Y.H., Terashima, A., Petralia, R.S., Wenthold, R.J., Isaac, J.T., Roche, K.W., and Roche, P.A. (2010). A neuronal role for SNAP-23 in postsynaptic glutamate receptor trafficking. Nat Neurosci *13*, 338-343.

Sumioka, A., Brown, T.E., Kato, A.S., Bredt, D.S., Kauer, J.A., and Tomita, S. (2011). PDZ binding of TARPgamma-8 controls synaptic transmission but not synaptic plasticity. Nat Neurosci *14*, 1410-1412.

Tafoya, L.C., Mameli, M., Miyashita, T., Guzowski, J.F., Valenzuela, C.F., and Wilson, M.C. (2006). Expression and function of SNAP-25 as a universal SNARE component in GABAergic neurons. J Neurosci *26*, 7826-7838.

Tao-Cheng, J.H., Crocker, V.T., Winters, C.A., Azzam, R., Chludzinski, J., and Reese, T.S. (2011). Trafficking of AMPA receptors at plasma membranes of hippocampal neurons. J Neurosci *31*, 4834-4843.

Tavares, G.A., Panepucci, E.H., and Brunger, A.T. (2001). Structural characterization of the intramolecular interaction between the SH3 and guanylate kinase domains of PSD-95. Molecular cell *8*, 1313-1325.

Tomita, S. (2010). Regulation of ionotropic glutamate receptors by their auxiliary subunits. Physiology *25*, 41-49.

Tomita, S., Adesnik, H., Sekiguchi, M., Zhang, W., Wada, K., Howe, J.R., Nicoll, R.A., and Bredt, D.S. (2005a). Stargazin modulates AMPA receptor gating and trafficking by distinct domains. Nature *435*, 1052-1058.

Tomita, S., Chen, L., Kawasaki, Y., Petralia, R.S., Wenthold, R.J., Nicoll, R.A., and Bredt, D.S. (2003). Functional studies and distribution define a family of transmembrane AMPA receptor regulatory proteins. The Journal of cell biology *161*, 805-816.

Tomita, S., Stein, V., Stocker, T.J., Nicoll, R.A., and Bredt, D.S. (2005b). Bidirectional synaptic plasticity regulated by phosphorylation of stargazin-like TARPs. Neuron *45*, 269-277.

Tonikian, R., Zhang, Y., Sazinsky, S.L., Currell, B., Yeh, J.H., Reva, B., Held, H.A., Appleton, B.A., Evangelista, M., Wu, Y., *et al.* (2008). A specificity map for the PDZ domain family. PLoS biology *6*, e239.

Toth, K., and McBain, C.J. (1998). Afferent-specific innervation of two distinct AMPA receptor subtypes on single hippocampal interneurons. Nat Neurosci *1*, 572-578.

Traynelis, S.F., Wollmuth, L.P., McBain, C.J., Menniti, F.S., Vance, K.M., Ogden, K.K., Hansen, K.B., Yuan, H., Myers, S.J., and Dingledine, R. (2010). Glutamate receptor ion channels: structure, regulation, and function. Pharmacological reviews *62*, 405-496.

Turrigiano, G.G. (2000). AMPA receptors unbound: membrane cycling and synaptic plasticity. Neuron *26*, 5-8.

Twomey, E.C., Yelshanskaya, M.V., Grassucci, R.A., Frank, J., and Sobolevsky, A.I. (2016). Elucidation of AMPA receptor-stargazin complexes by cryo-electron microscopy. Science *353*, 83-86.

Twomey, E.C., Yelshanskaya, M.V., Grassucci, R.A., Frank, J., and Sobolevsky, A.I. (2017). Channel opening and gating mechanism in AMPA-subtype glutamate receptors. Nature *549*, 60-65.

Urh, M., and Rosenberg, M. (2012). HaloTag, a Platform Technology for Protein Analysis. Current chemical genomics *6*, 72-78.

van der Sluijs, P., and Hoogenraad, C.C. (2011). New insights in endosomal dynamics and AMPA receptor trafficking. Seminars in cell & developmental biology *22*, 499-505.

Vandenberghe, W., Nicoll, R.A., and Bredt, D.S. (2005). Interaction with the unfolded protein response reveals a role for stargazin in biosynthetic AMPA receptor transport. J Neurosci *25*, 1095-1102.

Volianskis, A., Bannister, N., Collett, V.J., Irvine, M.W., Monaghan, D.T., Fitzjohn, S.M., Jensen, M.S., Jane, D.E., and Collingridge, G.L. (2013). Different NMDA receptor subtypes mediate induction of long-term potentiation and two forms of short-term potentiation at CA1 synapses in rat hippocampus in vitro. The Journal of physiology *591*, 955-972.

von Engelhardt, J. (2019). AMPA Receptor Auxiliary Proteins of the CKAMP Family. International journal of molecular sciences *20*.

von Engelhardt, J., Mack, V., Sprengel, R., Kavenstock, N., Li, K.W., Stern-Bach, Y., Smit, A.B., Seeburg, P.H., and Monyer, H. (2010). CKAMP44: a brain-specific protein attenuating short-term synaptic plasticity in the dentate gyrus. Science *327*, 1518-1522.

Wang, G., Gilbert, J., and Man, H.Y. (2012). AMPA receptor trafficking in homeostatic synaptic plasticity: functional molecules and signaling cascades. Neural plasticity *2012*, 825364.

Watson, J.F., Ho, H., and Greger, I.H. (2017). Synaptic transmission and plasticity require AMPA receptor anchoring via its N-terminal domain. eLife *6*.

Wo, Z.G., and Oswald, R.E. (1995). Unraveling the modular design of glutamate-gated ion channels. Trends in neurosciences *18*, 161-168.

Wu, H., Nash, J.E., Zamorano, P., and Garner, C.C. (2002). Interaction of SAP97 with minus-end-directed actin motor myosin VI. Implications for AMPA receptor trafficking. The Journal of biological chemistry *277*, 30928-30934.

Xia, J., Zhang, X., Staudinger, J., and Huganir, R.L. (1999). Clustering of AMPA receptors by the synaptic PDZ domain-containing protein PICK1. Neuron *22*, 179-187.

Xu, W. (2011). PSD-95-like membrane associated guanylate kinases (PSD-MAGUKs) and synaptic plasticity. Current opinion in neurobiology *21*, 306-312.

Yamamoto, A., Nagano, T., Takehara, S., Hibi, M., and Aizawa, S. (2005). Shisa promotes head formation through the inhibition of receptor protein maturation for the caudalizing factors, Wnt and FGF. Cell *120*, 223-235.

Yao, Y., Harrison, C.B., Freddolino, P.L., Schulten, K., and Mayer, M.L. (2008). Molecular mechanism of ligand recognition by NR3 subtype glutamate receptors. The EMBO journal *27*, 2158-2170.

Yu, Y.J., Dhavan, R., Chevalier, M.W., Yudowski, G.A., and von Zastrow, M. (2010). Rapid delivery of internalized signaling receptors to the somatodendritic surface by sequence-specific local insertion. J Neurosci *30*, 11703-11714.

Yudowski, G.A., Puthenveedu, M.A., Leonoudakis, D., Panicker, S., Thorn, K.S., Beattie, E.C., and von Zastrow, M. (2007). Real-time imaging of discrete exocytic events mediating surface delivery of AMPA receptors. J Neurosci *27*, 11112-11121.

Yudowski, G.A., and von Zastrow, M. (2011). Investigating G protein-coupled receptor endocytosis and trafficking by TIR-FM. Methods in molecular biology *756*, 325-332.

Zhang, W., St-Gelais, F., Grabner, C.P., Trinidad, J.C., Sumioka, A., Morimoto-Tomita, M., Kim, K.S., Straub, C., Burlingame, A.L., Howe, J.R., *et al.* (2009). A transmembrane accessory subunit that modulates kainate-type glutamate receptors. Neuron *61*, 385-396.

Zheng, C.Y., Chang, K., Suh, Y.H., and Roche, K.W. (2015a). TARP gamma-8 glycosylation regulates the surface expression of AMPA receptors. The Biochemical journal *465*, 471-477.

Zheng, N., Jeyifous, O., Munro, C., Montgomery, J.M., and Green, W.N. (2015b). Synaptic activity regulates AMPA receptor trafficking through different recycling pathways. eLife *4*.

Zheng, Y., Brockie, P.J., Mellem, J.E., Madsen, D.M., Walker, C.S., Francis, M.M., and Maricq, A.V. (2006). SOL-1 is an auxiliary subunit that modulates the gating of GLR-1 glutamate receptors in Caenorhabditis elegans. Proc Natl Acad Sci U S A *103*, 1100-1105.

Zhu, J.J., Esteban, J.A., Hayashi, Y., and Malinow, R. (2000). Postnatal synaptic potentiation: delivery of GluR4-containing AMPA receptors by spontaneous activity. Nat Neurosci *3*, 1098-1106.

# List of publications

Harb A., Vogel N., Frisch W., Shaib A., Becherer U., Bruns D., and Mohrmann R. Role of auxiliary subunits in AMPA receptor trafficking in hippocampal neurons. (*Manuscript being prepared to be submitted soon*)

Shaaban A., Dhara M., Frisch W., Harb A., Shaib A., Becherer U., Bruns D., and Mohrmann R (2019). The SNAP-25 linker supports fusion intermediates by local lipid interactions. Elife 8. pii: e41720.

Shaib, A.H., Staudt, A., Harb, A., Klose, M., Shaaban, A., Schirra, C., Mohrmann, R., Rettig, J., and Becherer, U. (2018). Paralogs of the Calcium-Dependent Activator Protein for Secretion Differentially Regulate Synaptic Transmission and Peptide Secretion in Sensory Neurons. Frontiers in cellular neuroscience *12*, 304.

Shehadi, M., Awada, F., Oleik, R., Chokr, A., Hamze, K., Abou Hamdan, H., Harb, A., and Kobaissi, A. (2014). Comparative Analysis of the Anti-bacterial Activity of Four Plant Extracts. International Journal of Current Research and Academic Review 01/2014; 2(6):83-94.

# Conferences

NWG 2019 (Göttingen Neuroscience conference, Germany): poster

BioBeirut8 2018 (Beirut, Lebanon): invited speaker. "*Role of Auxiliary Subunits in AMPA Receptor Trafficking in Hippocampal Neurons"*

Cell Physics 2017 (Saarbrücken, Germany): participant

Cell Physics 2016 (Saarbrücken, Germany): participant

Cell Physics 2014 (Saarbrücken, Germany): poster

# Acknowledgement

*First and foremost, I want to thank God almighty for his blessings and strength to achieve this PhD thesis!*

*I want to offer my special thanks and appreciation to my Doctoral supervisor Prof. Dr. Ralf Mohrmann who supported me through all my PhD period from the first day I started to work with him. Prof. Dr. Mohrmann accompanied me through all the ups and downs and gave me invaluable guidance and inspiration to solve many problems I faced, and enriched my confidence and knowledge in science and life, which I am very grateful for.*

*I want to thank Prof. Dr. Dieter Bruns for hosting me in his lab and considering the group of Prof. Mohrmann as part of his own. His participation and input in our work was of a great help that inspired me to think about new ideas and experiments. Away from science, I enjoyed the discussions with him about other interesting subjects during breaks and events.*

*I want to thank all the members of the group of Prof. Dr. Ralf Mohrmann and Prof. Dr. Dieter Bruns who contributed to my work and offered me joyful times including Walentina Frisch, Nils Vogel, Judith Arend, Vanessa Schmitt, and Madhurima Dhara.*

*I want to express my special gratitude to our lab manager Marina Wirth who always showed a strong support. I also thank Dr. Yvonne Schwarz for all her help and contribution throughout my PhD period.*

*I appreciate the generosity of Prof. Dr. Jens Rettig who allowed me to use his facility and microscopes to answer my scientific questions. I want to thank him for his interest in my project and encouragement to proceed. I would not forget to thank all his lab members including Dr. Elmar Krause, Dr. David Stevens, Dr. Claudia Schirra, Anja Ludes, and Margarete Klose for their scientific and technical support.*

*I have a great pleasure in expressing my gratitude to my former supervisor and current collaborator Dr. Ute Becherer for helping me establishing my project and always giving me some of her valuable time for nice discussions and advices on all levels.*

*I want to mention my dear friends who everyone by his own way helped and provided me with joyful times. I want to thank my dear friend Dr. Ali Shaib for all his contributions and help. I would not forget to remember Dr. Hawraa Bzeih, Marwa Sleiman, Maria Mantero Martinez, Mazen Makke, Ahmed Shaaban, Katharina Oleinikov, Ahsan Raza, and Arne Knörck, with whom I had unforgettable times and moments.*

*My forever enthusiastic, encouraging, and motivating family, uncles, and aunts: They were my source of hope and strength. I thank my beloved father Mustapha Harb and my beloved mother Siham Harb for believing in me and always pushing me forward. Their blessings and love brought me to where I am today. I thank my beloved brothers Mohammed and Hussein Harb who motivated me and were proud to see me progressing through all my life and studies. Of course, my newborn niece Manessa was also an inspiration for me to continue my last steps of my thesis.*